Inaugural Dissertation

zur

Erlangung der Doktorwüde

der

Naturwissenschaftlich-Mathematischen Gesamtfakultät

der

Ruprecht-Karls-Universität Heidelberg

Vorgelegt von

Haisen Ta

aus Nei Mongol, China

Tag der mündlichen Prüfung: 5. Februar 2010

A Novel Method for Quantitative and Structural Determination of Molecular Complexes by Photon Antibunching

Gutachter:

PD Dr. Dirk-Peter Herten

Prof. Dr. Roland Krämer

In memory of my grandmother

Acknowledgement

I owe everything to all the following people, who helped me on both my research work and daily life during my stay in Heidelberg. I can not imagine my life without their help and support.

I am very much grateful to my advisor, PD Dr. D.-P. Herten. Since I arrived at Heidelberg, his encouragement led me into this amazing field, his guidance enlightened the way of my research work and his support made me through all the difficulties during my study and research. His thoughtfulness made me feel very comfortable in my work and enjoy my life in a foreign country. Without him, it is not possible for me to come to this stage.

I thank Prof. Dr. J. Wolfrum and Prof. Dr. B. Bukau for giving me the chance to study in Heidelberg University.

I also thank Dr. A. Kiel, who helped me with the experiments and optical microscopes. And the discussions with him made me get into this field much easier and with more profound understandings.

I thank all the group members, Dr. K. Lymperopoulos, D. Barzan, J. Balbo, C. Spassova, T. Ehrhard, A. Kurz, A. Seefeld, Dr. K.-T. Han, Dr. P. Heinlein and so on. They gave me suggestions on research and helped me, who is a foreigner, with my daily life in Germany. Especially I thank Dr. C. Roth, who introduced Labview to me and gave me a lot of help on programming. I thank Dr. D. Siegberg, who helped me on the photostabilizing buffer. I also thank M. Schwering, who helped me on the labeling of DNA and also gave me many suggestions on my thesis. I thank A. Rybina and T. Lisauskas for their support during my thesis writing. I also thank Dr. Katharina Stoehr, who was the one I should have shared more time with.

I would like to thank Prof. Dr. M. Mayer, Dr. A. Mogk, Dr. G. Kramer, Dr. T. Haslberge and A. Sandikci for their collabrations during my Ph.D work.

I also thank Y. Wang for her proofreading of my thesis and support during my thesis writing.

I also thank the financial support of the Heinz Goetze Memorial Fellowship Program and Dr. D. Wuensche for her nice organization of the scholarship. I thank the financial support from Stipendien- und Betreuungsprogramm (STIBET) from DAAD during my dissertation preparation.

I owe a lot to my parents and my sister. Their unconditional love and support make me through all the difficulties and make me happy all the time no matter how far I am.

There are many many people having helped me in my Ph.D work, I can not list everyone here. Their help have benefited and will benefit me in my future research work and life.

Abbreviation

AOM	Acousto-Optic Modulator
APD	Avalanche Photodiodes
APS	amino-propyl silane
BSA	bovine serum albumin
CCD	Charge-Coupled Device
CW	Continuous Wave
DNA	deoxyribonucleic acid
FIDA	Fluorescence Intensity Distribution Analysis
FIFO	First-In-First-Out
FLIM	Fluorescence Lifetime Imaging
FRET	Fluorescence Resonance Energy Transfer
FWHM	Full Width at Half Maximum
HF	hydrofluoric acid
HPLC	High Performance Liquid Chromatography
IC	Internal Conversion
IRF	Instrument Response Function
LEDs	Light Emitting Diode
LM	Levenberg-Marquardt
NA	Numerical Aperture
PCH	Photon Counting Histogram

PLL	poly-l lysine
PMT	Photomultiplier Tube
ROXS	Reducing-Oxidizing System
SMD	Single Molecule Detection
SMFS	Single-Molecule Fluorescence Spectroscopy
SMS	Single Molecule Spectroscopy
SPC	Single Photon Counting
TCSPC	Time-Correlated Single Photon Counting
TIRF	Total Internal Reflection Fluorescence Microscopy
TTTR	Time-Tagged Time-Resolved
VR	Vibrational Relaxation

Abstract

In optical microscopy fluorescent molecules are used to label target structures like proteins or DNA. With confocal microscopy, a complex of multiple fluorescent molecules is detected as a point spread function due to the diffraction limit. A particular challenge is to determine the number of molecules hiding behind the point spread function. In this work an extended method for determining the number of fluorescent molecules is presented. The method is based on photon antibunching, which is the phenomenon that a single fluorescent molecule can emit only one photon at a time. A statistical analysis of coincidently detected photons can be used to determine the number of photon emitters. In previous works the maximal number of molecules that can be distinguished was about 3. This has now been extended by doubling the number of detectors from 2 to 4, so that up to 4 simultaneously emitted photons can be detected. A new data analysis procedure was established according to the changes of the scheme. Simulations have shown that in theory up to 50 molecules can be resolved under realistic conditions. These predictions were experimentally validated with immobilized dsDNA labeled with 5 fluorophores. The consideration of photobleaching in the data analysis and the use of a photo-stabilizer enable up to 15 molecules to be determined. Thus, this method provides a promising tool for determining the stoichiometry of various biomolecular complex, which can not be achieved by normal microscopic methods.

Kurzfassung

In der optischen Mikroskopie werden fluoreszierende Moleküle verwendet, um Zielstrukturen wie Proteine oder DNA zu markieren. Mit Hilfe der konfokalen Einzelmolekülmikroskopie können diese innerhalb der beugungsbegrenzten Auflösung als Punktabbildung detektiert werden. Eine besondere Herausforderung dabei ist es, die Anzahl der Moleküle, die sich hinter einer solchen Punktabbildung verbergen zu bestimmen. In dieser Arbeit wird eine, auf Photon- Antibunching basierende, Methode zur Bestimmung der Anzahl fluoreszierender Moleküle in einer solchen Abbildung erweitert. Photonen Antibunching basiert auf dem Phänomen, dass ein einzelnes fluoreszierendes Molekül nach Anregung nur maximal ein Photon emittieren kann. Anhand einer statistischen Analyse über gleichzeitig detektierte Photonen kann dann eine Abschätzung über die Anzahl der Emitter gegeben werden. In früheren Arbeiten konnte damit bis zu 3 Moleküle gezählt werden, eine höhere Anzahl konnte nicht mehr sicher bestimmt werden. In dieser Arbeit wurde dieser Ansatz erweitert. Die Anzahl Detektoren wurde verdoppelt, so dass bis zu 4 gleichzeitig emittierte Photonen detektiert werden konnten. Entsprechend wurde die statistische Auswertung angepasst. Mit Hilfe simulierter Daten konnte gezeigt werden, dass nun theoretisch bis zu 50 Moleküle gezählt werden können. Erste Experimente an immobilisiertem Konstrukt aus 5-fach Fluoreszenzmarkierten DNS Proben bestätigten die Methode. Unter Berücksichtigung der Photozerstörung in der Datenanalyse, sowie die Verwendung von Photostabilisatoren konnte die Methode bis zu 15 Moleküle sicher bestimmen. Damit stellt sie ein vielversprechendes Werkzeug zur Bestimmung der Stöchiometrie diverser Biomolekülkomplexe dar, die durch normale mikroskopische Verfahren nicht möglich ist.

Summary

Since the first detection of single molecules in solid host at cryogenic temperature by Moerner and Orrit [59, 55] and in solution at room temperature by Shera *et al.*, single molecule spectroscopy has been applied to an extending variety of problems in biological systems. The advantages of single molecule detection (SMD) over its bulk counterparts present it as an essential tool for modern biochemistry.

Ensemble measurements focus on the average behavior of many molecules, while single molecule detection (SMD) addresses mainly the behavior of individual molecules. When it comes to a moderate number of molecules, few methods are available to explore them. Furthermore, not all details of molecules can be resolved by modern optical microscopy. On one hand, resolution of optical microscopy is limited to $\sim 200\ nm$ by light diffraction. On the other hand, FRET (Fluorescence Resonance Energy Transfer) is only able to explore the interaction between molecules that are around $1 - 10$ nm apart from each other. The intermediate range of 10 nm to 200 nm is called resolution gap due to the lack of proper tools for investigation. Although the size of macromolecules in living systems, such as proteins, is in the range of nanometers, they tend to cooperate with each other to perform their functions in physiological environments. The sizes of macromolecular complexes frequently reside in several tens of nanometers, which exactly falls into the resolution gap. Recently, photon antibunching has provided a potential tool to quantify the stoichiometry of molecules collocalized within the distance of the resolution gap. Photon antibunching is a quantum nature of photon emission. It is a phenomenon that one fluorophore emits only one photon at one time. Therefore, if more than one photon is observed at the same time, the

signal must arise from several photon emitters. Several groups have used two single-photon sensitive detectors to identify simultaneous photon emissions and have determined the number of fluorophores in molecular complexes [79, 92]. But their methods are limited to around 3 fluorophores because of poor statistics of simultaneously detected photons.

In this work I describe a method to extend the counting ability of photon antibunching. First, in order to collect more simultaneously detected photons, a new scheme was built based on four detectors. Four detection channels are able to detect not only 1.5 times more two simultaneous photons than two detection channels, but also triple and quadruple simultaneous photons, which is not possible with two detection channels. Both the increased number of two simultaneous photons and the triple/quadruple simultaneous photons benefit the method by better photon statistics. I developed a new algorithm to quantify the number of fluorophores by photon antibunching based on the photon statistics (multiple simultaneous photons). Furthermore, a photostabilizing buffer is used to delay photobleaching and further increase the photon statistics. However, when the number of fluorophores increases, photobleaching becomes prominent even with the help of a photostabilizing buffer and results in the lack of enough simultaneously detected photons. In order to overcome this problem, I have modified the algorithm to consider fluorescent photobleaching, which has not been taken into account by former attempts. Therefore, theoretically all photons contribute to enhance the performance of the method. To evaluate the feasibility of this method, I performed numerical simulations, which demonstrate that the method is able to count up to 50 molecules with moderate errors. Validation of the method with experiments needs a system with a defined number of fluorophores. Therefore, I designed a double-stranded DNA (dsDNA) with 5 labels. The performance of the method on the defined system with known number of fluorophores confirms its feasibility on a low number (1-5) of fluorescent molecules. Moreover, it is demonstrated for the first time that photon antibunching is able to count up to 15 molecules by applying the method on dsDNA complexes with more fluorophores.

It is shown in this dissertation that more than 10 molecules can be resolve by using photon antibunching. The combination of a new scheme with four detection channels, a new algorithm considering photobleaching and a photostabilizing buffer make it possible to collect enough multiple simultaneously detected photons and use all the photon statistics to quantify the stoichiometry of fluorescent molecules. Because the method is deduced from the nature of photon emission and is not limited by the resolution of optical microscopy, it provides perspectives on many applications in biological systems, such as determining the stoichiometry of receptors clusters on the cell membrane and quantifying the number of copies in protein aggregation, which are difficult to resolve by modern optical microscopy.

Contents

1 Introduction

As envisioned by Richard P. Feynman in 1959, particles are intensively examined, fabricated and manipulated at nanometer scale nowadays. Due to the perfection at their dimension, nano particles, such as single molecules, nanocrystals, nanodiamonds and nanotubes, behave very differently from their bulk counterparts [58, 4, 76, 21]. Single molecule spectroscopy (SMS) provides a powerful tool to examine nano particles at single molecule or particle level. Many microscopic methods including confocal microscopy are developed to extract from an experiment the fluorescence emission properties, such as the spectrum, degree of energy transfer, stoichiometry and spatial position [91, 54].

SMS has advantages over the ensemble counterparts in two aspects. First, SMS is able to characterize subpopulations, while ensemble experiments only measure the average value of all subpopulations. As an explanation in Fig.1.1, both figures are composed of red or blue squares alternatively. The figure on the right is the amplification of a small part of the left. The structure in the left figure is so small that only the average color can be identified by

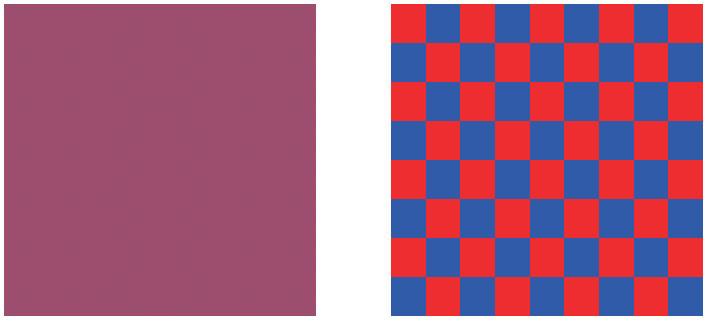

Figure 1.1: Explanation of subpopulations in SMS: The figure on the right is the amplification of a part of the left by 100×100 times.

naked eyes, which is magenta. However, if we magnify a small part of it by 100×100 times as shown in the right, the fine-tuned structure appears. Thus, we are able to examine the color of the squares one by one and separate them into two subpopulations, one of which contains red squares and the other blue. Actually, there is nothing in magenta. For the same reason, SMS can resolve the subpopulations which are hidden in ensemble measurements. Second, SMS is able to trace the dynamics of single particles, which are not detectable in ensemble measurements due to the lack of synchronization of all particles. A similar example is that if all squares on the left of Fig.1.1 are changing color randomly between red and blue, it still looks like magenta under the circumstance that the average dwell times of all squares in red and blue are the same. However, if the color of each square can be traced individually in respect of time, the characteristic time of color changing can be determined by examining one square at one time. Tracing one molecule at a time enables the observation of the dynamics of reactions, even in equilibrium. Because of the ability of identifying the existence and dynamics of sub-populations, the applications of SMS in physics, chemistry, and biophysics have broadened and deepened our knowledge of many basic phenomena [49, 53, 74].

Although modern optical microscopies can resolve structures as small as 200 nm, it is still not possible to resolve the fine structure of most biomolecules. The reason is that the size of biomolecules is in the range of 10 nm and smaller than the resolution of confocal microscopies. Therefore, in order to examine one molecule at a time, molecules have to be separated from each other, which means the concentration of the molecules is lower than $0.2\ molecule/\mu m^2$ on a surface [70] or $10^{-8}M$ in solution [68]. On the other hand, if several molecules associate with each other within the size below the optical resolution, it is not possible for optical microscopes to distinguish whether there is only one molecule or not. However, a unique evidence of the existence of single molecules is photon antibunching.

Photon antibunching of resonance fluorescence is a phenomenon that one fluorescent molecule can not emit more than one photon at a time. Fluorescent molecules can be excited from ground state (low energy) to excited state (high energy). Fluorescence emission occurs

only when the molecules return from excited state to ground state. Mostly, fluorescent molecules are in ground state at room temperature. Once a molecule is excited to a higher energetic state, it stays there for a while (nanoseconds for most organic dyes), such as t_i

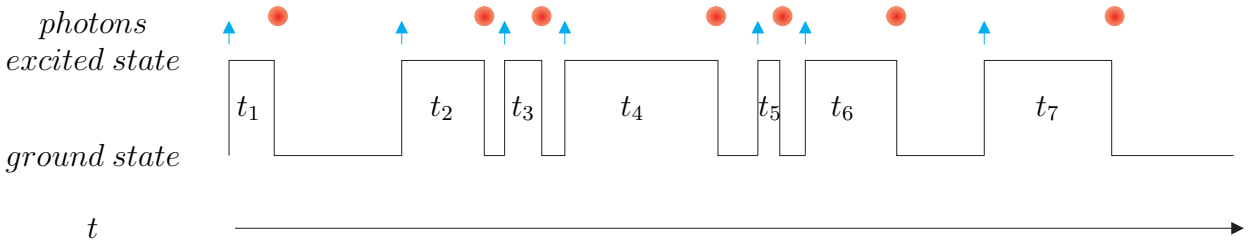

Figure 1.2: An explanation of photon antibunching: If a fluorophore have two states (ground state and excited state), photon emission happens only when the fluorophore returns to ground state from excited state. Arrows indicate the time when the fluorophore is excited and t_i, $i = 1,2,...,7$, are the dwell times of the excited state.

($i = 1,2,...,7$) in Fig. 1.2. Consequently, the next photon emission from the same molecule is always lagged due to the dwell time in excited state. The temporal spacing between two photon emissions from the same fluorophore is called photon antibunching. Therefore, photon antibunching has been used as a proof of single fluorescent molecules. On the other hand, two-simultaneous-photon emission is an indication of multiple fluorescent molecules, which means that decreased photon antibunching carries the information about the stoichiometry of the fluorescent molecules. Actually, photon antibunching has been used to quantify the number of fluorescent molecules both on a surface and in solution [79, 92]. However, the number of molecules that former attempts were able to count is limited to around 3, which is far from the demands of biological applications to determine the stoichiometry of macromolecular systems, such as receptor clusters on cell membrane and protein aggregates. The motivation of this thesis is to develop a new model based on photon antibunching to count more molecules which are immobilized on a surface at room temperature.

1.1 Brief history of photon antibunching in single molecule detection

Single molecule detection (SMD) has been applied under numerous circumstances in many fields and photon antibunching is frequently used as a tag of the existence of single molecules.

Historically, photon antibunching in resonance fluorescence with atoms was firstly observed by Kimble, Mandel, and Dagenais in 1977 [39] as predicted by Stoler $et\ al.$ in 1974 [78]. Although many works about photon antibunching and photon statistics of atomic beam were performed in the following decade [1, 40, 73, 27], photon antibunching of single molecules was not identified since single molecules had not been observed until 1989, when Moener $et\ al.$ successfully detected single pentacene molecules in a host crystal at cryogenic temperatures [55]. Shortly after the first SMD, the observation of photon antibunching of single molecules was reported in 1992. Basche $et\ al.$ pumped single pentacene molecules optically in a host of a solid and observed photon antibunching as well as the decrease of photon antibunching when two molecules were pumped at the same time [8].

Later, Betzig $et\ al.$ and Ambrose $et\ al.$ independently detected immobilized single molecules on a surface at room temperature [12, 5]. However, at that time, good statistics of photon antibunching with immobilized fluorescent molecules were limited by photobleaching, photochemical destruction of fluorescent molecules, and detector saturation, which is resulted from the long dead time of detectors. In 1997 Ambrose $et\ al.$ successfully circumvented detector saturation by turning off continuous wave (CW) laser excitation with an acousto-optic modulator (AOM) for periods longer than the detector dead time, consequently observed photon antibunching of single fluorescent molecules with an excitation power high enough to saturate the fluorescent molecules [62].

Since time-correlated single photon counting (TCSPC), essentially a ”stopwatch” technique

to precisely record photon arrival times, was introduced in 1961 by Bollinger and Thomas [16], it is widely used and is one of the best ways to define the time resolution of photon arrivals. In 2002 Weston $et\ al.$ took the advantages of TCSPC, adapted photon antibunching in TCSPC scheme and obtained the number of fluorescent labels of single molecule complexes immobilized on a surface by comparing simultaneous photon pairs and non-simultaneous photon pairs [92]. They were able to see the arrival times of photon pairs with one TCSPC card by delaying one of the signals from two single-photon sensitive detectors. TCSPC also enabled them to determine the excited-state lifetime of the fluorescent molecules at the same time. However, because photobleaching results in poor photon statistics, simultaneous photon pairs saturate fast when the number of fluorophores increases and limit the counting ability by photon antibunching.

On the other hand, the first photon antibunching effect in solution was observed by Kask $et\ al.$ in 1985 by the correlations of photon arrival times in nanosecond time range. Although there were more than one molecule in the observation volume, photon antibunching was still observable [37]. Later the first SMD in solution at room temperature was done by Shera $et\ al.$ in 1990 [17]. Bursts of fluorescent emission are attributed to single molecules and autocorrelation of photon bursts yielded information of transit time of the molecule through the excitation volume. In 2007, Sykora $et\ al.$ measured fluorescent photon antibunching by accumulating data over a large number of molecules diffusing in solution to obtain the average number of labels on one molecule [79]. The number of fluorophores was determined by the combinations of the correlations at zero, intermediate and infinite lag time. But excitonic coupling between the fluorophores limited the number of molecules that they were able to count.

Nevertheless, both the applications of photon antibunching methods on immobilized molecules on a surface and molecular complexes diffusing in solution have a similar limit, which is around 3 molecules. Recently, we extended the scheme of photon antibunching by using four detection channels [80]. A theoretical model to estimate the number of molecules

and molecular brightness was built and the simulations showed that it is possible to count more molecules under realistic experimental conditions.

At the same time, because photostability, such as photobleaching and blinking, plays an important role in the applications of fluorophores, including photon antibunching, it has been studied specifically for many commercial fluorophores [93, 71, 32, 86]. Some oxygen depleting systems [10, 3] have been used to decrease photobleaching rates in solution because oxygen is primarily responsible for photobleaching of fluorophores. Although the remove of oxygen increased the photostability of fluorophores, it also introduced blinking in millisecond time scale at the same time. This is because oxygen is also a good anti-blinking agent. As a result, the fluorescence intensity is reduced and consequently decreased the occurrences of correlated photon pairs. Additional Trolox [66] or a reducing-oxidizing system [86] has successfully been used to diminish blinking and prolong the lifetime of some fluorophores at the same time, which generates nonblinking and longlasting fluorescent molecules. The applications of fluorophores, including photon antibunching, have benefited from their stability and brightness [66].

Meanwhile, photon antibunching on different single quantum system has also been intensively explored. Since quantum dots or semiconductor nanocrystals were firstly reported [69], they have gained many interests and been applied in many fields [38, 51]. Quantum dots tend to be brighter than most organic dyes due to their large extinction coefficients [30, 7]. They also resist bleaching over a long period of time (hours). Although quantum dots blink [57], photon antibunching of quantum dots has been observed at room temperature by Michler $et\ al.$ in 2000 [52] due to the difference in the time scale of photon antibunching and blinking. The typical photon antibunching curve with continuous-wave laser excitation has also been used to obtain the excited-state lifetime of quantum dots [46]. Moreover, the first non-blinking semiconductor nanocrystals were reported by Wang $et\ al.$ in 2009 [89] and may enable substantial advances in many fields, including the applications of photon antibunching in determining stoichiometry of molecules.

Recently, fluorescent nanodiamonds attract many attentions due to their inertness, small size and surface structure. They are well-suited for biological applications, such as labeling and drug delivery [96]. Photon antibunching in resonance fluorescence emitted from a single nitrogen vacancy center in diamond at room temperature was observed in 2000 [18, 13]. Some nanodiamonds with different deficits, such as silicon-vacancy, showed even brighter fluorescence [85]. Therefore, because of their resistance to photobleaching and reasonable molecular brightness, nanodiamonds are good candidates to count more molecules by photon antibunching.

Moreover, photon antibunching of a single tetrachromophoric dendritic system demonstrate that efficient singlet-singlet annihilation ensures that only one photon is emitted even when several excitations are generated in an individual multichromophoric molecule [82].

Since photon antibunching is observable only if the number of fluorophores is low, it has always been connected to SMD by either proving the existence of single molecules or quantifying the number of fluorescent copies in molecular complexes. Furthermore, as a quantum nature of photon emission, photon antibunching is able to provide stoichiometric information even below the optical resolution of modern microscopy. Therefore, it will continuously play an important role in SMD and help to provide quantitative information of biological systems.

1.2 Methods to investigate stoichiometry of molecules

In order to determine the stoichiometry in biological systems, such as macromolecular complexes in the cytoplasm and receptor clusters on the cell membrane, there are many techniques developed to investigate the stoichiometry of fluorescent molecules in solution or on surfaces.

Although photobleaching is not favored in most cases, it has been exploited to study the stoichiometry of biomolecules [50]. The fluorescence intensity drops as shown in Fig. 1.3 are probably due to the bleaching of individual fluorophores. Therefore, the initial number

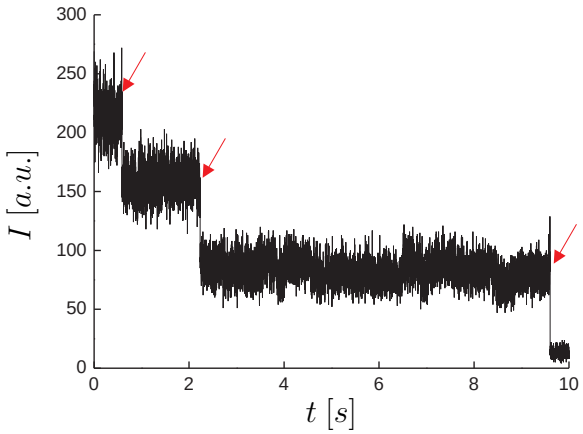

Figure 1.3: Fluorescence intensity drops induced by bleaching: a scheme of counting molecules by bleaching steps. Three fluorescence intensity drops at $0.7s$, $2.2s$ and $9.7s$ (indicated by arrows) probably correspond to photonbleaching of three individual fluorophores respectively. I is the fluorescence intensity with arbitrary unit and t is the time in second.

of fluorophores can be determined by counting the bleaching steps. It has been used in some biological systems, such as determining the number of pRNA of the DNA-packaging motor of bacteriophage [77] and determining the stoichiometry of protein complexes on rabbit red blood cell membranes [25]. However, although it can determine the stoichiometry of biomolecules, bleaching step is not a direct proof of single molecule bleaching. Moreover, the resolving ability of counting bleaching steps is limited by the fluorophores and the overlapping of bleaching steps, which occurs frequently when the number of fluorophores increases.

Moreover, triple-color correlation analysis provides direct observation of higher order molecular complex formation in the confocal volume, which also gives information of

the number of molecules up to three [34]. However, multicolor labeling is usually labor demanding and limited by the difficulties in choosing fluorophores resulted from the laser excitation band and the emission spectrum spacing of fluorophores.

Furthermore, there are also several non-correlation methods to investigate the stoichiometry of fluorescent molecules in solution. One of them is called photon counting histogram (PCH). It is based on the photon counting histogram of fluorescent molecules diffusing in solution and uses the information of additional fluorescence intensity broadening from a Poisson distribution to extract the average number of molecules within the excitation volume and the molecular brightness [23, 24, 95]. A similar approach, called fluorescence intensity distribution analysis (FIDA), was developed independently and is able to determine the concentrations and specific brightness values of a number of individual fluorescent species in solution [36, 35, 61]. Furthermore, a method called burst analysis spectroscopy was used to measure the population distributions of fluorescent molecules at very low sample concentrations [64]. All methods have been successfully applied to biological systems [94, 24, 95]. Another method, named N & B analysis, is based on moment-analysis and can map the number of molecules and brightness out of video frames from standard imaging instruments [28]. It has been used to detect molecular complexes and measure their stoichiometry in living cells from simultaneous fluctuations of the fluorescence intensity in two image channels [29].

Most of these methods depend on the fluorescent brightness or fluctuation of fluorescent brightness of mobile part of the fluorophores, therefore molecular brightness calibration is needed in one way or another. Moreover, they only derived the average distribution of fluorophores. At the same time, photon antibunching is also able to determine the stoichiometry of fluorescent molecules. It has advantages over its counterparts because photon antibunching does not need calibration and is suitable for fluorescent molecules both immobilized on surfaces and diffusing in solution [79, 92]. However, there are some disadvantages of photon antibunching as well. For example, it requires highly photostable fluorophores to collect enough simultaneous photon pairs. The near-field interactions between fluorophores may

change the behavior of fluorescence emission and make it difficult to interpret the observations with photon antibunching [82].

1.3 Outline of the rest of the dissertation

In this dissertation, a method based on four detection channels and a new mathematical model are described to determine the stoichiometry of fluorescent molecules followed by verification of simulations and experiments. The outline of the rest of this thesis is as follows.

The theoretical background is briefly described in Chapter 2 *Theory*, such as the basics of fluorescence and photon antibunching as well as TCSPC (Time correlated single photon counting). Afterwards, in Chapter 3 *Instruments and Materials*, the materials which were used in this work are listed, as well as the instruments with their specifications and the software for data acquisition and analysis. Furthermore, in Chapter 4 *Experiments and Results*, a mathematical model based on multiple detection channels is introduced and verified by both simulations and experiments. In the end, in Chapter 5 *Discussion and outlook*, are discussions about the model as well as the simulations and experiments. The potential applications of the method in real biological systems, further developments of the method and photon antibunching are also explored in this chapter.

2 Theory

2.1 Basics of fluorescence

Luminescence is an emission of ultraviolet, visible or infrared light from species at electronically excited state. Fluorescence and phosphorescence are two particular cases of luminescence, which has been intensively studied and applied to many fields. Fluorescence was first brought into scientific realm in 1952 by Sir G. G. Stokes [84]. The fluorescence process happens nearly instantly after the absorption of the excitation light due to the relatively short time delay between light absorption and emission, ranging usually from nanoseconds to microseconds in duration. While phosphorescence refers to the emission very much delayed after the excitation process, and the delay can be in the range of milliseconds to minutes or even hours.

2.1.1 Absorption and emission Processes

According to quantum theory, the nature of light includes the notion of wave-particle duality. The particle of light is called photon, which has an energy, E, proportional to its frequency, f, by

$$E = hf = \frac{hc}{\lambda} \tag{2.1}$$

where h is Planck's constant, λ is the wavelength and c is the speed of light. The energy of a photon can be absorbed by a molecule via electronic transition. An electronic transition is the promotion of an electron from a lower energy ground state to a higher energy excited

state. The atoms in a molecule have some degrees of freedom to rotate and vibrate with respect to each other. The vibrational and rotational energy is also quantized and can be considered as being packed on top of each electronic level. The electron at the ground state

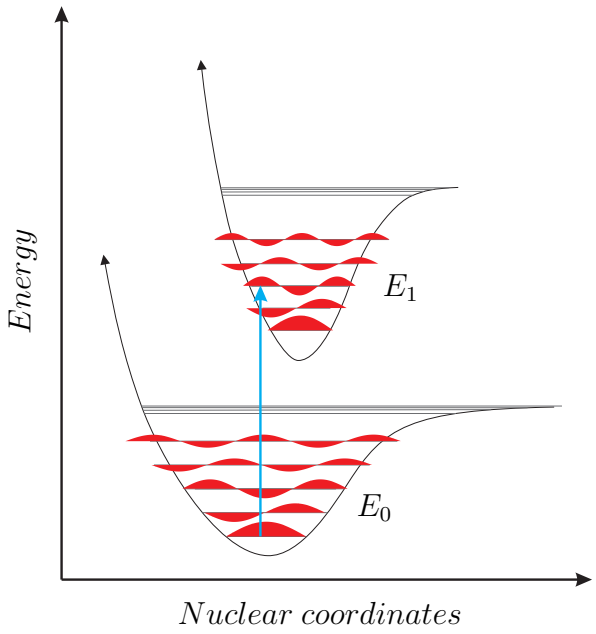

Figure 2.1: A scheme of Fronck-Condon principle: Potential energy diagrams with vertical transitions.

can be excited by any kind of perturbation having energy corresponding to the energy gap between ground and excited states. The absorption of photons is the only concern of the electronic excitation in this thesis. The probability of electronic transition mainly depends on Frank-Condon principle: an electronic transition is most likely to occur without changes in the positions of the nuclei in the molecular and its environments. The transition is called vertical transition, as illustrated by the diagram of Fig.2.1. It is important to note that absorption happens very fast ($\sim 10^{-15}s$) in comparison with all other processes.

The absorption of UV/visible radiation in organic molecules is confined to certain functional groups (chromophores) which contain valence electrons with low excitation energy. The absorption spectrum of molecules which contain such chromophores is complex due to the superposition of rotational and vibrational transitions on the electronic transitions.

Therefore, the absorption band is more continuous than being composed of many peaks.

Absorption $A(\lambda)$ in ensemble measurements can be described and quantified by the Lambert-Beer law:

$$A(\lambda) = \log_{10} \frac{I_0}{I(\lambda)} = \varepsilon(\lambda) c d \tag{2.2}$$

where λ is the wavelength of the incident light, ε is the molar absorption coefficient (commonly expressed in $L\ mol^{-1} cm^{-1}$), c is the molar concentration(in $mol\ L^{-1}$) of absorbing species and d is the absorption path length (in cm).

It is noteworthy that there are several conditions to keep Lambert-Beer law valid. First, the absorbers should be independently to each other. Second, the medium has to be homogeneously distributed and scatter of the radiation is ignorable or can be corrected by an additional baseline measurement. Third, the incident radiation should be parallel and the ideal incident radiation should be monochromatic, or have, in practical, at least a wavelength width that is narrower than the absorbing transition. Finally, the incidence radiation should not cause optical saturation, which will deplete the molecules at lower energy level and lead to nonlinear effect, or even possibly give rise to stimulated emission. Attention has to be paid to obtain reliable absorptions.

A Jablonski diagram as shown in Fig.2.2 is convenient to visualize the possible processes of an electronic transition. After excitation, the molecule quickly relaxes to the lowest vibrational level of the first excited state $S_{1,\nu=0}$, ν is the vibrational quantum number, by vibrational relaxation (VR), which gives the energy to the surrounding molecules by collision. Illuminated with higher energy photon than that for excitation to S_1, the molecule can be excited to other excited states S_n ($n > 1$) and again quickly relax to $S_{1,\nu=0}$ via internal conversion (IC) and VR non-radiatively. Therefore, all the processes before the molecule go to $S_{1,\nu=0}$ have no memory effect to the processes afterwards because IC and VR are much faster than other processes. The time scales of these processes are listed in Tab. 2.1.

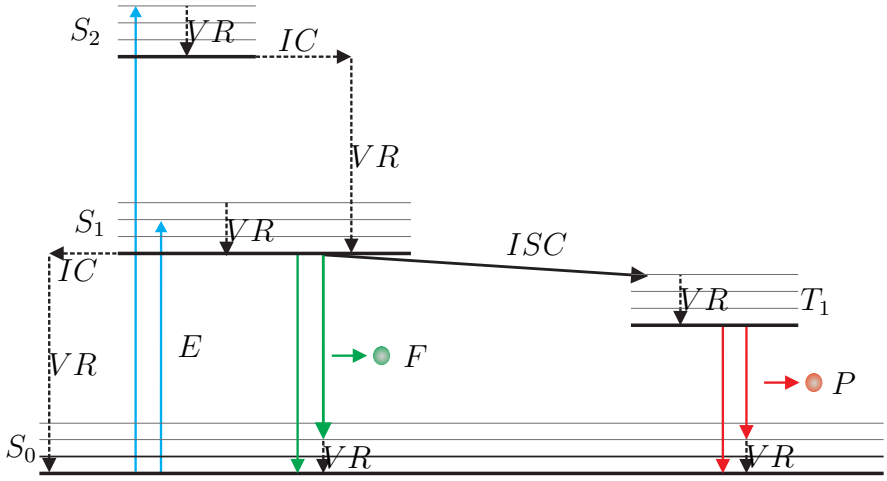

Figure 2.2: Jablonski diagram: Photophysical pathways to the ground state after an electronic excitation E are shown schematically. S_0, $S1$, $S2$ and $T1$ are singlet ground state, singlet first and second excited state and triplet first, respectively.

The molecule in $S_{1,\nu=0}$ relaxes to ground state S_0 either radiatively or non-radiatively. Radiative de-excitation with emission of photons is called fluorescence. Mostly fluorescence emission occurs from S_1 to S_0 and, therefore, its characteristics do not depend on the excitation wavelength.

When non-radiative de-excitation from the triplet state T_1 is predominant over radiative de-excitation, the phenomenon of phosphorescence occurs. Normally the transition from T_1 to S_0 is spin forbidden and the radiative rate is very low. Only under certain conditions, such as at low temperatures or in a rigid medium, phosphorescence can be observed due to the long triplet state lifetime.

There are also other possible processes, such as triplet-triplet annihilation and delayed fluorescence. Details about these processes are described in many textbooks.

Table 2.1: Characteristic times of absorption and relaxation [84].

Characteristic times	
absorption	$10^{-15}s$
vibrational relaxation	$10^{-12} - 10^{-10}s$
lifetime of the excited state S_1	$10^{-10} - 10^{-7}s$
intersystem crossing	$10^{-10} - 10^{-8}s$
internal conversion	$10^{-11} - 10^{-9}s$
lifetime of the excited state T_1	$10^{-6} - 1s$

2.1.2 Excited state lifetime

Excited molecule can return to ground state either radiatively or non-radiatively. So the excited state decay rate constant k is the sum of radiative (k_r) and non-radiative (k_{nf}) decay rate.

$$k = k_r + k_{nr} \tag{2.3}$$

Given a dilute solution of a fluorescent species A with concentration of [A] (in $mol\ L^{-1}$), a very short pulse of light at time 0 excites a certain number of molecules A to the S_1 state and then return to S_0, radiatively or non-radiatively. The excited state decay rate is proportional to the populations of the molecules in $S_{1,\nu=0}$. The kinetics is expressed by the following differential equation:

$$-\frac{d[^1A^*]}{dt} = (k_r + k_{nr})[^1A^*] \tag{2.4}$$

Integration of this equation yields the concentration of excited molecules $[^1A^*]$. If $[^1A^*]_0$ is the concentration of excited molecules at time 0, integration leads to

$$[^1A^*] = [^1A^*]_0 \exp(-\frac{t}{\tau_s}) \tag{2.5}$$

where τ_s is the lifetime of excited state S_1. τ_s is given by

$$\tau_s = \frac{1}{k_r + k_{nr}} \tag{2.6}$$

The fluorescence intensity i_f is given by

$$i_f(t) = k_r[^1A^*] = k_r[^1A^*]_0 \exp(-\frac{t}{\tau_s}) \tag{2.7}$$

$i_f(t)$ is the δ-pulse response of the system, decreases single-exponentially.

In any practical measurements of fluorescence intensity, the measured intensity I_f is proportional to i_f and the proportional factor depends on instrumental conditions.

2.1.3 Quantum yields

The fluorescence quantum yield Φ_f is defined as the fraction of excited molecules that return to the ground state S_1 by emission of fluorescence photons:

$$\Phi_f = \frac{k_r}{k_r + k_{nr}} = k_r\tau_s \tag{2.8}$$

In other words, the fluorescence quantum yield is the ratio of the number of emitted photons to the number of absorbed photons. The number of absorbed photon at time t is

$$\frac{i_f(t)}{[^1A^*]_0} = k_r \exp(-\frac{t}{\tau_s}) \tag{2.9}$$

after integration of Eq. 2.9, the quantum yield Φ_f is given by

$$\Phi_f = k_r\tau_s = \frac{1}{[^1A^*]_0} \int_0^\infty i_f(t)dt \tag{2.10}$$

The quantum yield of intersystem crossing and phosphorescence can be defined in the same way.

Therefore, any factor which influences the radiative or non-radiative rates will change the lifetime and quantum yield of the fluorophore, such as dynamic collision quenching, near-field dipole-dipole interaction and intersystem crossing. It is known that dioxygen is a

quencher of fluorescence. Oxygen quenching is a collision process and controlled by diffusion. Therefore, the effects of oxygen on quantum yields and lifetimes depend on the compound and the medium. Fluorophores with long lifetime are particularly sensitive to the presence of oxygen.

2.2 Time-correlated single photon counting

The most comprehensive description about time-correlated single photon counting (TCSPC) is that of D.V.O'Connor and D. Phillips, "Time-Correlated Single Photon Counting", in 1984 [31]. TCSPC was mainly used to record fluorescence decay function at the beginning. Because of its amazing sensitivity and excellent time resolution TCSPC has been adapted by many techniques, such as Fluorescence Lifetime Imaging (FLIM) of living cell [11] and single molecule detection (SMD) in standard confocal microscope or laser scanning confocal microscope. TCSPC is also the main SMD platform of the work in this thesis.

In TCSPC, pulsed laser provides both the excitation source and the clock. The detection of TCSPC is based on single-photon sensitive detectors. Photon arrival times are recorded according to the laser pulses. Therefore, the histogram of the photon arrival times with respect to the corresponding excitation laser pulses reflects the decay of fluorescent excited state. Because a single-photon sensitive detector has a dead time much longer than the lifetime of fluorescent excited state, it can not detect two or more photons in one laser cycle. Therefore, very low excitation intensity is a must and the fluorescence intensity is low enough that the probability for detecting more than one photon in one laser cycle is negligible (rare events). The principle is shown in Fig.2.3. Most of the laser cycles contain no photons, and others have one photon pulse. The arrival times of photons in the laser cycles is measured. After many laser cycles, a large number of photons are collected and a histogram of photon arrival times is built. If the photons come from a fluorophore, the histogram corresponds to the measured fluorescence intensity decay I_F and the lifetime of excited state S_1 can be deduced from it.

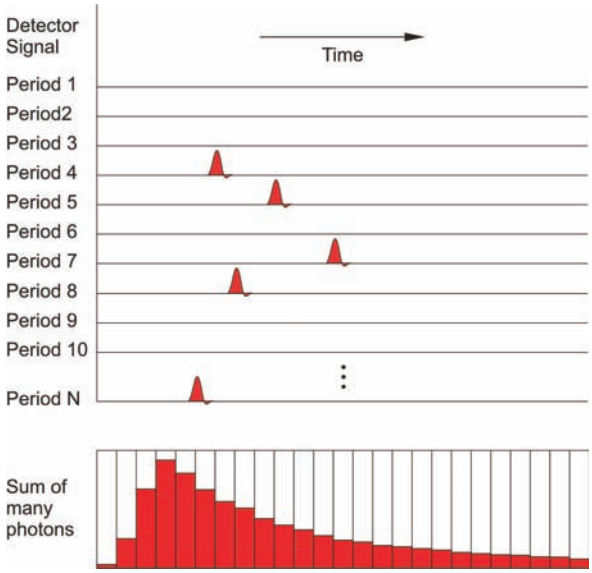

Figure 2.3: A scheme of TCSPC [9]: Photon arrival times are recorded according to the laser pulses which excite the fluorophore. An histogram of the photon arrival times is built based on many photon arrival times and reflect the decay of the excited states.

It is also possible to record the photon arrival times in a stream, store them to a hard disk of a PC and reconstruct the histogram off-line or perform further analysis. Facilitated with multiple synchronized parallel channels [88], TCSPC can achieve a photon count rate as high as 20 MHz, which has many advanced applications including counting molecules by photon antibunching.

2.3 Photon antibunching

Photon antibunching is a quantum phenomenon that the emission of one photon reduces the probability that another photon is emitted immediately afterward. In this work, photon antibunching of resonance fluorescence is concerned.

In 1956, Robert Hanbury Brown and Richard Twiss used two detectors, with one to start and the other to stop the measurements, to measure the time interval between photons from

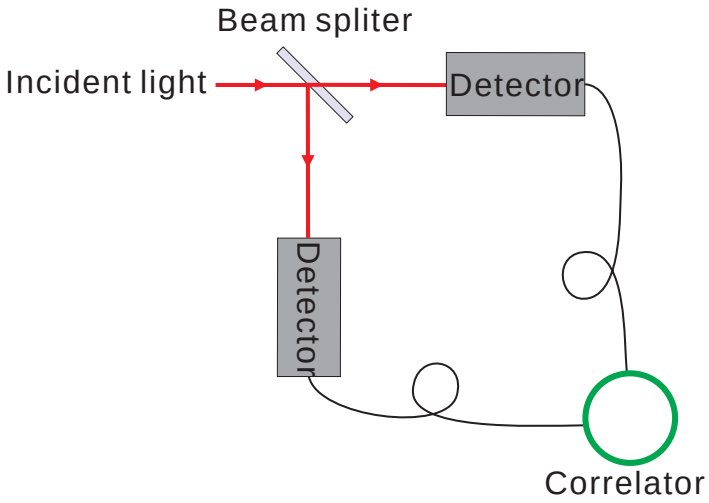

Figure 2.4: A scheme of a Hanbury Brown-Twiss setup: An incident light beam is split to two by a beam splitter. Two beams reach two detectors. One of the detector starts the measurement and the other stops.

a thermal light source as shown in Fig. 2.4 [65]. They observed that the detected photons 'bunched', which means if a photon was detected at one of the detectors, there is also a high chance to observe another photon at the other detector at the same time. However, if the light source is a single two-level quantum emitter, such as an atom or a fluorescent molecule, anti-correlated photon detection will be observed. That is, photon detection at one detector results in a less chance of detecting another photon at the other detector. The distribution of the photon number in a time window is a sub-Poissonian, which means the variance of the photon number distribution is less than the mean of it. This sub-Poisson distribution of photon intensity generally refers to photon antibunching. Photon antibunching in resonant fluorescence was first observed by Kimbel *et al* in 1970's. [39].

The physics of photon antibunching is easy to understand: if a two-level atom or molecule emits a photon at time 0, it is impossible for it to emit another one immediately, even it is excited right after. The reason is that a photon emitter has to stay in the excited state for a while and the next photon can only be emitted when the photon emitter returns to ground state from excited state. The average dwell time in excited state is the lifetime of excited state. However, if there are many photon emitters in the light source, the emission

of a second photon is not excluded by the first one any more and the photon emission follows Poisson distribution. Therefore, photon antibunching is considered as evidence that the source of the radiation field is a single quantum system, while the lack of photon antibunching is a sign of multiple photon emitters in the light source.

Photon bunching or antibunching can be interpreted by the correlation function or the joint probability density of two successive photon emissions.

The normalized intensity correlation function of a radiation field can be expressed [39] as

$$\lambda(\tau) = \frac{\langle \Delta I(t) \Delta I(t+\tau) \rangle}{\langle I(t) \rangle \langle I(t+\tau) \rangle} \tag{2.11}$$

where t is the time, τ is the lag time, $I(t)$ is the instantaneous intensity of the radiation emission and $\Delta I \equiv I - \langle I \rangle$, $\langle \cdot \rangle$ means temporal average.

The joint probability density of photon detection is given by

$$P_2(t,t+\tau) = \alpha^2 \langle I(t) I(t+\tau) \rangle \tag{2.12}$$

where α is a constant characterizing the efficiency of the detector. Eq. 2.12 can be reexpressed by substituting $\langle I(t) I(t+\tau) \rangle$ with $\lambda(\tau)$ in Eq.2.11

$$P_2(t,t+\tau) = \alpha^2 \langle I(t) \rangle \langle I(t+\tau) \rangle [1 + \lambda(\tau)] \tag{2.13}$$

When $\lambda(\tau) \leq \lambda(0)$ and $\lambda(\infty) = 0$, photon emission bunches, such as in thermal source of light. It indicates that the two-fold detection probability is greater for time intervals τ near zero than for long intervals. On the other hand, when the correlation at zero lag time $\lambda(0) < 0$, and the joint probability density $P_2(t,t+\tau)$ increases with time interval τ increasing when $\tau = 0$. This initial rise in $\lambda(\tau)$ or $P_2(t,t+\tau)$ is defined as photon antibunching [39].

Photon antibunching of individual quantum systems has been first measured by fluorescent correlation function at room temperature with CW laser excitation [62] and pulsed laser illumination [81, 47]. All of the measurement have been performed in Hanbury Brown-Twiss setups [67].

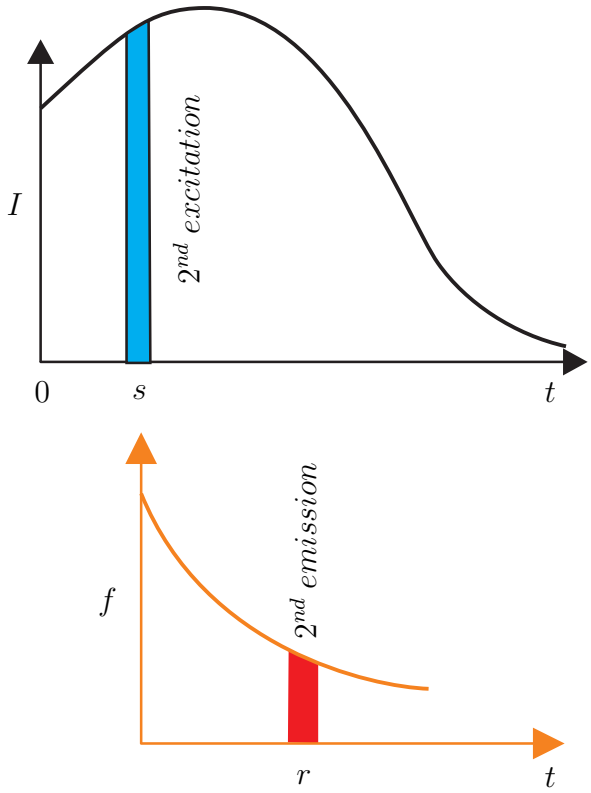

Figure 2.5: Correlation of two photon emission: A photon emission happens at time 0. A laser with intensity I excites the fluorophore at time s to excited state and results in a second photon emission at time r. The correlation of two photon emission is the probability of a second photon emission after the first photon emission by a lag time τ. f is the fluorescence intensity.

A Hanbury Brown-Twiss setup measures the correlation of two photon emissions. Given a single photon emitter is illuminated by a laser with intensity $I(t)$ (in $photon/cm^2/s$) and a photon is emitted at time 0. The photon emitter is excited for the second time at time s and emit another photon at time r, where $s < r$, as shown in Fig. 2.5. The probability density to

excite the molecule at time s is given by

$$A_2 = \sigma I(s) \tag{2.14}$$

where σ is the molecule absorption cross section (in $cm^2/molecule$).

The probability density of the second photon emission is given by fluorescence intensity i_f (Eq. 2.7) as

$$E_2 = \sigma I(s) k_r \exp(-\frac{t-s}{\tau_s}) \tag{2.15}$$

where k_r is the radiative decay rate in s^{-1}. Integration of the probability density, the correlation function $G^{(2)}(\tau)$ is yield as

$$G^{(2)}(\tau) = \int_0^\tau \sigma I(s) k_r \exp(-\frac{t-s}{\tau_s}) ds \tag{2.16}$$

If the incident radiation flux $I(t)$ is constant, then $G^{(2)}(\tau)$ is given by

$$G^{(2)}(\tau) = \sigma I k_r \tau_s (1 - \exp(-\frac{\tau}{\tau_s})) \tag{2.17}$$

By noticing that quantum yield $\Phi_f = k_r \tau_s$, $G^{(2)}(\tau)$ can also be expressed as

$$G^{(2)}(\tau) = \sigma \Phi_f I (1 - \exp(-\frac{\tau}{\tau_s})) \tag{2.18}$$

An example of the $G^{(2)}(\tau)$ is given in Fig. 2.6. The initial rising at time 0 is a typical photon antibunching trend, which is a single exponential increase. It is worth to note that the chance to observe two photon emissions at time 0 from a single photon emission is zero. In practice, $G^{(2)}(0)$ will not be exact but close to zero because of background photons. As long as the number of photon emitter increases, the photon antibunching curve will not be perfect. If the number of photon emitters is huge, such as in ensemble experiments, $G^{(2)}(\tau)$ will be flat at time 0. Moreover, the characteristic time of the exponential increasing is exactly the excited state lifetime τ_s of the photon emitter. Consequently photon antibunching curve provides a way to determine the lifetime τ_s.

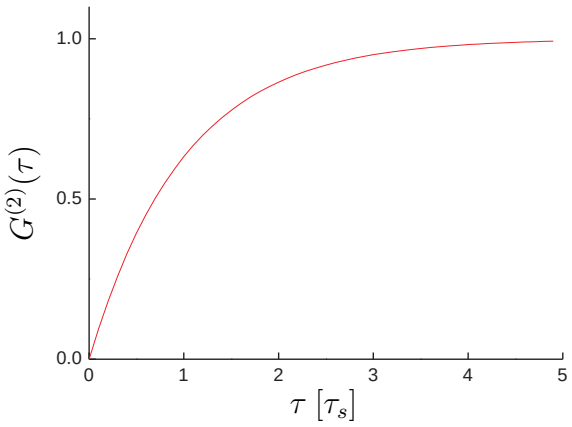

Figure 2.6: Normalized correlation function $G^{(2)}(\tau)$ according to $G^{(2)}(\infty)$. $G^{(2)}(\tau)$ increases from zero to $G^{(2)}(\infty)$ as τ increases from 0 to ∞.

The measured correlation function is proportional to $G^{(2)}(\tau)$ and is given by

$$\widetilde{G}^{(2)} = \alpha^2 G^{(2)}(\tau) = \alpha^2 \sigma \Phi_f I(1 - \exp(-\frac{\tau}{\tau_s})) \tag{2.19}$$

where α is the collection efficiency of the instruments. In the case of continuous wave (CW) laser, the laser intensity is constant and therefore Eq. 2.19 describes the photon antibunching curve of single photon emitters.

When it comes to pulsed laser excitation, specifically with very short pulse duration, in TCSPC, the interpretation of photon antibunching changes. Suppose that the full width at half maximum (FWHM) of the laser pulse is around $100\ ps$, while the excited-state lifetime of a fluorophore is normally several nanosecond. It means, the duration of the laser pulse is much shorter than the excited-state lifetime of a fluorophore. Once the fluorophore is excited by a laser pulse, it takes about several nanosecond in average for the fluorophore to return to ground state radiatively or non-radiatively. Therefore, there is almost no chance for the fluorophore to be excited again by the same laser pulse. The adaption of photon antibunching in TCSPC with pulsed laser results in that only one photon can be emitted by one fluorophore

in a laser cycle.

2.4 Basics of Single Molecule Spectroscopy

The far field imaging of a single molecule is one of the greatest challenges for chemists and biologists due to the diffraction limit described by Abbe in 1873:

$$\delta_x = \frac{0.61\lambda}{NA} \tag{2.20}$$

where λ is the wavelength of the light and NA is the numerical aperture of the optical element. This limit tells that the best resolution can be reached is about 200 nm under the best conditions, with a wavelength of 400 nm and a high numerical aperture of 1.4. However, the size of single molecules is far below this limit. Therefore, when it comes to single molecule spectroscopy (SMS) and single molecule detection (SMD), only the photons from single molecules are detected and the behavior of the single molecules is indirectly reported. For the same reason, the concentration of the molecules has to be low enough that only one molecule is under investigation at a time, which leads to the concentration of $10^{-10} Mol$ with a probe volume of $10\ fL$ in a confocal microscope with high numerical aperture of 1.4.

Several types of microscopes can achieve severe background reduction, high detection efficiency and spatially selective imaging necessary for single molecules detection, such as near-field microscopy, confocal microscopy, wide-field microscopy and total internal reflection microscopy as shown in Fig. 2.7.

Near-field microscopy, as in Fig. 2.7 (1), has the smallest illumination volume, but has also the disadvantage of invasion to the sample, which may introduce some interactions between the probe tips with samples. Confocal microscopy, as in Fig. 2.7(2), is a standard far field microscope and allows to use sample chambers for liquid immersion. Both near-field microscopy and confocal microscope can only probe a very small volume once,

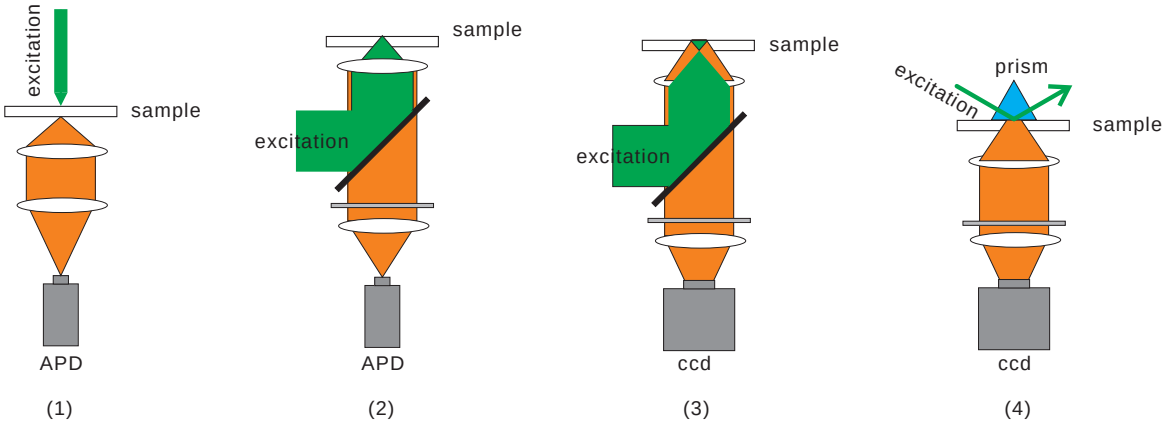

Figure 2.7: Microscopes for SMS: (1) near-field microscopy, (2) confocal microscopy, (3) wide-field microscopy and (4) total internal reflection microscopy.

and scanning is a must for large area detection. Wide-field microscopy, as in Fig. 2.7(3), and total internal reflection fluorescence microscopy (TIRF), as in Fig. 2.7(4), are both for imaging samples, therefore many molecules can be examined at the same time. TIRF microscopy only illuminates a small depth of volume of the sample, and consequently suppress the background dramatically, which is a shortcoming of wide-field microscopy. But both wide-field microscopy and TIRF microscopy have a lower time resolution due to the time response of CCD (Charge-coupled device) cameras (sub-second) comparing to that of Avalanche Photodiodes (APD) (sub-microsecond).

In order to achieve as large as possible signal to noise ratio, many considerations have to be taken. Some of them are listed: reducing background by proper aligning optical beam path and using right filters, choosing the right laser for excitation to get better fluorescence intensity, selecting fluorophores with high photostability and quantum yield, using photostabilizing agents to prolong the life time of fluorophores and so on. In this work, fluorescence single molecule spectroscopy at room temperature is mainly concerned and a confocal microscope with APD as detectors is the main platform for SMD.

2.4.1 Counting molecules with 2 detectors

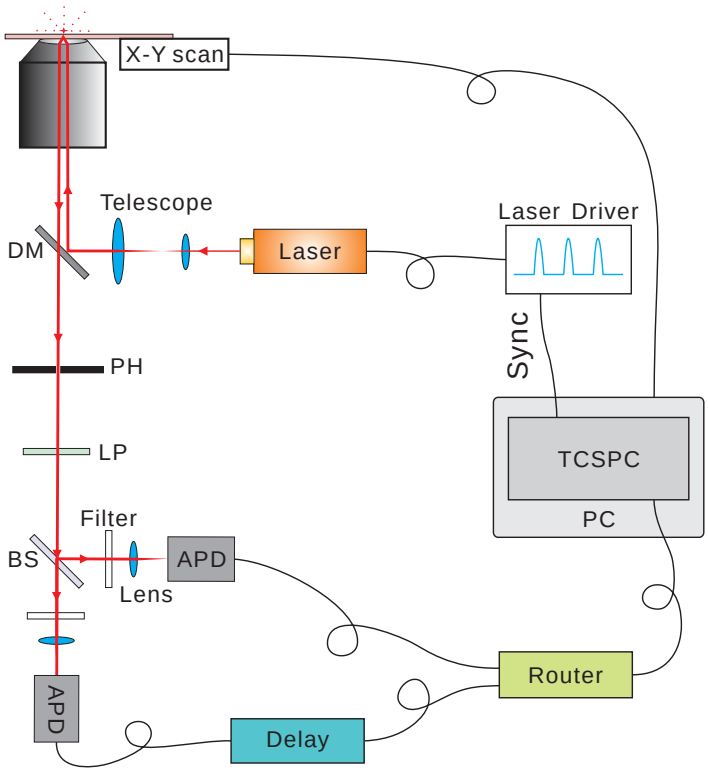

Figure 2.8: Two-detector TCSPC setup: A pulse laser diode is driven by a laser driver, the incident laser is directed into the objective by a dichroic mirror (DM) after passing a telescope. The fluorescence from a sample is selected by the same dichroic mirror and selected again by a pinhole (PH). After passing a long pass filter (LP), the detection beam is split to two by a 50:50 beam splitter (BS) and focus to two independent APDs after filtered by band-pass filters. One of the two detection channel signal is delayed and both the signals are passed to TCSPC card via a router. A piezo stage is controlled by the same PC in which the TCSPC card is plugged.

Confocal microscopy has been used to determine the stoichiometry of fluorescent molecules immobilized on surfaces [92] or diffusing in solution [79] by photon antibunching. Both of the groups use pulsed diode laser system and two detection channels. As an example, the confocal microscope equipped with a TCSPC card used by Weston *et al* will be described.

As shown in the Fig. 2.8, one of the detection signals is delayed to retrieve the photon arrival

times in the past. Therefore, the simultaneous photon pairs introduced by the same laser pulse can be distinguished with one TCSPC card by comparing the signal arrival times. The coincidence ratio $N_c/\bar{N}_L$ of simultaneously detected photon pairs N_c to non-simultaneously detected photon pairs $\bar{N}_L$ indicates the number of fluorophores n.

$$\frac{N_c}{\bar{N}_L} = 1 - \frac{1}{n} \tag{2.21}$$

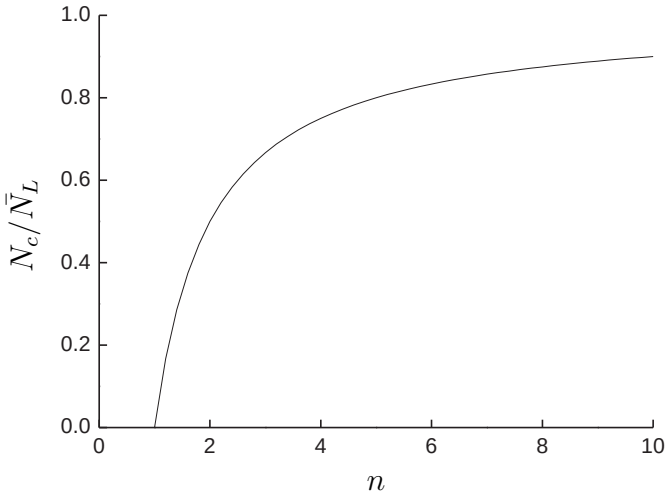

Figure 2.9: Coincidence ratio of simultaneously detected photon pairs N_c to non-simultaneously detected photon pairs $\bar{N}_L$: As the number of molecule n increases, the coincidence ratio $N_c/\bar{N}_L$ saturates and converges to 1.

However, $N_c/\bar{N}_L$ saturates very fast when n increases as shown in Fig. 2.9. Consequently, the counting of fluorescent molecules by photon antibunching is limited to about 3 molecules [92].

2.5 Basics of DNA

Deoxyribonucleic acid (DNA) plays an essential role in all living organisms and some viruses for it carries genetic information and transmits them from generation to generation. Therefore it is one of the best studied biomolecules.

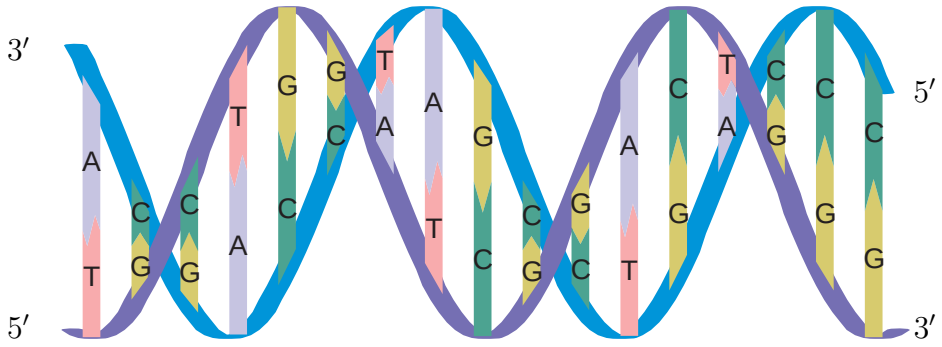

Figure 2.10: A scheme of dsDNA Helix: dsDNA has two single strands, which are anti-parallel (one is from 5’ to 3’ while the other from 3’ to 5’). Each strand is composed by a sequence of four bases: adenine (A), cytosine (C), guanine (G) and thymine (T). Two strands are associated by base paring: A only bonds to T and C bonds to G by hydrogen bonds.

DNA contains two long polymers of monomeric units called nucleotides. A nucleotide consists of three parts: sugar, base and phosphate. The sugar and phospate are joined by ester bond and form the backbone of each strand. In dsDNA, the two strands are anti-parallel, which means they are in opposite directions to each other. They entwine like vines, in the shape of a double helix as shown in Fig. 2.10. There are four different types of nucleotides with different base attached to the sugar. The four bases are adenine (A), cytosine (C), guanine (G) and thymine (T). These four bases are attached to the sugar/phosphate to form the complete nucleotide [20]. Each type of base on one strand forms hydrogen bonds with just one type of base on the other strand. This is called complementary base pairing. A bonds only to T, and C bonds only to G. This arrangement of two nucleotides binding together across the double helix is called a base pair. It is the sequence of these four bases in the strands that encodes information. The DNA chain is 2.2 to 2.6 nm wide, and one nucleotide

unit is 0.33 nm long [48]. Although dsDNA can be twisted by DNA supercoiling into more complex structure, the dsDNA helix is rather rigid as long as the number of base pair is not high. Therefore, the coupling of oligonucleotides (DNA) is well defined and the length of it with a certain number of base pairs can be predicted very well. Furthermore, the coupling of dsDNA provides a reliable way to bring molecules together with a defined distance. It is even possible to build complex structures with designed DNA sequences [6].

Moreover, the concentration of double-strand DNA (dsDNA) in solution can be determined by the UV absorption at 260 nm. The extinction coefficient depends on the occurrences of the four different bases. On the other hand, DNA denaturation, also called DNA melting, is the process that dsDNA unwinds and separates into single strands by breaking the hydrogen bonding between the bases. The melting temperature is the temperature at which half of the DNA strands are in the double-helical state and half are in the ”random-coil” states. The melting temperature depends on both the length of the molecule, the specific nucleotide sequence and concentration of salts.

Table 2.2: Unified nearest-neighbor parameters for DNA/DNA duplexes [72].

Nearest-neighbor sequence (5’-3’/5’-3’)	ΔH $kcal/mol$	ΔS $cal/(mol \cdot K)$
AA/TT	-7.9	-22.2
AG/CT	-7.8	-21.0
AT/AT	-7.2	-20.4
AC/GT	-8.4	-22.4
GA/TC	-8.2	-22.2
GG/CC	-8.0	-19.9
GC/GC	-9.8	-24.4
TA/TA	-7.2	-21.3
TG/CA	-8.5	-22.7
CG/CG	-10.6	-27.2
Terminal A-T base pair	2.3	4.1
Terminal G-C base pair	0.1	-2.8

There are several empirical formulas to calculate the melting point. One of the methods,

called nearest-neighbor method, is frequently used to predict melting temperatures of nucleic acid duplexes. The nearest-neighbor model accounts for this by considering adjacent bases along the backbone two-at-a-time [72]. The melting temperature can be expressed as

$$T_m = \frac{\Delta H}{\Delta S + R \ln(C_1 - \frac{C_2}{2})} \tag{2.22}$$

where ΔH is the standard enthalpy and ΔS is the standard entropy for formation of the duplex from two single strands (The standard enthalpy and entropy of nearest-neighbor pases are listed in Tab. 2.2), C_1 is the initial concentration of the single strand that is in excess (usually probe, primer), C_2 is the initial concentration of the complementary strand that is limiting (usually target), R is the universal gas constant $\left(1.987 \frac{\text{cal}}{\text{mol}\cdot\text{K}}\right)$.

Standard enthalpies and entropies are negative for the annealing reaction and are assumed to be temperature independent. If $C_1 >> C_2$ then C_2 can be neglected and Eq. refeq:meltingtemp becomes simpler.

As a conclusion, it is easy to build molecule origami from DNA with well defined structure by designing the sequences. Therefore, DNA is chosen to calibrate photon antibunching method by providing molecule complexes with a certain number of fluorophores and a well defined structure.

3 Materials and Methods

3.1 Material and chemicals

All chemicals were from Sigma-Aldrich GmbH (Munich, Germany) and Fluka GmbH (Ebersdorf) if not specified. All aqueous solutions and buffers were prepared with double distilled water with less than 5 ppb impurities. The phosphate buffered saline (PBS) buffer with PH 7.4 was from Sigma-Aldrich to 10 mM prepared in water (containing 130 mM sodium chloride and 2.7 mM potassium chloride).

Lab-Tek Chambers with 8 wells, consisting of 8 wells with a cover slide at the bottom and plastic walls, was ordered from Nunc GmbH (Wiesbaden, Germany) and used for immobilization of the double strand DNA (dsDNA). The volume of each well was around 800 μL.

The dyes used in this work were Atto 620 and Atto 647N (NHS-Ester) from ATTO-TEC GmbH (Siegen, Germany)

3.2 dsDNA with multiple labels

A dsDNA with multiple labels was constructed for single-molecule experiments in this work. The scheme of the dsDNA is shown in Fig.3.1. Both the ssDNA strands were ordered from IBA GmbH (Goettingen, Germany). The DNA sequences were follows

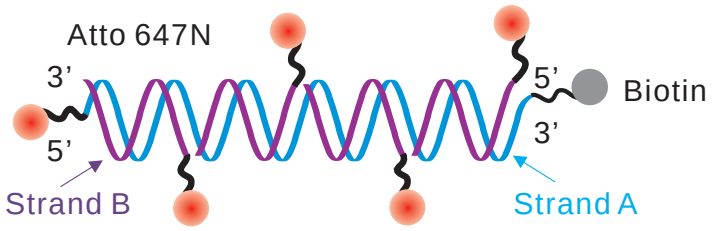

Figure 3.1: A scheme of dsDNA with multiple labels.

- Strand A (92 baspairs or bps): 5'-/Atto 647N/ AAC GAG GAG GAC CCC TAT CCC AAA ACG AGG AGG ACC CCT ATC CCA AAA CGA GGA GGA CCC CTA TCC CAA AAC GAG GAG GAC CCC TAT CCC AA /biotin/-3'

- Strand B (23 bps): 5'-/Atto 647N/ TTG GGA TAG GGG TCC TCC TCG TT-3'

The long strand A was composed of four repeated 23 bps sequences. The short strand B was the complementary sequence of the repeated sequence in strand A. The strand A was biotinylated at one end (3') and modified with NH2 group, which was coupled with an Atto-647N at the other end (5'). The sequence B was labeled with an Atto-647N at one end (5'). The dsDNA was annealed as follows. The strand A and the strand B were mixed in 1:4 molar ratio in a PBS buffer. The mixture was cooled on a heating block from $90°C$ to room temperature over the course of $3 \sim 4$ hours. After hybridization the final dsDNA had around 5 fluorophores.

The following protocol was used for conjugation of oligonucleotides to dyes: One equivalent of activated fluorescence dye was dissolved in anhydrous DMF in a concentration of 2 mg/ml and a 5 fold excess of oligonucleotide in 0.05 M carbonate buffer (pH 9.0) was added. After 16 h stirring at room temperature, the product was purified by HPLC (High performance liquid chromatography) using a linear solvent gradient of 0.75 M acetonitrile in 0.1 M aqueous triethylammonium acetate.

For purification of oligonucleotide an HPLC from Agilent (Waldbronn, Germany) series 1100 was used. It consisted of the degasser G1322A, the binary pump G1312A, the diode array detector G1315A and the fluorescence detector G1321A. Separation was achieved by a reverse-phase column, length 250 mm with an inner diameter of 4 mm from Knauer (Berlin, Germany), which was packed with ODS Hypersil size 5 μm.

3.3 Immobilization of dsDNA

We use several method to prepare surfaces for immobilization of dsDNAs. All immobilizing procedures involve a glass surface cleaning step with incubation of the glass surface or Labtek chambers with $0.2 - 1\%$ hydrofluoric acid (HF) for 1 minute followed by a washing step with ddH2o.

- APS coating surface

  DNAs was immobilized onto amino-propyl silane (APS) modified glass surface [15]. The immobilization is considered to be a non-covalently process. A DNA oligonucleotides interacts with the polycationic surface by coulombic attraction. The surface was prepared as: After cleaned with diluted HF, the cover slides were incubated with APS solution (2.5% in mathanol) for 5 minutes. After another washing step, the colver slide was dry by nitrogen gas flow or compressed air flow.

- Poly-L Lysine coating slides

  Another unspecific immobilization of dsDNA with Poly-L Lysine (PLL) modified surface. The surface coated with PLL, which was charged and could associated dsDNA due to negative charges of dsDNA backbone by coulomb interaction. After Labtek champers were cleaned by diluted HF, 250 μL 20% extran (in dd water) was used to incubate the surface for 15 minutes. After another washing step, let the chambers dry in the air for at least 30 minutes. Afterwards the chambers were incubated with poly-l-lysine (70 mug/ml in water) solution for 15 minutes and washed again with water.

The chambers have to be dry before using for unspecific immobilizing samples.

- BSA-biotin surface

  A specific immobilization of dsDNAs was to use streptavidin-biotin system. Following chemicals were used for surface preparation:

  – Biotin-modified bovine serum albumin, (biotin-BSA) (Sigma-Aldrich)

  – Bovine serum albumin (BSA) (Fluka, Neu-Ulm, Germany)

  – Streptavidin (Roche Diagnostics, Mannheim Germany)

  The association of biotin and streptavidin is specific and strong, which makes streptavidin-biotin a widely used linker of biomolecules. Cleaned Labtek chambers were incubated with a mixture solution of biotin-BSA and BSA for 2 hours. The mixing ratio of biotin-BSA and BSA was chosen the way that the density of biotin-BSA on the surface was low enough to separate from each other to be resolved by single molecule detection instruments. Then after washing 3 times with PBS buffer, a solution of streptavidin ($0.5\ mg/ml$ in PBS, $10\ mM$) was incubated with the surface for 20 minutes. After washing 5 times with PBS buffer, the surface was ready for immobilizing biotin-dsDNAs.

3.4 Photostabilizing ROXS system

A photostabilizing system, called reducing-oxidizing system (ROXS), was used to prolong the illuminating time of the dye, Atto 647N [86]. The components and their concentrations of ROXS are listed in Tab. 3.1.

Because Oxygen has to be excluded, the Labtek chamber was sealed with Parafilm (Pechiney Plastics Packaging Company, Chicago, USA) on the top of the well. Care is needed to avoid sealing air bubbles in the chamber.

Table 3.1: ROXS system [86].

Chemicals	Concentration
Methylviologen	$1\ mM$
Trolox	$2\ mM$
TCEP	$1\ mM$
Catalase	$8000\ units$
Glucose	$0.22\ M$
Glucose oxidase	$80\ units$
4x PBS-buffer	

3.5 Single molecule detection instrument

The scheme of the setup to perform the single-molecule experiment is shown in Fig.3.2. Basically it is a confocal microscope in TCSPC mode and all the photon arrival times are collected by the data acquisition card and stored to the hard disk of a PC.

The excitation source is a pulsed diode laser with a wavelength of 635 nm and a maximum excitation power of 2 mW (PicoQuant GmbH, Berlin, Germany). The diameter of the laser beam is adjusted to 0.5 cm by a telescope. The parallel laser beam is cleaned by a narrow-band excitation filter (HQ 635/10, AHF analysentechnik AG, Tubingen, Germany) and then directed into the side port of an inverted microscope (Axiovert s100 TV, Carl Zeiss, Jena, Germany). Within the microscope, the beam is reflected by a dichroic mirror (F53-488, AHF analysentechnik AG) and focused to a spot by an oil-immersion objective (planApo 100 x, NA 1.4, Olympus Corp., Japan). The fluorescence is collected by the same objective and goes through the same dichroic mirror. By a convex lens, the fluorescence is focused and then selected by a pinhole (120 mm in diameter). By another lens the fluorescence turns into parallel beam. After a long pass filter (F43-651, AHF analysentechnik AG), the fluorescence beam is divided into two by a 1:1 beam splitter (BS016, Thorlabs, Munich, Germany) and then converged by two identical lens (f 20cm). Finally the two fluorescence beams are divided into four by two 1:1 beam splitters, filtered by four identical band-pass filters (F42-019, AHF analysentechnik AG) and then focused to the active areas of four

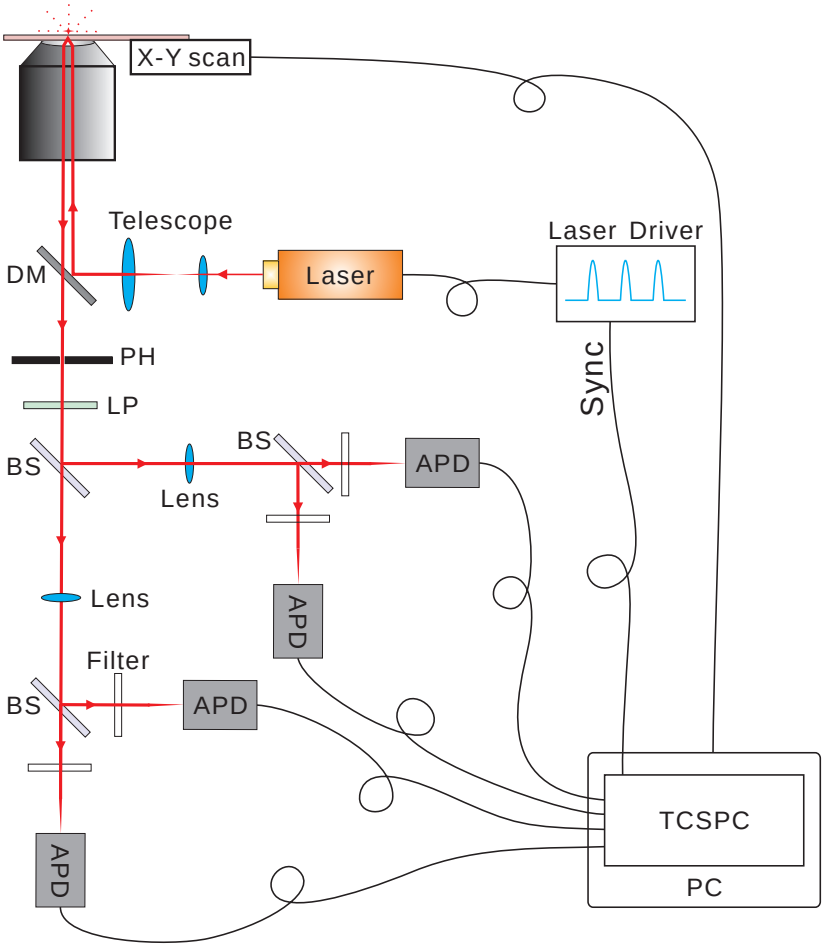

Figure 3.2: A scheme of a single molecule setup: A pulse laser diode is driven by a laser driver. After passing a telescope and a cleaning filter, the incident laser is directed into the objective by a dichroic mirror (DM). The fluorescence from a sample is selected by the same dichroic mirror and selected again by a pinhole (PH). After passing a long pass filter (LP), the detection beam is split into two and again split into four equally by three 50:50 beam splitters (BS) and focus to four identical APDs after passing band-pass filters. Four identical cables connect the signals from APDs to four independent TCSPC cards. A piezo stage is controlled by the same PC in which the TCSPC card is plugged.

identical APDs. The signal from APD is connected either to the four independent channels of PC plug-in TCSPC card, (SPC134, Becker & Hickl GmbH, Berlin, Germany) or to a USB interface HydraHarp 400 (PicoQuant GmbH, Berlin, Germany).

The SPC 134 card is used for 2D surface raster scanning and performs in first-in-first-out (FIFO) mode [9]. Data acquisition software is home-made, called DAQLineScan. The HydraHarp 400 is used for fluorescence intensity trace recording in Time-Tagged Time-Resolved (TTTR) mode [87]. Both the data acquisition instruments are synchronized with the laser driver. The surface scan is also controlled by the same data acquisition PC via a scanning stage.

3.5.1 Parameters of some instruments

1. The excitation source

   A pulse laser diode with a wavelength of 635 nm is used as the excitation source. The laser is driven by a pulse driver with a repetition rate tunable in steps between 10 and 80 MHz (PDL800B, Picoquant GmbH, Berlin). For photon antibunching experiments, 10 MHz was the working repetition rate. 10 MHz was chosen in order to keep photon counting rate low because the photon counting rate is proportional to the repetition rate. The maximum laser power is 30 mW. The pulse width of the laser beam is about 50 ps FWHM, which depends on the excitation intensity. The exact emission wavelength is dependent on the temperature. Therefore, an excitation cleaning filter is needed in the setup.

2. Detectors

   The detection of fluorescence was carried out by four single photon sensitive avalanche photodiodes (APD), SPCM-AQR-14 from Perkin Elmer (MA, USA). The diameter of the active surfaces of the APD is approximately $180\ \mu m$. The detection efficiency is above 50% in the spectral range between 550 and 800 nm and maximally $\sim 65\%$ at around 700 nm as shown in Fig. 3.3. In addition, they have a very low electronic dark

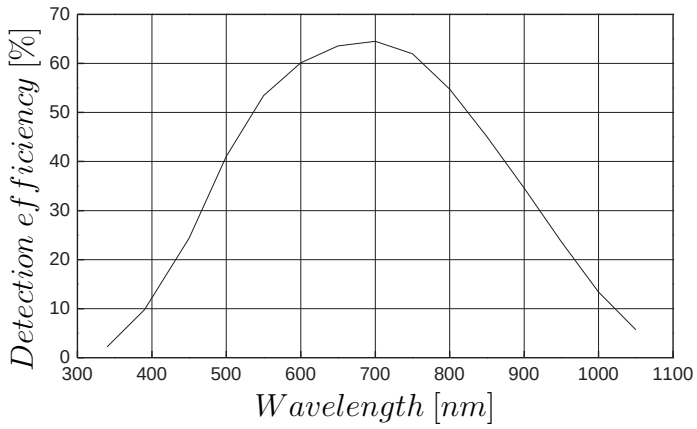

Figure 3.3: Photon detection efficiency of an APD of the AQR-14 series at different wavelengths: The maximum detection efficiency is reached around 700 nm, in the region where the excitation wavelength of the red dye used in this work.

count rate of less than 100 Hz. The dead time of the APDs is about 50 ns and the output counting rate before saturation is higher than 1MHz.

3. The scanning stage

   The x-y scanning and positioning is achieved by a three-dimensional piezoelectric scanner P561.3CL (Physik Instrumente (PI), Karlsruhe, Germany) together with a capacitive sensor control unit E509.C3A (Physik Instrumente) and a three-channel amplifier E-503.00 (Physik Instrumente). The active area is 100 microns x 100 microns x 20 microns and controlled by a linear voltage increase of 1 V / micron. The voltage is provided by an analog output board (NI PCI-6713, National Instruments, Austin, TX, USA) along with home made software coded in LabView 7.1 (National Instruments). The software also synchronizes the stage scanning and data acquisition.

4. Data acquisition cards

   The PC plug-in card SPC 134 from Becker & Hickl GmbH (Berlin, Germany) for Time-Correlated Single-Photon Counting (TCSPC) is in charge of the fluorescence intensity measurements during the 2D raster scanning. A USB interface Hydraharp 400 (Picoquant, Berlin, Germany) is responsible for the photon arrival time recording.

Some of the configurations of the two TCSPC data acquisition cards are listed in Tab. 3.2.

Table 3.2: Specification of SPC 134 and Hydraharp 400.

Specifications	SPC 134	HydraHarp 400
Dead time	125 $ns(FIFO)$	80 ns
Time resolution	5 ps	1 ps
PC interface	PCI	$USB2.0$
Maximum count rate per channel	5 MHz	$12.5MHz$

The reason for using two different TCSPC data acquisition cards is that the four channels of SPC 134 were not well synchronized at that time. Therefore, HydraHarp 400 was used to record photon events for photon antibunching experiments. The SPC 134 was used for 2D scanning due to the software compatibility.

Four independent detection channels were used and synchronized with each other. In order to test the synchronization of the four cards, an experiment was performed as shown in Fig. 3.4. The signal from an APD is split into four (by three T shape signal

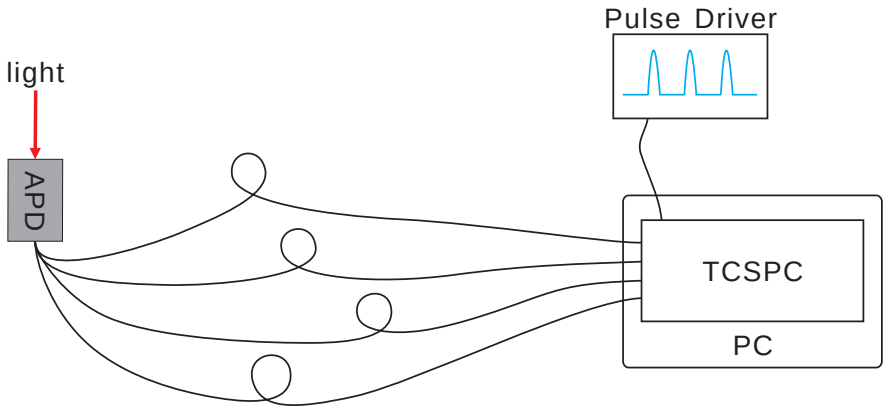

Figure 3.4: Synchronization examination: The synchronization of the four independent TCSPC cards of SPC 134 is examined. The signal from one APD is split to four and directed to the four cards of SPC 134 by four identical cables. A pulse driver provides a time clock for TCSPC cards.

splitters). By using four cables with the same length, four data acquisition cards should have the same signals in theory if they are synchronized. In practice, the correspondent signals (photon arrival times) fall into the same pulse cycle. The small deviations of signals within the same pulse cycle are due to the differences in the length of the cables, the jitter of the signals as well as the different response of the signal splitters.

5. Filters and mirrors

   The transmission of the dichroic mirror and the filters used in the experiment is shown in Fig. 3.5. The combination of the dichroic mirror (black), long pass filter (red) and

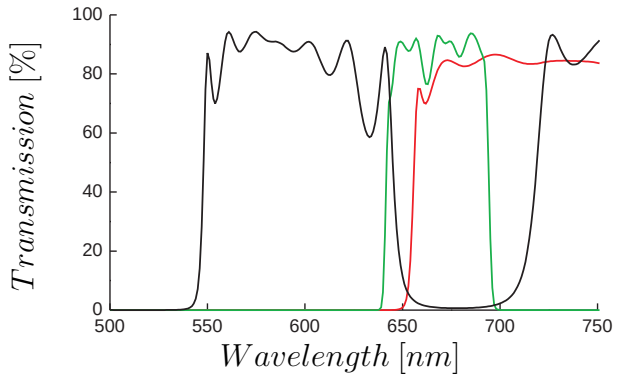

Figure 3.5: Transmission of dichroic mirror and filters: Transmission of dichroic mirror (black), long pass filter (red), band pass filter (green).

   the band pass (green) filter secures the separation of the excitation laser light and the fluorescence from the dye Atto 647N .

3.6 Data acquisition and analysis

- Data acquisition:

  2D raster scanning were controlled by a home-made software, called DAQLineScan, developed in Labview 7.1 (National Instruments) and C. The scanning were synchronized with data acquisition of SPC134 by DAQLineScan. A 2D fluorescence

intensity picture was generated on-line during the scan. The interested spots were picked automatically or manually right after the scanning. Then the stage moved the spots into the laser focus one by one and the spots were illuminated until all the fluorophores were bleached. During the illumination, a HydraHarp 400 recorded the photon arrival times for off-line analysis.

- Data analysis:

  In single-molecule experiments, photon arrival times were recorded by HydraHarp 400, which generated a data format of ”ht3” in TTTR mode. The ”ht3” format was converted into a ”std” format, which is a 64-bit-integer stream of photon arrival times, by a home-made C program. A routine coded in Matlab was used to visualize the fluorescence intensity trace. The interface with an example trace is shown as in Fig. 3.6. A photon counting trace is displayed in both sub-windows (upper and

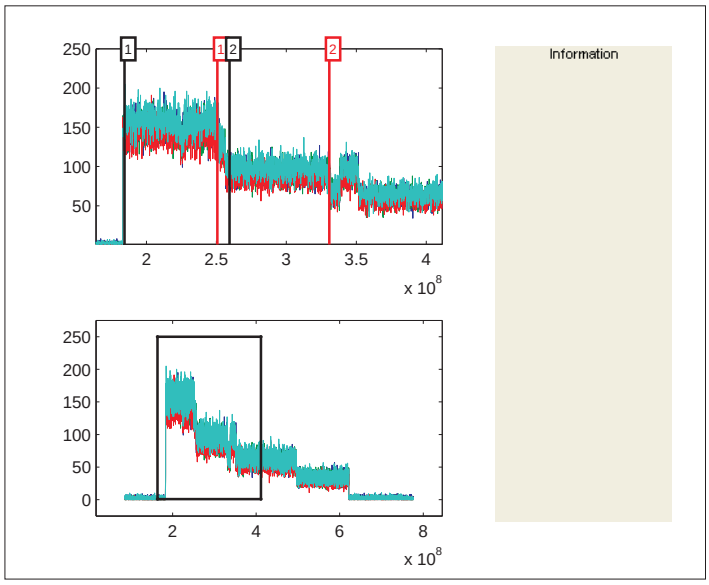

Figure 3.6: Data analysis software interface: Two sub-windows on the left display the fluorescence intensity trace. The upper window is the zoom of the black box in the lower one.

lower). The upper one is the zoom image of the solid square in the lower one. Users can select time intervals in the upper window manually for further operations. Two

types of coincidence analysis are developed. One is based on stable fluorescence intensity (no-bleaching) and the other takes photobleaching into account. After time intervals are selected, the coincidence analysis can be performed as the user requests. Background correction can be included if the background photon probability is given. In order to accelerate the calculations, coincidence photon events are found and stored in standalone files by a C code routine. Therefore, the Matlab program can access the coincidence photons without processing the photon streams, which accelerates the calculations dramatically.

All the figures in this dissertation are generated by Origin 8SR4 (OriginLab, Massachusetts, USA), Coredraw X4 (Corel, Ottawa, Canada) and Matlab (The Mathworks, Natick, MA,USA).

3.7 Fluorescence absorption and emission

The absorption spectra and emission spectra were recorded in quartz glass ultra-micro cuvettes (104.002F Suprasil, Hellma, Muellheim, Germany).

UV/Vis absorption spectra were recorded by a Carey 500 Scan spectrometer Varian (Darmstadt, Germany). The emission spectra were recorded with a Cary Eclipse 500 fluorescence spectrometer from Varian (Darmstadt, Germany). The excitation source is a xenon flash lamp. The emission spectra were corrected with respect to the intensity of the xenon flash light at different wavelength automatically. The temperature in the sample holder was precisely electro-thermally controlled.

The fluorescence lifetime was determined by the FluoTime 100 (PicoQuant, Berlin, Germany). The excitation light source is pulsed LEDs (Light Emitting Diode) with wavelengths of 370, 450, 500 or 600 nm. The pulse duration is around 300 ps and the repetition rate is

tunable from 2.5 MHz to 40 MHz stepwise by a pulse driver (PDL-800B, PicoQuant). The detector is an integrated photomultiplier tubes (PMT) with a time-correlated single photon counting (TCSPC, TimeHarp 200, PicoQuant) card. The lifetime fitting is performed with software, called FluoFit, from PicoQuant.

4 Experiments and Results

Noninvasive far-field single-molecule fluorescence spectroscopy (SMFS) is frequently used to characterize biomolecules in their physiological conditions. The stoichiometry of biomolecules, as one of the important concerns of biologists, has intensively been explored by SMFS. One of the methods is to analyze correlated photon pairs with photon antibunching, a quantum nature of photon emission as described in Section 2.3. Although several attempts have been performed to quantify the number of molecules by photon antibunching, the counting was limited to about three molecules [92, 79].

In this part, a theoretical model, called coincidence analysis, is presented to extend the molecule-counting ability. The model is based on the adaption of photon antibunching in a system with the combination of time-correlated single photon counting (TCSPC, see Section 2.2) and pulsed laser excitation. The feasibility of the model is evaluated by simulations and experiments.

4.1 Mathematical model

TCSPC combined with picosecond-pulsed laser excitation provides a way to record photon arrival times precisely (picosend resolution). Recently an unprecedented high single photon counting rate (more than 10 MHz) has been reached by using multiple detection channels in TCSPC [88]. It enables a large number of photons from a pool with more than ten fluorophores to be collected in a short time (seconds to minutes).

Furthermore, multiple-photon-detection events in one laser cycle can be recorded with the help of multiple-detection-channel TCSPC and picosecond-pulsed laser excitation. A stochastic model is built to estimate the number of fluorophores out of the occurrences of multiple-photon-detection events.

4.1.1 Assumptions

In order to establish a theoretical model, some assumptions are needed:

1. A single fluorophore can emit at most one photon per laser cycle by using picosecond-pulsed laser excitation

   Photon antibunching is the phenomenon that one fluorophore can only emit one photon at one time (see Section 2.3). However, it has different representations according to the excitation schemes. On one hand, photon antibunching of resonance fluorescence induced by CW lasers can be quantified by the second order correlation of fluorescence intensity. The correlation function from a single fluorophore is described by Eq. 2.19 and the initial rising at 0 lag time (Fig. 2.6) is the indication of photon antibunching. The characteristic time of the initial rising is the excited-state lifetime of the fluorophore. On the other hand, when it comes to pulsed laser excitation, the interpretation of photon antibunching results in that only one photon can be emit by one fluorophore in one laser cycle. An analytical approach helps to understand it.

   Assume that only one photon emitter is illuminated by an incident laser with a flux intensity of $I(t)$ (in $photon/cm^2/s$, $I(t)$ is a function of time t). Two successive photon emissions are of interest and the initial state of the photon emitter is the electronic ground state S_0.

   Suppose the photon emitter is excited at time r and u, $r < u$ (Fig. 4.1). Af-

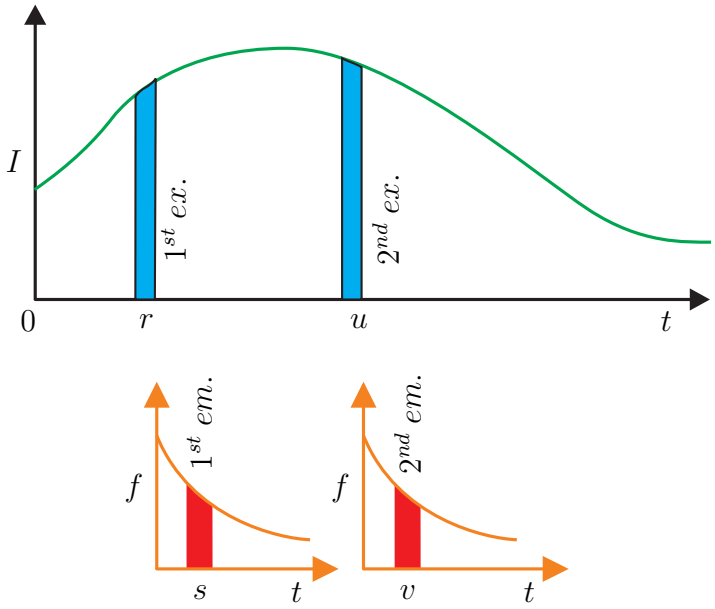

Figure 4.1: Probability of two photon emission: A laser with intensity I excite the fluorophore twice at time r and u. Both excitation result in photon emission at time s and v, respectively. f is the fluorescence intensity and t is time.

ter each excitation photon emission occurs at time s and v, $r < s < u < v$. The probability of observing two (or more) photon emissions can be expressed analytically.

The probability density of the first excitation is

$$A_1 = \sigma I(r) \tag{4.1}$$

where σ is the absorption cross section of the photon emitter (in cm^2).

The probability density of the first photon emission depends on the probability of excitation of the photon emitter and can be given by

$$E_1 = A_1 k_r \exp(-\frac{s-r}{\tau_s}) \tag{4.2}$$

where k_r is the radiative decay rate (in s^{-1}).

Similarly, the second photon emission probability density can be expressed as

$$E_2 = A_2 k_r \exp(-\frac{v-u}{\tau_s}) \tag{4.3}$$

where $A_2 = \sigma I(u)$ is the probability density of the second excitation.
By combining and integrating the two photon emission probability density, the probability of observing two photon emissions is given by

$$P^{(2)} = \int_0^\infty \int_r^\infty \int_s^\infty \int_u^\infty A_1 k_r \exp(-\frac{s-r}{\tau_s}) A_2 k_r \exp(-\frac{v-u}{\tau_s}) dv du ds dr \tag{4.4}$$

Since the integration of v can be expressed explicitly and A_1 and A_2 have specific expressions, the probability becomes

$$P^{(2)} = \sigma^2 k_r^2 \tau_s \int_0^\infty \int_r^\infty \int_s^\infty I(r) I(u) \exp(-\frac{s-r}{\tau_s}) du ds dr \tag{4.5}$$

If the laser intensity $I(t)$ is a rectangular function with a width of a and is given by

$$I(t) = \begin{cases} l, \text{ if } 0 \leq t \leq a \\ 0, \text{ if } t > a \end{cases} \tag{4.6}$$

By specifying $I(t)$ and noticing $\Phi_f = k_f \tau_s$, the probability of two photon emissions can be turned into

$$P^{(2)} = \sigma^2 \Phi_f^2 l^2 \tau_s^2 (1 - \frac{a}{\tau_s} + \frac{1}{2}(\frac{a}{\tau_s})^2 - exp(-\frac{a}{\tau_s})) \tag{4.7}$$

Assume that the duration a of the laser intensity is much smaller than the excited lifetime τ_s of the photon emitter, Eq. 4.7 can be further simplified by Taylor expansion as

$$P^{(2)} = (\sigma \Phi_f l a)^2 (a/\tau_s)/6 = (\sigma \Phi_f E)^2 (a/\tau_s)/6 \tag{4.8}$$

where $E = la$ is the power of the laser.

Meanwhile, the probability of at least one photon detection events is given by integrating Eq. 4.2 as

$$P^{(1)} = \int_0^\infty \int_r^\infty \sigma I(r) k_r \exp(-\frac{s-r}{\tau_s}) ds dr = \sigma \Phi_f l a = \sigma \Phi_f E \tag{4.9}$$

In practice, the incident laser pulses can roughly be considered as rectangular function. The width of the rectangular function a can be approximately given by the FWHM of the laser pulses. The measured probabilities of one or more photon emission and two or more photon emission are given by

$$\widetilde{P}^{(1)} = \alpha P^{(1)} = \alpha \sigma \Phi_f E \tag{4.10}$$

$$\widetilde{P}^{(2)} = \alpha^2 P^{(2)} = (\alpha \sigma \Phi_f E)^2 (a/\tau_s)/6 \tag{4.11}$$

where α is the proportional coefficient given by instrument conditions. However, because photon detection is a rare events with low probability ($<< 1$), the probability of one- or more-photon detection can be considered as that of one-photon detection and the probability of two- or more-photon detection as that of two-photon detection. Furthermore, in normal experimental conditions, $\alpha \sigma \Phi_f E << 1$. Thus, the probability of two-photon detection is much lower than one-photon detection.

In addition, if the power of a laser pulse E is fixed, the probability to observe one-photon-detection events remains constant. However, the shorter the width of the laser pulses, the lower the chance to observe two-photon-detection events. Due to the low probability of two-photon-detection events, it is reasonable to consider that only one photon can be emitted from one photon emitter in TCSPC, if the duration of the laser pulse is much shorter than the excited-state lifetime of the photon emitter. This assumption plays an important role in counting molecules by photon antibunching in TCSPC.

It is worth to note that the probability to detect two photons from the same fluorophore is not absolute zero although it is considerably low. There remains a tiny chance to observe a single fluorophore being excited more than once. For example, if the first fluorescent emission occurs so fast that the laser pulse still has significant intensity to excite the fluorophore again and finally a second photon is emitted. Thus, two photons may both be detected by chance. However, the influence of more than one-photon-detection from a single molecule in one laser cycle is low enough that it does not influence the calculation in this work.

2. Constant fluorescence intensity

   The second assumption is that all fluorophores have the same fluorescence intensity and are stable during the observation time, such as no blinking. That is to say, there is no intensity fluctuation, bleaching, cross talk among fluorophores and so on.

   The laser intensity irradiated on all molecules stays constant since the lateral size of the laser focus profile is around $300\ nm$ for red laser excitation and much larger than a typical molecular complex. For example the size of a ribosome is about $20 - 30$ nanometers. If the fluorophores are all located near the center of the Gaussian profile of the laser focus, where the intensity of the laser has less deviation in a rather large spatial area and is high enough to excite the fluorophores efficiently, all fluorophores experience the same laser intensity.

   Furthermore, the variation in quantum yield of different fluorophores is neglected. Suppose the local environments of all molecules stay nearly the same and dynamic collisional quenching is the same for all fluorophores; near-field dipole-dipole interaction and resonance energy transfer, such as heterotransfer and homotransfer, are not significant; internal conversion and intersystem crossing remain small enough. Therefore, the fluorescence intensities of all the molecules are the same during

the observation time. Although this assumption is not always true in reality, it is convenient to model a rather simple system first and study the influences of all the conditions later. The influences of variations of fluorescent brightness among fluorophores is also discussed in Section 4.2.5 and 4.3.5.

3. Background emission

   Background emission in confocal microscope is mainly from Rayleigh and Raman scattering of solvent and noise from electronic device, e.g., dark count current of detectors. However, signal to background ratio in SMD, which is around 10 or even higher, is good and it is reasonable to ignore the background to simplify the problem as much as possible at the beginning and take it into account as a given condition later.

4.1.2 Coincidence probabilities

In order to identify correlated photons in TCSPC scheme, it is necessary to resolve two or more photons in one laser cycle. Technically, current single-photon sensitive detectors can only detect one photon in one laser cycle since the dead times of the detectors and data acquisition cards are comparable to one laser cycle. For example, the dead time of an APD is about $50\ ns$ and that of single photon counting (SPC) card is about $100\ ns$, while a laser period is $25 - 100\ ns$ in my case. That is, if more than one photon arrive at the same detector in one laser cycle, only the first photon is counted and the others are ignored. A straightforward solution is to use two or more independent detection channels to resolve very close photon arrival times [67, 39, 81]. We also use TCSPC scheme to record the arrival times of photons with multiple detection channels as shown in figure 4.2. The probabilities of multiple-photon-detection in one laser cycle can be evaluated by taking into account the number and molecular brightness of fluorophores.

- Coincidence probabilities without background

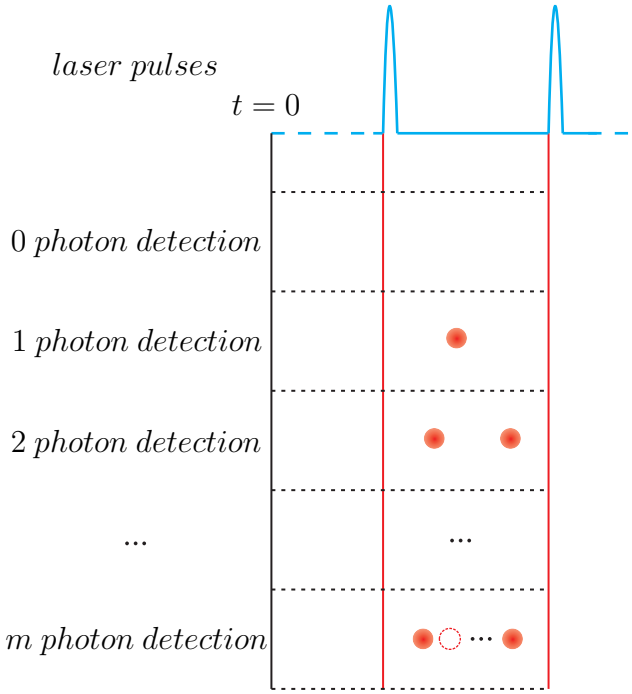

Figure 4.2: Multiple-photon-detection events: $0, 1,..., m$-photon-detection events in one laser cycle can be resolved with m independent detection channels.

Assume that a detection beam path is equally divided into m pathways and the fluorescent photons are collected by m identical synchronized detection channels. By comparing the arrival times, the occurrences of multiple-photon-detection events in one laser cycle can be determined as shown in figure 4.3.

The probability to observe i photon detection events by i detectors in one laser cycle is a multinomial distribution, $i = 0, 1, ..., m$, and can be calculated as

$$P(n,p,i) = \begin{pmatrix} m \\ i \end{pmatrix} ((i \cdot \frac{p}{m} + 1 - p)^n - \sum_{k=0,k>0}^{i-1} \frac{\begin{pmatrix} i \\ k \end{pmatrix}}{\begin{pmatrix} m \\ k \end{pmatrix}} P(n,p,k)) \tag{4.12}$$

where n is the number of fluorophores under investigation, p is normalized molecular brightness according to the frequency of the laser pulses shed on the fluorophores, or

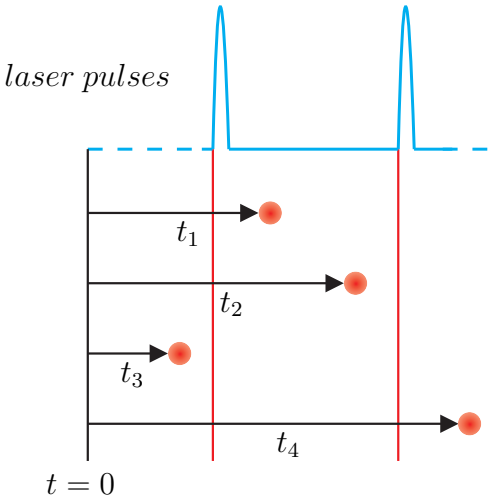

Figure 4.3: Comparison of photon arrival times: It can be determined by comparing the photon arrival times and synchronization signal whether two photons arrive in the same laser cycle. The first two photon arrive at time t_1 and t_2 and fall in the same laser cycle and are recorded as a two-photon-detection events. As a comparison, the third and fourth photons at t_3 and t_4 fall in different laser cycles and do not contribute on multiple-photon-detection events. Red dots are photon arrival events.

specifically the probability that a single fluorophore emits a photon and consequently the photon is detected in one laser cycle. It means, $p = g\sigma\Phi_f E$, where g accounts for the collection efficiency of a TCSPC setup, σ is the molecular absorption cross-section, Φ_f is the fluorescence quantum yield, E is the power of a laser pulse. These probabilities $P(n,p,i)$ are also called coincidence probabilities for convenience in this dissertation.

The first part of Eq. 4.12 is the probability for no more than i photon detection events while the second recursive part is the sum of all probabilities for less than i photon detection events. An explicit expression can be deduced by specifying the number of detection channels m.

If the number of detection channels $m = 2$, Eq. 4.12 can be explicitly expressed as

$$\begin{aligned} P_2\,(n,p,i=0) &= (1-p)^n \\ P_2\,(n,p,i=1) &= -2(1-p)^n + 2(-\tfrac{1}{2}p+1)^n \\ P_2\,(n,p,i=2) &= 1+(1-p)^n - 2(-\tfrac{1}{2}p+1)^n \end{aligned} \tag{4.13}$$

Since, in reality, the normalized molecular brightness p is low, the first noticeable degree approximation of Eq. 4.13 with respect of p is a very good approximation of the probabilities, shown as

$$\begin{aligned} P_2\,(n,p,i=0) &= 1+o(1) \\ P_2\,(n,p,i=1) &= np+o(p) \\ P_2\,(n,p,i=2) &= \tfrac{1}{4}n(n-1)p^2+o(p^2) \end{aligned} \tag{4.14}$$

According to Eq. 4.14 the one-photon-detection probability is almost proportional to the normalized molecular brightness p and the number of fluorophores n, and the probability for two-photon-detection events is proportional to $n(n-1)$ and p^2.

Simple relations of coincidence probabilities with the number of fluorophores n and normalized molecular brightness p can be deduced from Eq. 4.14

$$n = \frac{P_2(n,p,i=1)^2}{P_2(n,p,i=1)^2 - 4P_2(n,p,i=2)} \tag{4.15}$$

$$p = P_2(n,p,i=1) - \frac{4P_2(n,p,i=2)}{P_2(n,p,i=1)} \tag{4.16}$$

When $np << 1$, Eq. 4.15 provides a good estimation of n. It gives the same result as Weston *et al.* explained in 2002 [92]. When np is not low, the equations 4.14 are not valid anymore and the relation between one- and two-photon-detection probabilities with the number of fluorophore is not as simple as described in Eq. 4.15. Additionally, Eq. 4.16 also provides a simple way to estimate p with the combination

of $P_2(n,p,i=1)$ and $P_2(n,p,i=2)$.

By extending the number of detection channels m to 4, Eq. 4.12 turns into

$$\begin{aligned}
P_4(n,p,i=0) &= (1-p)^n \\
P_4(n,p,i=1) &= -4(1-p)^n + 4(-\frac{3}{4}p+1)^n \\
P_4(n,p,i=2) &= 6(1-p)^n - 12(-\frac{3}{4}p+1)^n \\
&\quad + 6(-\frac{1}{2}p+1)^n \\
P_4(n,p,i=3) &= -4(1-p)^n + 12(-\frac{3}{4}p+1)^n \\
&\quad - 12(-\frac{1}{2}p+1)^n + 4(-\frac{1}{4}p+1)^n \\
P_4(n,p,i=4) &= 1 + (1-p)^n - 4(-\frac{3}{4}p+1)^n \\
&\quad + 6(-\frac{1}{2}p+1)^n - 4(-\frac{1}{4}p+1)^n
\end{aligned} \tag{4.17}$$

As the number of detection channels m increases, a higher number of photon detection events can be resolved. Although the expression becomes much more complicated as Eq. 4.17, it is still convenient to perform the calculation by computer routines.

The first noticeable degree approximation of equations 4.17 with respect of p is given by

$$\begin{aligned}
P_4(n,p,i=0) &= 1 + o(1) \\
P_4(n,p,i=1) &= np + o(p) \\
P_4(n,p,i=2) &= \frac{3}{8}n(n-1)p^2 + o(p^2) \\
P_4(n,p,i=3) &= \frac{1}{16}n(n-1)(n-2)p^3 + o(p^3) \\
P_4(n,p,i=4) &= \frac{1}{256}n(n-1)(n-2)(n-3)p^4 + o(p^4)
\end{aligned} \tag{4.18}$$

As long as $np << 1$, these formulas provide good approximations of the coincidence probabilities. the According to these formulas the one-photon-detection probability

is nearly proportional to n and p and two-photon-detection probability is to p^2 as in the two detection channel scheme. Furthermore, the three- and four-photon-detection probabilities are proportional to the third and fourth power of p respectively.

By using the same manipulations as applied on two detection channel calculations, the relations of one- and two-photon-detection probabilities with the number of fluorophores n and normalized molecular brightness p can be approximately approached by

$$n = \frac{3P_4(n,p,i=1)^2}{3P_4(n,p,i=1)^2 - 8P_4(n,p,i=2)} \tag{4.19}$$

$$p = P_4(n,p,i=1) - \frac{8P_4(n,p,i=2)}{3P_4(n,p,i=1)} \tag{4.20}$$

It is worth to emphasis that the condition of equations 4.19 and 4.20 is that $np << 1$.

Assume that the same fluorophores are measured by both two- and four-detection-channel setups and the fluorescence detection is optimized by careful selection of objectives, detector aperture dimensions, dichroic mirror and emission filters, as well as precise alignment of optical beam pathway, the fluorescence collection efficiency remains the same in both setups. Therefore, the normalized molecular brightness p of a single fluorophore remains constant in both platforms. A direct conclusion from Eq. 4.14 and Eq. 4.18 is that two- and four-detection-channel setups can collect the same number of one-photon-detection events in the same period. By comparing the two-photon-detection probabilities, a simple relation $P_4(n,p,i=2) = \frac{3}{2}P_2(n,p,i=2)$ is obtained, which means that four-channel setup can collect 1.5 times more two-photon emissions than two-channel setup with all the experimental conditions kept constant.

- Coincidence probabilities with background

  Because background photons always occur in SMD experiments, it is necessary to

take them into account in the model. The distribution of photons coming from the background can be modeled as a Poisson distribution. Background photons occur only about $10^3 Hz$ and the probability is about 10^{-4} after normalized by the laser repetition rate (10MHz). Due to the rareness of background photons, it is reasonable to consider that there is at most one background photon in one laser cycle. In a typical observation time (seconds to a minute), with laser pulse frequency of $10MHz$, the chance to observe two or more background photons is low and ignorable in comparison to multiple-photon-detection events from fluorophores. Assume that all the assumptions of Eq. 4.12 are the same except for the background photons, the coincidence probability calculation is similar to the case without background correction if the background photons are regarded as from an additional fluorophore with a rather low normalized molecular brightness:

$$\begin{aligned} P(n,p,i) = & \begin{pmatrix} m \\ i \end{pmatrix} ((i \cdot \frac{p}{m} + 1 - p)^n (i \cdot \frac{p_b}{m} + 1 - p_b) \\ & - \sum_{k=0,k>0}^{i-1} \frac{\begin{pmatrix} i \\ k \end{pmatrix}}{\begin{pmatrix} m \\ k \end{pmatrix}} P(n,p,k)) \end{aligned} \tag{4.21}$$

where, p_b is the probability of background photons in one laser cycle. By replacing m with 2 or 4, the probabilities of all the photon detection events in two or four detection channel setup can be explicitly formulated.

- Coincidence probabilities with photobleaching

  Unfortunately, most of fluorophores show photobleaching after a certain period of excitation by high energy output laser [91]. Fluorophores can emit a certain number of photons before being photodestructed and falling into a permanent fluorescent dark state. Suppose that a pool of fluorophores is illuminated by a high energy laser, some of the fluorophores will experience photodestruction statistically very fast without emitting sufficient photons for coincidence analysis, especially when the number of fluorophores increases to more than 10. Since photobleaching can not be circumvented easily, a practical way is to modify the model to characterize the bleaching of fluorophores.

  As a part of the fluorophores are undergoing photobleaching, I assume the molecular brightness of the fluorophores remains unchanged as do the other parameters. Therefore, the overall fluorescence intensity I_t at time t is determined only by the number of fluorophores left at fluorescent on-state n_t as well as the normalized molecular brightness p or the initial fluorescence intensity I_0:

  $$I_t = n_t p = \frac{n_t}{n_0} I_0 \text{ or } n_t = \frac{I_t}{I_0} n_0 \tag{4.22}$$

  where I_0 is the initial intensity of the fluorescence at time t_0.
  Therefore, the coincidence probabilities at time t are

  $$P(n_t,p,i) = P(\frac{I_t}{I_0} n_0,p,i) \tag{4.23}$$

  where, $i = 0,1,...,m$ is the number of detection channels that detect a photon and m is the total number of detection channels.

Suppose the observation time is from t_0 to t_1, the coincidence probability densities are

$$f(n_t,p,i) = \frac{1}{t_1 - t_0} P(\frac{I_t}{I_0} n_0,p,i) \tag{4.24}$$

By integrating Eq. 4.24, the overall coincidence probabilities can be formulated as

$$F(n_0,p,i) = \frac{1}{(t_1 - t_0)} \int_{t_0}^{t_1} P(\frac{I_t}{I_0} n_0,p,i) dt \tag{4.25}$$

As long as the instant fluorescence intensity I_t is given as well as the initial number of fluorophores n_0 and normalized molecular brightness p, the probabilities can be calculated. In reality, the intensity of fluorescence can be approximately given by the measured intensity of fluorescence. By substituting different coincidence probabilities as in Eq. 4.12 or 4.21, different conditions can be included in this model. There is no explicit expression of Eq. 4.25 since the function I_t is not known beforehand.

4.1.3 Parameter estimation

Excited by laser pulses with high repetition frequency, such as 10 MHz or 20 MHz in our setup, fluorophores can be illuminated more than 10^7 times in several seconds. The multiple-photon-detection events Y_i, $i = 0,1,...,m$, are observable as a realization of a multinomial distribution in experiments. Their probabilities can be described by Eq. 4.12, 4.21 or 4.25. As the probabilities for Y_i depend on two variables under our assumptions, the number of fluorophores n and the normalized molecular brightness p, the Levenberg-Marquardt (LM) algorithm is chosen to find the best estimation of the parameters n and p. That is to optimize n and p of the coincidence probabilities $P_m(n,p,i)$ so that the sum of the squares of the deviations

$$S(n,p) = \sum_{m}^{i=0} (Y_i - P_m(n,p,i))^2 \tag{4.26}$$

becomes minimal [75].

LM algorithm provides an iterative procedure to find the parameters n and p,

$$(J^T J + \lambda\, diag(J^T J))\delta = J^T(Y - P(\beta)) \tag{4.27}$$

where J is the Jacobian matrix of $P_m(n,p,i)$, Y and $P(\beta)$ are vectors with i^{th} component Y_i and $P_m(n,p,i)$ respectively, and β is a vector of $(n\ p)^T$, δ is the step of a new estimation from β, and λ is the damping parameter [63]. It is very convenient to perform LM algorithm by using a software package available in C, MATLAB or other programming languages.

It is worth to point out that not all the $m+1$ multiple-photon-detection events are independent to each other, since the sum of them is the total number of laser pulses N shed on the sample. However, the correlations of coincidence probabilities

$$Corr(Y_i, Y_j) = -\sqrt{\frac{P(n,p,i)P(n,p,j)}{(1-P(n,p,i))(1-P(n,p,j)}} \tag{4.28}$$

are all small when p is low, where $i \neq j$ and $i,\ j = 0,1,...,m$, except that $Corr(Y_0,Y_1)$ is close to -1. It is convenient and practical to consider them independent to each other.

4.2 Numerical simulations

Before the model described in Section 4.1 is subjected to real experiments, its feasibility is examined by numerical simulations.

Multiple-photon-detection events are multinomial distributed and Monte Carlo method is engaged to generate the multinomial random numbers. By combining different sets of parameters, such as varying the number of fluorophores n, normalized molecular brightness p and the number of excitation laser pulses N, the relation of the parameters and the distribution of the estimation are elaborated. I also apply the estimation to the simulated data sets with molecular brightness varying from molecule to molecule, which is the

case in reality. In the simulations, I concentrate on the case of four-detection channels. Theoretically, the analysis can be extended to any number of detection channels.

4.2.1 Coincidence probabilities

According to the Abbe's prediction in 1870's, with a $100X$ objective having a high numerical aperture (NA) of 1.4, the focal volume of a confocal microscope is limited by light diffraction. If a $635\ nm$ laser is in use, the lateral diameter of the focal volume is around half of the excitation wavelength, which is $\sim 300\ nm$. The light flux on the specimen is about $10\ \mu W$ in my case, so the light intensity at the focus is about $8\ kW/cm^2$, which corresponds to $3 \cdot 10^{22}\ photon/(cm^2 s)$. The collection efficiency of a confocal microscope with NA 1.4 is around 30% depending on the collection angle. The transmission efficiency of a dichroic mirror is around 90% and that of the filters, the 1:1 beam splitters and the band pass filters are about 95%, 80% and 50% respectively. The quantum yield of an APD is around 60% at red light range ($650 - 750nm$) and the efficiency of a data acquisition card is close to 1. Finally the overall collection efficiency of a single-molecule detection microscope is in the order of 1%. The absorption cross-section of a single fluorophore is about $3 \cdot 10^{-16} cm^2/molecule$, the quantum yield of a very bright organic dye is close to 1, and the final fluorescent photon yield is about $24\ kHz$. When illuminated with laser pulses with very short pulse duration, one fluorophore can be excited only once in each pulse, so fluorescence emission highly depends on the frequency of the laser. For instance, if the frequency of the laser pulse is $10\ MHz$, the probability p to detect a photon in one laser cycle (or normalized molecular brightness) is in the range of 10^{-3}. p is taken as $10^{-3} - 4 \cdot 10^{-3}$ in my simulations.

In aqueous environment the total amount of fluorescence from each fluorophore is limited to roughly 10^6 photons by photobleaching [56]. 100 times more photons (10^8 photons) can be emitted from one fluorophore with the help of photostabilizing agents [86]. However, only

about 1% of the photons can be collected by a standard confocal setup, which is $10^4 - \cdot 10^6$ photons. As the probability to detect a photon is about 10^{-3}, an average number of the laser pulses shed on a fluorophore is around $10^7 - 10^9$ times before photodestruction happens. N is chosen as $10^8 - 4 \cdot 10^8$ in my simulations.

The coincidence probability distributions described in Eq. 4.12 are plotted as functions of the number of fluorophores n in Fig. 4.4(a) for a normalized molecular brightness of $p = 10^{-3}$. The probability for not detecting any photon decreases slowly as expected

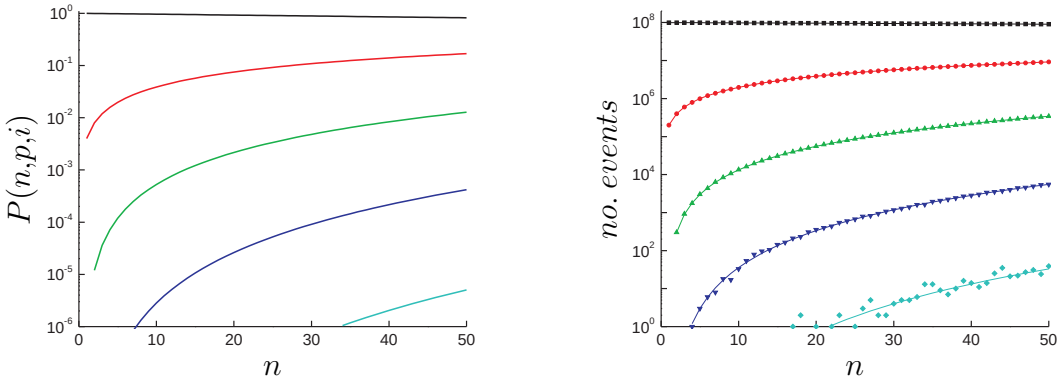

(a) (b)

Figure 4.4: (a) Coincidence probabilities distributions $P(n,p,i)$ for i-photon-detection events within one laser cycle in dependence of the number of fluorophores n for an ideal four-detector setup. (b) The Monte Carlo simulations (dots) of i-photon-detection events in comparison with calculations (lines) for an ideal four-detector setup. ($i = 0$: black, 1: red, 2: green, 3: blue, 4: cyan). The normalized molecular brightness p is 10^{-3}, the number of excitation laser pulses N is 10^8 and n is from 1 to 50.

with n increasing (black line). The probabilities for one- (red), two-(green) three- (blue) and four-photon-detection events (cyan) within a single excitation cycle increases with increasing n. The reason why the probabilities of two-, three- and four-photon detection do not extend to $n = 1$ is that the scale is logarithmic and there is no probability to observe more photons in one laser cycle than the number of fluorophores n.

Monte Carlo simulations are performed to obtain the number of multiple-photon-detection events on a parameter set of $N = 10^8$, $p = 10^{-3}$ and $n = 1, 2, ..., 50$. The destination of each photon from every fluorophores is determined by generating a random number. Multiple-photon-detection events are recorded and summarized out of millions of random experiments. Simulations (dots) of multiple-photon-detection events are in good agreement with their predictions (lines) as shown in Fig. 4.4(b), which supports the suitability of the Eq. 4.12. The deviation of three- and four-photon-detection events from the theory are noticeable or moderate since the absolute occurrence numbers are low and inclined to be influenced by shot noise.

4.2.2 Estimation based on simulation

Given the multiple-photon-detection events by simulations, the LM algorithm is applied to find the estimated fluorophore numbers n and the normalized molecular brightness p. The averages of the estimated number of fluorophores $\overline{n}_{est}$ with typical parameter sets of $N = 10^8$, $2 \cdot 10^8$ or $4 \cdot 10^8$, $p = 10^{-3}$ and $n = 1,2,...,50$ are in good agreement with the simulated numbers of fluorophores n very well (Fig. 4.5(a)). The deviations $\overline{n}_{est} - n$ increase from 0 at $n = 1$ to $0.6 - 1.5$ (depends on the number of laser excitation pulses N) at $n = 50$ as shown in Fig. 4.5(b). The estimation is perfect when $n = 1$, because there is no more than one-photon emission due to the existence of only one fluorophore. It is worth to note that the number of fluorophores is a little overestimated since $\overline{n}_{est} - n > 0$ for $n > 1$ (Fig. 4.5(b)). This is due to the nonlinear effect of the estimator. Moreover, while increasing N, the deviations $\overline{n}_{est} - n$ from the simulated number of fluorophore n becomes smaller (Fig. 4.5(b)). It is reasonable because more photons are collected by increasing the number of excitation laser pulses or prolonging the illumination time.

Nevertheless, although there is a small overestimation in the estimated number of fluorophores, the proposed method is able to provide reasonable estimations up to 50 molecules.

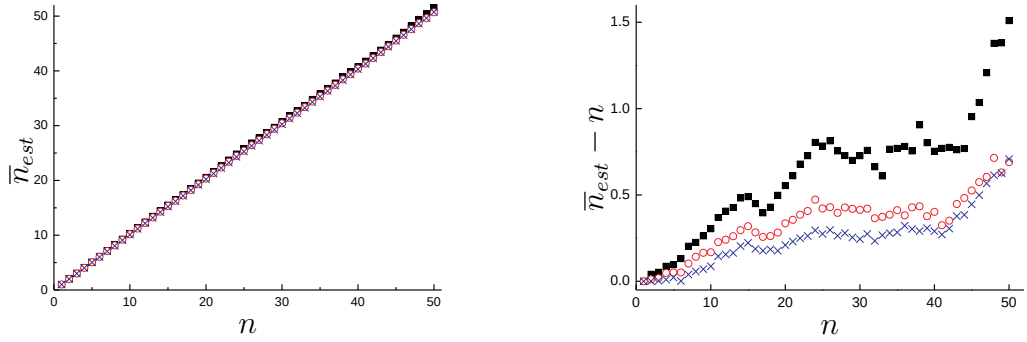

(a) (b)

Figure 4.5: Estimation on fluorophore numbers: The average $\overline{n}_{est}$ (a) of the estimated number of fluorophores and the deviation $\overline{n}_{est} - n$ (b) from the simulated number of fluorophores n are plotted against n with different number of excitation laser pulses N. $N = 10^8$: black square, $2 \cdot 10^8$: red circle and $4 \cdot 10^8$: blue cross. $p = 10^{-3}$ and the statistics are based on 500 simulations.

4.2.3 Estimation distribution

Multiple-photon-detection events are stochastic processes, so the estimation based on them also has a certain distribution. In a four-detector scheme one- and two-photon-detection events $Y1$ and $Y2$ are much more frequent than three- or four-photon-detection events $Y3$ and $Y4$. Therefore, $Y1$ and $Y2$ mainly determine the distribution of estimation. As described in Eq. 4.19, when $np << 1$, the number of fluorophores n can be roughly given by the combination of one- and two-photon-detection probabilities $P_4(n,p,i = 1)$ and $P_4(n,p,i = 2)$ or $P(1)$ and $P(2)$ in short.

Eq. 4.19 can be rewritten as

$$\frac{1}{n} = 1 - \frac{8P(2)}{3P(1)^2} \tag{4.29}$$

The observations of $P(1)$ and $P(2)$ are $\frac{Y1}{N}$ and $\frac{Y2}{N}$ respectively. The distribution of $1/n$ is thus in dependence of $1 - \frac{8}{3}\frac{Y2}{N}/(\frac{Y1}{N})^2$ or $\frac{Y2}{N}/(\frac{Y1}{N})^2$. Because $Y1$ and $Y2$ are very close to Poisson distribution, the standard deviations of them are $\sigma(Y1) = \sqrt{Y1}$ and $\sigma(Y2) = \sqrt{Y2}$,

where $\sigma(\bullet)$ is the standard deviation. Therefore, the standard deviation of $\frac{Y2}{N}$ is much higher than that of $\frac{Y1}{N}$ since

$$\sigma(\frac{Y2}{N})/\sigma(\frac{Y1}{N}) = \sqrt{\frac{Y1}{Y2}} \tag{4.30}$$

and $Y1$ is several magnitudes higher than $Y2$.

Therefore, the distribution of $\frac{Y2}{N}/(\frac{Y1}{N})^2$ is close to that of $\frac{Y2}{N}/P(1)^2$. Because $Y2$ is close to normally distributed due to the central limit theorem, the reciprocal of the estimated number of fluorophore $1/n_{est}$ can also be considered as a normal distribution. It can be shown by the estimation on the simulated data as well. The histograms of the estimated number of fluorophores n_{est} show tails at the right side (Fig. 4.6(a)), which is not accessible to simple fits. However, the histograms of their reciprocal $1/n_{est}$ are close to normal distribution

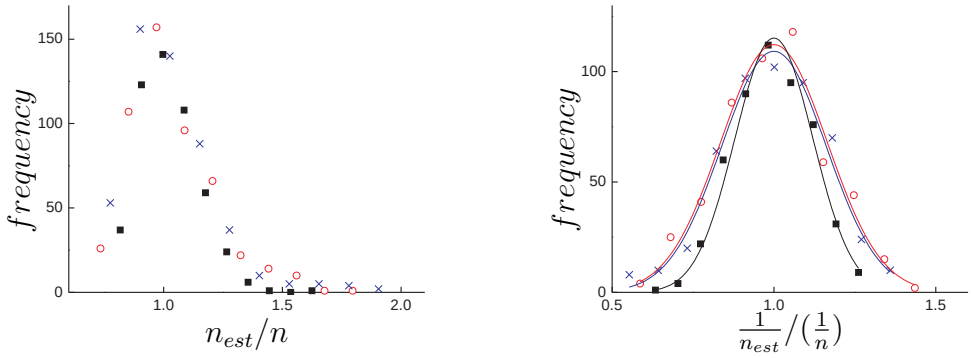

(a) (b)

Figure 4.6: Distribution of the estimated fluorophore number: The histograms of the estimated numbers of fluorophores n_{est} normalized by the simulated number of fluorophores n (a) and the histograms of the reciprocal of the estimated numbers of fluorophores $1/n_{est}$ normalized by $1/n$ (b) with different n. $n = 2$: black square, 10: red circle or 50: blue cross. The histograms of $1/n_{est}$ are fit by Gaussian functions. The number of excitation laser pulses N is 10^8, the normalized molecular brightness p is 10^{-3} and the histograms are based on 500 simulations.

(Fig. 4.6(b)).

Furthermore, by substituting P(1) with its approximation in Eq. 4.18, the standard deviation of $1/n_{est}$ is thus given by

$$\sigma(\frac{1}{n_{est}}) = \sigma(1 - \frac{8P(2)}{3P(1)^2}) \approx \sigma(\frac{8Y2}{3NP(1)^2}) = \sqrt{\frac{8(n-1)}{3n^3}}\frac{1}{p}\frac{1}{\sqrt{N}} \tag{4.31}$$

It means, the standard deviation $\sigma(1/n_{est})$ is inversely proportional to the normalized molecular brightness p times the square root of the number of excitation laser pulses N. Although this dependency concerns $\sigma(1/n_{est})$ instead of the standard deviation σ_n of the estimated number of fluorophores, it provides the information that the estimation on the number of fluorophore becomes better when the number of excitation laser pulses or the normalized molecular brightness increases. Moreover, a more direct way to study the dependency of them is simulation.

On one hand, if the number of excitation laser pulses N increases two or four times from 10^8 to $2 \cdot 10^8$ or $4 \cdot 10^8$, the relative standard deviations σ_n/n of the estimated number of fluorophores n become smaller as expected (Fig. 4.7(a)). Actually, the standard deviations σ_n when $N = 2 \cdot 10^8$ or $4 \cdot 10^8$ are $\sqrt{2}$ and 2 times better than that when $N = 10^8$, which is demonstrated in Fig. 4.7(b) by plotting the ratio of the standard deviation σ_n when $N = 10^8$ or $2 \cdot 10^8$ to that when $N = 4 \cdot 10^8$.

On the other hand, by changing p from 10^{-3} to $2 \cdot 10^{-3}$ or $4 \cdot 10^{-3}$, the relative standard deviations σ_n/n decrease as shown in Fig. 4.8. Further comparisons demonstrate that two or four folds decrease in σ_n/n results from doubled or quadrupled p.

Accordingly, simulations clearly show that the standard deviation of the estimated number of fluorophores is inversely proportional to the normalized molecular brightness p and the square root of the number of excitation laser pulses N.

Therefore, in order to improve the estimation, it is recommended to use brighter fluo-

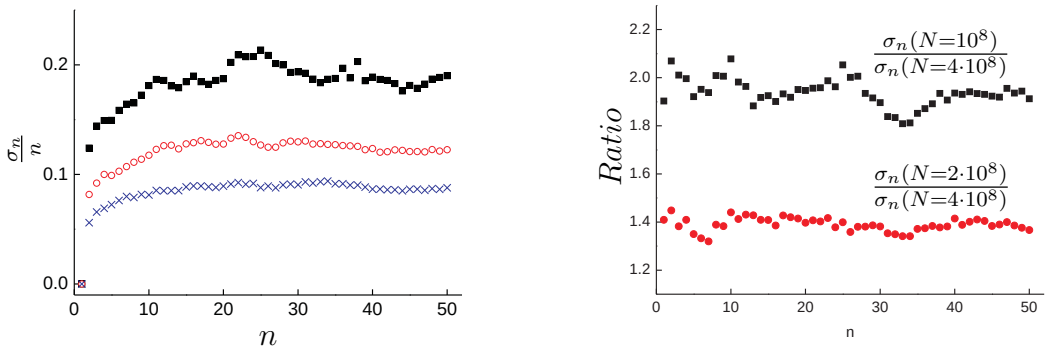

(a) (b)

Figure 4.7: Dependency of the estimated number of fluorophores on the number of excitation laser pulses: (a) Relative standard deviations σ_n/n of the estimated number of fluorophores n are plotted in dependence of n with different number of excitation laser pulses N ($N = 10^8$: black square, $2 \cdot 10^8$: red circle and $4 \cdot 10^8$: blue cross). (b) Ratio $\frac{\sigma_n(N=10^8)}{\sigma_n(N=4\cdot10^8)}$ and $\frac{\sigma_n(N=2\cdot10^8)}{\sigma_n(N=4\cdot10^8)}$ of two standard deviations σ_n of the estimated number of fluorophores are plotted against n (black square: ratio of σ_n with $N = 10^8$ to that with $N = 4 \cdot 10^8$; red dot: ratio of σ_n with $N = 2 \cdot 10^8$ to that with $N = 4 \cdot 10^8$). The normalized molecular brightness p is 10^{-3} and the statistics are based on 500 simulations.

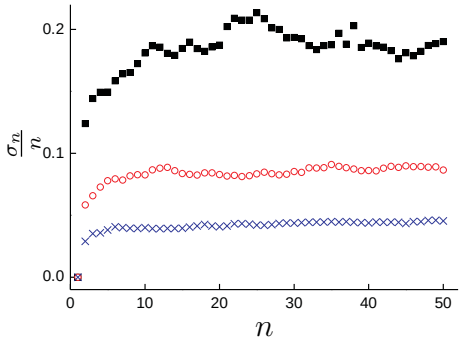

Figure 4.8: Estimation of the number of fluorophores with different normalized molecular brightness: The relative standard deviation $\frac{\sigma_n}{n}$ with different normalized molecular brightness p ($p = 10^{-3}$: black square, $2 \cdot 10^{-3}$: red circle and $4 \cdot 10^{-3}$: blue cross) are plotted against the simulated number of fluorophores n. The number of excitation laser pulses N is 10^8 and the statistics are based on 500 simulations.

rophores instead of only increasing photostability to extend the excitation exposure time. Unfortunately, there is not much room to increase the molecular brightness of widely used organic dyes due to the limit of their molecular cross-section and quantum yield. Actually, an optimized optical beam path is able to collect more photons and therefore helps to improve the estimation. However, the attempt to increase the excitation exposure time by decreasing the laser power shed on fluorophores can not improve the resolution of photon antibunching analysis. On the other hand, it is not possible to increase molecular brightness when the fluorophore is already saturated by further increasing the laser power. At the same time, high laser power, especially when fluorophores are saturated, causes fluorophores to blink or bleach by driving them into triplet or radical states [86]. This will result in shortening the lifetime of the fluorophores and decreasing their exposure time. Therefore, there is a compromise between increasing the laser power and prolonging the exposure time. Moreover, there are also many attempts to use Trolox [66] or a reducing-oxidizing system (ROXS) [86] to avoid blinking and delay photobleaching. Higher photostability and increased molecular brightness both benefit the estimation by coincidence analysis.

Moreover, according to Eq. 4.31, $1/n_{est}$ depends on the number of fluorophores n as well. In fact, the relative standard deviation of $1/n$ can be given by slightly changing Eq. 4.31, which is

$$\sigma(\frac{1}{n})/\frac{1}{n} \approx \sqrt{8(n-1)/(3np^2N)} \tag{4.32}$$

This means that the relative standard deviation $\sigma(\frac{1}{n})/\frac{1}{n}$ saturates as n increases and converges to a value of $\sqrt{8/(3Np^2)}$. It is informative that coincidence analysis is only limited by the condition of the analysis, which is $np << 1$. Therefore, if the normalized molecular brightness p is around 10^{-3}, the number of fluorophores n can be up to 100. When np is comparable to 1, such as higher than $1/10$, further analysis is needed.

For the same reason, the distribution of the estimated normalized molecular brightness p is very close to Gaussian distribution according to Eq. 4.20. The same manipulation as done on

$1/n$ provides the standard deviation of estimation on the normalized molecular brightness p

$$\sigma_p \approx \sqrt{\frac{8(n-1)}{3nN}} \tag{4.33}$$

This relation shows that there is no dependency between the standard deviation σ_p and the normalized molecular brightness p. As long as n and N are fixed, the standard deviation of the estimated normalized molecular brightness is constant. However, the brighter the fluorophore, the better the relative standard deviation of estimated p. The histograms of the estimation on p of 500 simulations are plotted in Fig. 4.9. The Gaussian fitting of the

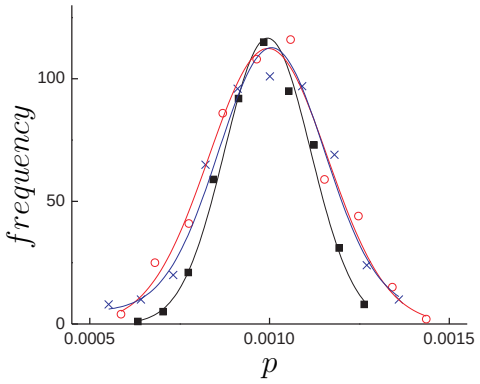

Figure 4.9: Distribution of estimated normalized molecular brightness: The histogram of the estimated normalized molecular brightness p with simulated number of fluorophores $n = 2$ (black square), 10 (red circle) and 50 (blue cross) are fit by Gaussian functions. The number of excitation laser pulses N is 10^8, the normalized molecular brightness p is 10^{-3} and the histograms are based on 500 simulations.

histograms demonstrates that all the histograms center at the expected p value of 10^{-3} with relative standard deviations from 12% to 16%, which are close to the calculations by Eq. 4.33. The small differences between the simulations and calculations are due to the approximations of the coincidence probabilities $P(1)$ and $P(2)$ as well as the neglection of three- and four-photon-detection events.

Furthermore, by increasing the number of excitation laser pulses N in simulations, the

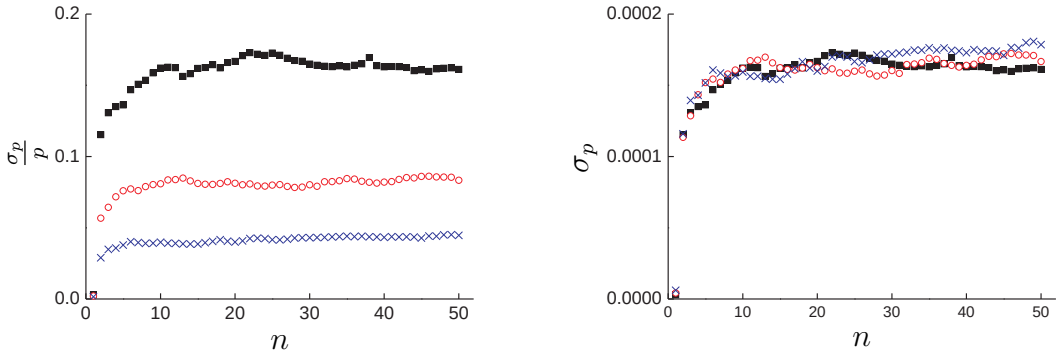

(a) (b)

Figure 4.10: Estimation on normalized molecular brightness with different parameters: (a) The relative standard deviations $\frac{\sigma_p}{p}$ of the normalized molecular brightness p are plotted against n with different number of excitation laser pulses N ($N = 10^8$: black square, $2{\cdot}10^8$: red circle and $4{\cdot}10^8$: blue cross). p is 10^{-3}. (b) The standard deviations σ_p with different normalized molecular brightness p ($p = 10^{-3}$: black square, $2 \cdot 10^{-3}$: red circle and $4 \cdot 10^{-3}$: blue cross) are plotted against n. $N = 10^8$. The statistics in both figures are based on 500 simulations.

relative standard deviation $\frac{\sigma_p}{p}$ of the estimated normalized molecular brightness p decreases (Fig. 4.10(a)). In fact, when the number of excitation laser pulses N doubles or quadruples, the estimation of p is about $\sqrt{2}$ or 2 times better, which is in agreement with the prediction of Eq. 4.33. It makes sense that the longer the illumination, the better the estimation. On the other hand, the standard deviation of the estimated p does not change while p increases (Fig. 4.10(b)), which is expected according to Eq. 4.33. Moreover, as the number of fluorophores n increases, the standard deviation of the estimated normalized molecular brightness turns to be constant (Fig. 4.10(b)). This tendency can be easily explained by increasing n to infinity in Eq. 4.33.

Above all, although the theoretical approximation is based on one- and two-photon-detection events, it also keeps true when all the multiple-photon-detection events are included according to simulations.

4.2.4 Influence of background

Until now, the background has not been taken into account. However, it is important to study the effect of background on the estimation of the number of fluorophores, because Rayleigh scattering, Raman scattering from the solvent and noise from electronic devices always occur in single molecule experiments. Actually, it is convenient to study the influence of background by simulations. An additional fluorophore was introduced in simulations to present the background from all the sources. According to the standard conditions of single-molecule experiment, the normalized intensity of background photons is about 10^{-4} (10% of a typical normalized molacular brightness). Thereby, the estimation on the same simulated data indicates that the average of the estimated numbers of fluorophores $\overline{n}_{est}$ without background correction has a small shift to a higher number from that with background correction as shown in Fig. 4.11(a). The reason is that the background photons

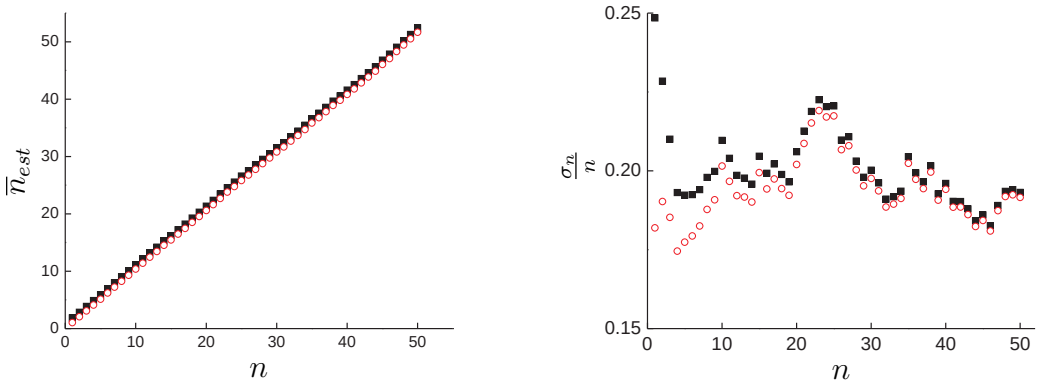

(a) (b)

Figure 4.11: Estimation with background correction: Comparison of estimation without (black square) and with (red circle) background correction on the same set of simulated data. The average $\overline{n}_{est}$ of the estimated number of fluorophores (a) and the relative standard deviation $\frac{\sigma_n}{n}$ of estimated number of fluorophores (b) are plotted against the simulated number of fluorophores n. The probability of background photon p_b is $5{\cdot}10^{-4}$ and the normalized molecular brightness p is 10^{-3}. The number of excitation laser pulses N is 10^8 and all statistics are based on 500 simulations. p_b is taken as a known condition in background correction estimation.

behave like an additional fluorophore. It is clear that background photons are independent from the number of fluorophores. Consequently, when the number of fluorophores increases background photons still remain the same and the signal to noise ratio becomes better. This is also indicated by the relative standard deviation σ_n/n in Fig. 4.11(b). The relative standard deviations σ_n/n without background correction (black square) is much higher than that with (red circle) when the number of fluorophores n is less than 5. As n increases, the influence of background photons diminish very fast. The strong correlation between the estimation with and without background correction in Fig. 4.11(b) is because the same set of simulated data is used in both cases.

4.2.5 Influence of variation in normalized molecular brightness

Although the model is based on the assumption that all the fluorophores have the same normalized molecular brightness, this assumption is not always true in reality due to the fluctuation of local environment of individual fluorophores, inhomogeneous laser intensity and so on. By applying the model to simulations with normalized molecular brightness varying from molecule to molecule, the fidelity of the model on slight violation can be investigated. The normalized molecular brightness p of the fluorophores is modeled as a random variable from a Gaussian distribution and generated by a Gaussian random number generator with a given mean and standard deviation. Afterwards, the probabilities of the multiple-photon detection are calculated with the generated normalized molecular brightness p. Finally, the multiple-photon-detection events are generated by a multinomial distribution random number generator. The estimation on the simulated data demonstrates that the averages $\overline{n}_{est}$ of the estimated n are still very close to the expected values n with slightly different deviations as shown in Fig. 4.12(a). The deviations $\overline{n}_{est} - n$ from the expected value n change from overestimation to underestimation when the variation of normalized molecular brightness p increases from 0% to 20% (Fig. 4.12(b)). The relative standard deviation $\frac{\sigma_n}{n}$ of the estimated n remains without big changes as shwon in Fig. 4.12(c).

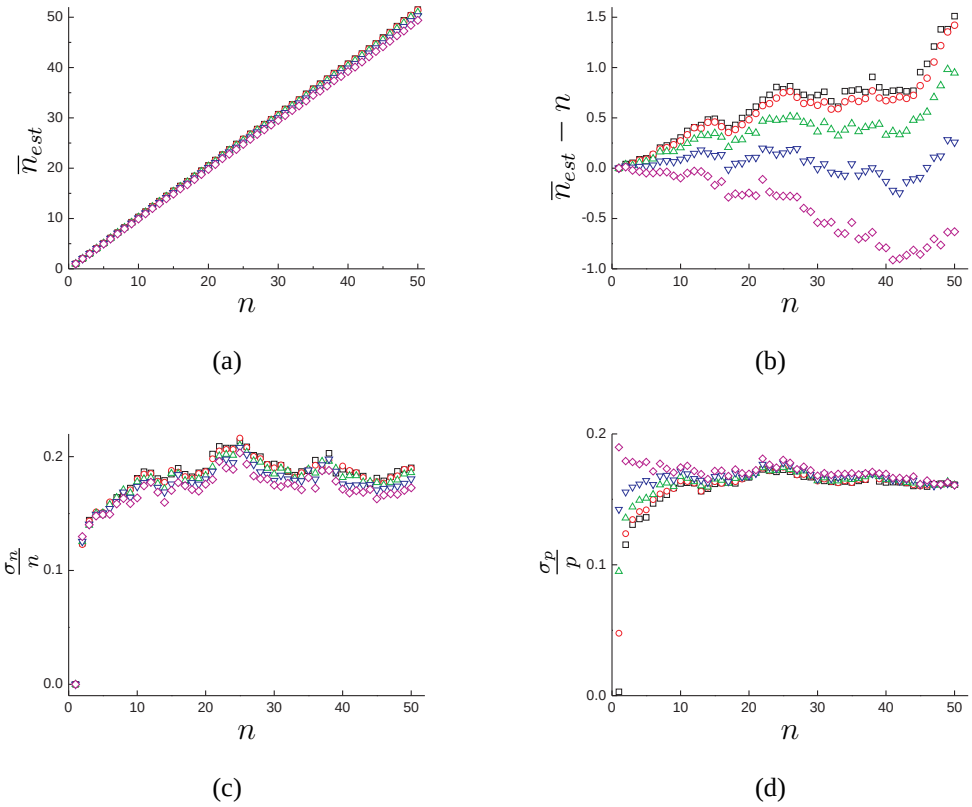

Figure 4.12: Estimation with molecular brightness varying: The average $\overline{n}_{est}$ of the estimated number of fluorophores (a), the deviation $\overline{n}_{est} - n$ of estimated number from the simulated number of fluorophores (b), the relative standard deviation σ_n/n of the estimated number of fluorophores (c) and the relative standard deviation $\frac{\sigma_p}{p}$ of the estimated normalized molecular brightness (d) are plotted against the simulated n. The variation of the normalized molecular brightness in the simulation ranges from 0 (black square), 5% (red circle), 10% (green up triangle), 15% (blue down triangle) to 20% (magenta diamond). The number of exciation laser pulses $N = 10^8$, the average normalized molecular brightness is 10^{-3} and all statistics are based on 500 simulations.

The relative standard deviation $\frac{\sigma_p}{p}$ of estimated p converges to same values when n is big (> 10) as shown in Fig. 4.12(d). But when n is less than 10, $\frac{\sigma_p}{p}$ increases while increasing the varation of p. The reason is that the variation in p of individual fluorophores leads to big variation in p of the overall fluorophores when the number of fluorophores is small. As a conclusion, the proposed model still works well when the fluctuation of the normalized molecular brightness is about 20%.

4.3 Experimental validation of coincidence analysis

In order to evaluate the proposed method, a setup was built to perform single molecule experiments. The scheme of the setup is shown in Fig. 3.2. Basically, it is a confocal microscopy working in TCSPC (Time-correlated single photon counting) mode. The excitation is a picosecond-pulsed laser. TCSPC uses the laser pulses as a clock and is able to record photon arrival times precisely (1ps resolution in this work) according to the clock. The fluorescence beam path is divided into four equal parts by three 1:1 beam splitters. Therefore, the setup is able to detect the multiple-photon emission in one laser cycle equipped with four identical single-photon sensitive detectors (APD). The multiple-photon-detection events can be applied in the model to estimate the number of fluorophores in the confocal focus volume. All the following experiments were performed with the home made single molecule microscope.

4.3.1 Localization of single dsDNA

In order to evaluate the model experimentally, a system with well defined number of fluorophores is needed. Therefore, I designed a dsDNA with multiple labels. The scheme of the dsDNA is shown in Fig. 4.13. The dsDNA is constructed as follows: one of the strands is long with a four times repeated sequence and the others are four identical short sequences complementary to the repeated sequence in the long one. The long strand is

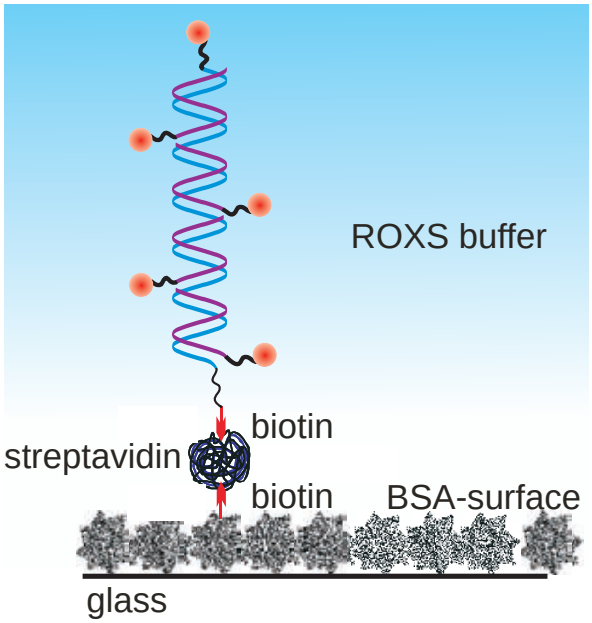

Figure 4.13: A scheme of immobilized dsDNA with a defined number of labels: dsDNA is labeled with 5 Atto 647N and immobilized on a surface via streptavidin-biotin system. Glass surface is modified by BSA and BSA-biotin mixture. Photo-stabilizing buffer (ROXS) is used.

biotinylated at one end (3') and modified with NH2 group at the other end (5'), which is coupled to Atto-647N. The short sequence has an Atto-647N labeled at one end (5'). After hybridization, the final dsDNA has probably 5 fluorophores.

In order to investigate single complexes at one time, dsDNA was immobilized on a surface. The immobilization was realized by streptavidin-biotin system. As a tetramer, streptavidin has four biotin-binding sites forming strong and specific bonds with biotin molecules. The glass surface was first coated with a mixture of biotinylated BSA and BSA. The surface accessible biotin was linked to the biotin end of the dsDNA via streptavidin.

After the labeled dsDNA was immobilized on the surface, raster scanning was carried out to precisely locate single fluorescence spots on the surface. Scan images like Fig. 4.14 were acquired by recording fluorescence intensity of labeled dsDNA. A 600×600 pixel image ($1\ \mu s$ per pixel) represents a $30 \times 30\ \mu m^2$ field of view. The density of the immobilized

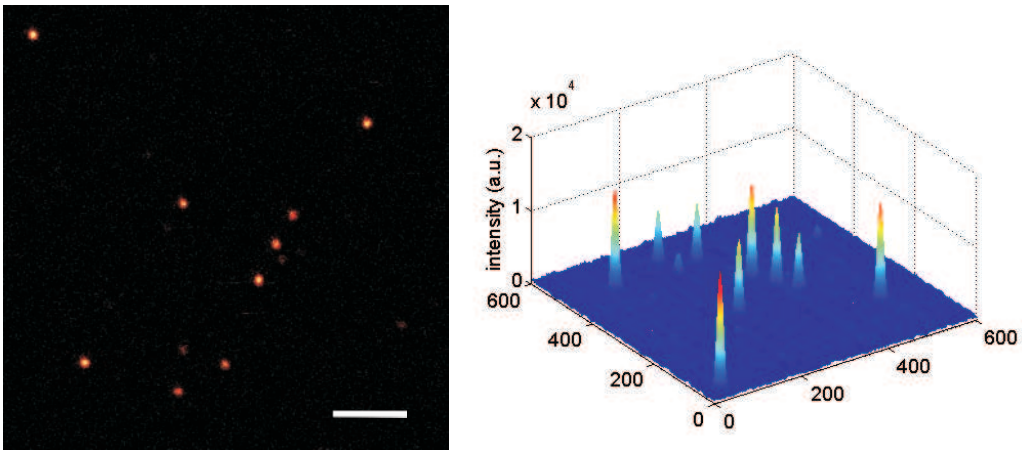

(a) (b)

Figure 4.14: Surface raster scan: $30 \times 30\ \mu m$ 2D raster scanned fluorescence intensity picture, 2D (a) and 3D (b). The excitation dwell time of each pixel is $1\ \mu s$ and scale bar in (a) is $5\ \mu m$.

single spots was as low as 0.015 molecules per μm^2. A good range of single molecule density was suggested to be less than $0.2\ spots/\mu m^2$ [70]. The laser power used for raster scanning was $3\ \mu W$, which corresponded to $2.5\ KW/cm^2$. $1\ \mu s$ pixel dwell time and $3\ \mu W$ laser power were selected as a compromise between avoiding photo bleaching of fluorophores and precisely locating fluorescence spots.

After located by raster scan, dsDNAs were moved into the focus of a $635\ nm$ laser one after another and were illuminated until all the fluorophores were bleached. Fluorescent photons were collected by a setup as shown in Fig. 3.2 and the photon arrival times were recorded and stored to hard disk of PC for off-line data analysis. Multiple-photon-detection events were recognized by comparing the arrival time of fluorescent photons of all four detection channels. The multiple-photon-detection events were used to estimate the number and normalized molecular brightness of fluorophores by LM algorithm. Although the numbers of multiple-photon-detection events range over a wide scale, LM algorithm provides a very good fit.

4.3.2 Estimation on dsDNA with 5 fluorophores

A typical fluorescence intensity trace is shown in Fig. 4.15 and fluorescence intensity drops as the fluorophores experience photo bleaching. Although photo bleaching leads to a loss of

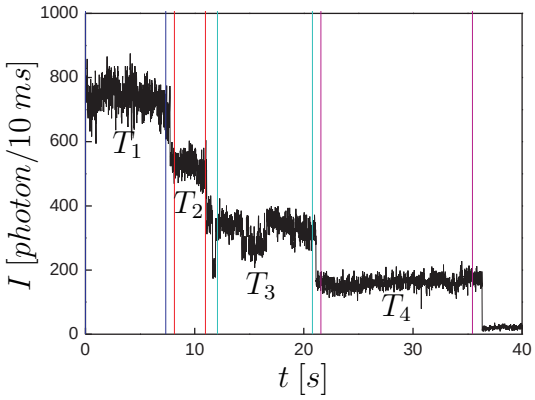

Figure 4.15: A typical fluorescence intensity trace: The fluorescence intensity time trace of a dsDNA labeled with multiple Atto-647N dyes shows clear individual bleaching steps. dsDNA is immobilized via streptavidin to the biotin modified BSA and BSA mixture coated glass surface. Fluorescent photon count I with $10\ ms$ bin time of a typical single spot is plotted independence of time t. Estimation on four time intervals is listed in Tab. 4.1. The frequency of excitation pulse laser is $10\ Hz$ with laser intensity $8\ kW/cm^2$ at the focus. A photostabilizing buffer (ROXS) is used to delay the photobleaching of the Atto-647N dyes.

fluorescence emission and is not favorable to most biological application of fluorophores, it can also be used to determine the stoichiometry of biomolecules indirectly, especially when the number of molecules is not high [25, 77, 50]. By adding photostabilizing agents, such as a ROXS system [86], the bleaching of individual fluorophore is delayed and the spacing of multiple bleaching steps statistically increases. Consequently, it is possible to count higher number of molecules. The bleaching steps of multiple Atto-647N labeled dsDNA immobilized on a glass surface clearly show that there were 4 fluorophores at $t = 0$ as shown in Fig. 4.15. After the first $7.5\ s$, one of the fluorophores turned into permanently dark state by photodestruction, the second fluorophore at $11\ s$, the third at $21\ s$ and finally all the fluorophores bleached away around $37\ s$. The fluorescence intensity plateaus between every

Table 4.1: Estimation of the number of fluorophores on different time windows.

Time intervals	Time	n_{est}	p_{est}
T_1	$0 - 7.3\ s$	4.16 ± 0.86	$p = 1.73 \cdot 10^{-3} \pm 2.9 \cdot 10^{-4}$
T_2	$8.1 - 11.0\ s$	3.04 ± 0.62	$p = 1.65 \cdot 10^{-3} \pm 2.8 \cdot 10^{-4}$
T_3	$12.1 - 20.8\ s$	2.08 ± 0.42	$p = 1.46 \cdot 10^{-3} \pm 2.5 \cdot 10^{-4}$
T_4	$21.6 - 35.5\ s$	1.01 ± 0.20	$p = 1.38 \cdot 10^{-3} \pm 2.3 \cdot 10^{-4}$

two successive bleaching steps are stable, except in the time interval T_3. The fluctuation in T_3 is probably due to the blinking or homo-energy transfer competing with fluorescence. Coincidence probabilities of Eq. 4.21 were chosen in LM algorithm and the estimation is performed on four time intervals T_1, T_2, T_3 and T_4 as shown in Fig. 4.15. The estimation gives similar results as the bleaching steps, which is listed in Tab. 4.1. The decreasing estimated normalized molecular brightness p (from $1.73 \cdot 10^{-3}$ to $1.38 \cdot 10^{-3}$) is probably due to the variation of the molecule brightness of fluorophores. All the combinations of p (increasing, stable and decreasing) have been observed. The background correction is performed by giving the background photon probability determined on the region after all the fluorophores are photo bleached. It is noteworthy that the estimation is based on the photon antibunching nature of resonance fluorescence instead of bleaching steps which may not be possible because individual bleaching steps may no longer be discerned when the number of fluorophores is high.

By choosing 188 time intervals, which show very clear bleaching steps and stable fluorescence intensity for photon antibunching analysis, a statistics of estimation n_a by the model was obtained. The estimated n_a versus the bleaching steps n_b are plotted in Fig. 4.16. The bleaching steps are taken as references in this plot and estimation based on photon antibunching shows a slight overestimation. It is probably due to the imperfection of background correction, which has rather big influences on the estimation when the number of fluorophores is low as has been explored in Section 4.2.4. The standard deviation of the estimation of photon antibunching analysis increases, which is consistent with the former analysis in simulations. The plot cannot be extended to higher number of fluorophores

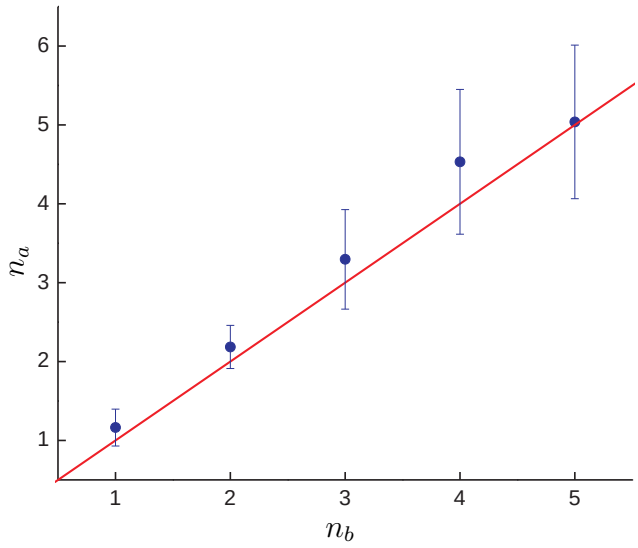

Figure 4.16: Statistics of estimation on less than 5 fluorophores: Statistics of estimated number of fluorophores n_a in dependence of the number of fluorophores by counting bleaching steps n_b. Red line is $y = x$, statistics are calculated based on 188 time intervals and background correction is considered in photon antibunching analysis.

because of both the maximum number of labels in the dsDNA and the limitation of the resolving individual bleaching steps.

The estimation based on the model which considers photobleaching as in Eq. 4.25 gives much more freedom to choose a time interval. For example in Fig. 4.17, a time interval with a fixed time duration of $20\ s$ (corresponds to $2 \cdot 10^8$ excitation laser pulses) is chosen and moved stepwise from the beginning of the fluorescence intensity trace to the end. At each step, the estimated number of fluorophores n_{est} (red circle with standard deviation as error bar) and the estimated normalized molecular brightness p_{est} (blue triangle) are plotted in Fig. 4.17(a) and Fig. 4.17(b) respectively as well as the fluorescence intensity time trace I (black line). All estimations n_{est} coincide with the fluorescence intensity indicating that the estimation reflects the real number of fluorophores very well as fluorescence intensity is proportional to the number of fluorophores at fluorescent-on state. At the same time the estimation p_{est} is constant until all the fluorophores are bleached, which again verifies the

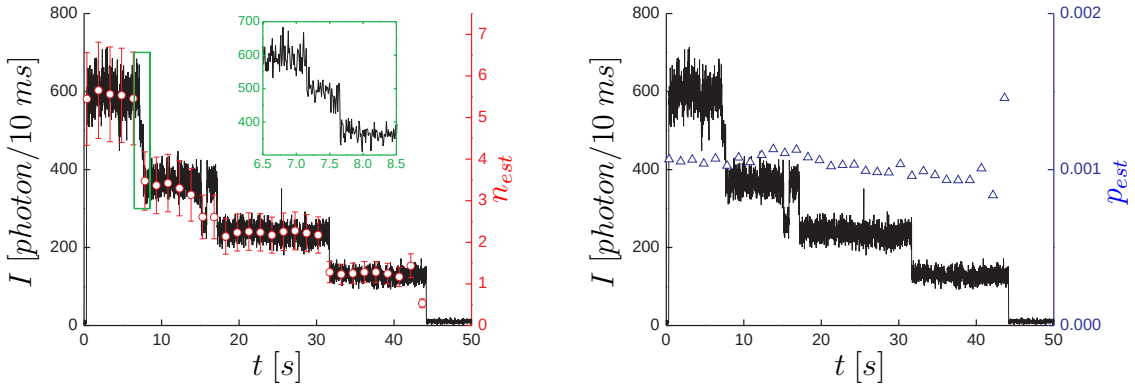

(a) (b)

Figure 4.17: Estimation on a fluorescent trace: Estimation on the number of fluorophores (a) and normalized molecular brightness (b) with the fluorescence intensity. Inset in (a) is the zoom in of the green box of the fluorescence intensity trace to show two successive bleaching steps in a short time. Background correction is included in the estimation and background photon probability is determined after all the fluorophores are bleached, which is 10^{-4}. Frequency of the excitation of 635nm laser is $10\ MHz$ and laser power is $10\ \mu W$ or $8\ KW/cm^2$ at the focus.

estimation.

Occasionally, two bleaching steps occur one after the other in a short time at round $7.2\ s$ and $7.6\ s$ shown in the inset of Fig. 4.17(a), the estimation also tells the same that the number of fluorophores drops from 5.5 before $7\ s$ to 3.4 after $8\ s$.

The statistics of the estimated normalized molecular brightness p of a double strand dsDNA as shown in Fig. 4.17 shows the mean value is $1.02 \cdot 10^{-3}$ and the standard deviation is $6.6 \cdot 10^{-5}$ or 6.4%. It is comparable to the statistics of the former simulation, as shown in Fig. 4.10(a) with settings of $N = 2 \cdot 10^8$ or $4 \cdot 10^8$ and $p = 10^{-3}$.

When it comes to the standard deviations of the estimated number of fluorophores in the same sample, the whole trace has to be split into several parts because bleaching results in

different number of fluorophores at fluorescence-on state. For example, the estimation at the 5 points on the first plateau (0-7s) gives a statistics of 5.53 ± 0.083, 9 points at the third plateau (18-30s) gives 2.22 ± 0.046 (Fig. 4.17(a)). Therefore, the standard deviation of the estimated n is about a few percentage of the estimated n. It is very close to the simulations in Section 4.2.3. However, the error bar (standard deviation) of n_{est} inherited from the statistics of many single dsDNAs is around 15% of n_{est} (Fig. 4.17(a)), which is much larger than the one from single dsDNA fluorescence intensity trace. The reason is probably that many conditions in one specific case remain untouched during the observation time. For instance, the molecular brightness of each fluorophores in one dsDNA keeps constant, but there are always differences between two complexes due to the heterogeneity of local environment and local laser intensity.

4.3.3 Estimation on more than 10 fluorophores

Most of the single dsDNA spots show around 5 fluorophores, but I also observed some fluorescence intensity traces which have probably more than 5 fluorophores as black line shown in Fig. 4.18. The bleaching steps at the initial time from $t = 0\ s$ to around $10\ s$ are overlapping and hard to distinguish. Therefore, it is not convenient to count molecules by bleaching steps. However, by applying the method based on photon antibunching, it is possible to provide the information of the number of fluorophores. I used the model which considers photobleaching as in Eq. 4.25 and chose a time interval of $4\ s$ or $4 \cdot 10^7$ excitation laser pulses. By moving the time interval stepwise the estimation on the number of fluorophores n_{est} and the normalized molecular brightness p_{est} at 100 time points is shown in Fig. 4.18(a) and Fig. 4.18(b) respectively. n_{est} fits to the fluorescence intensity very well after rescaling and indicates the initial number of fluorophores was around 15 and in the first $10\ s$ more than half of them bleached leaving only 6 fluorophores. After $80\ s$, all fluorophores were photodestructed in a stepwise manner. The estimated normalized molecular brightness p_{est} is stable around the mean value of $1.35 \cdot 10^{-3}$ with small standard

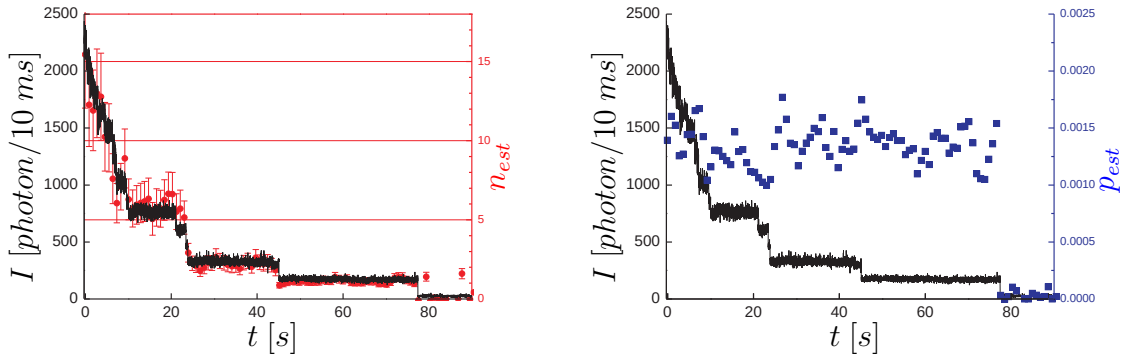

(a) (b)

Figure 4.18: Estimation of a fluorescent trace with 15 fluorophores: Estimation on the number of fluorophores n_{est} with error bar extrapolated from the statistics of less than 5 fluorophores by linear fitting of the relative standard deviation (a) and normalized molecular brightness p_{est} (b) as well as the fluorescence intensity are plotted in dependence of time t. Background correction is included in the estimation and background is determined after all the fluorophores are bleached, which is $2.5 \cdot 10^{-4}$. Frequency of the excitation of 635nm laser is $10\ MHz$, laser intensity is $10\ \mu W$ or $8\ KW/cm^2$ at the focal plane and a photostabilizing buffer (ROXS) is used.

deviations of $1.7 \cdot 10^{-4}$ or 7.4% until all fluorophores were bleached away. The error of the estimated number of fluorophores n_{est} is extrapolated from the statistics of less than 5 fluorophores by linear fitting of the relative standard deviation. According to the simulations in Section 4.2.3, the relative standard deviation stays constant in respect of the number of fluorophores n after the initial rising. Therefore, linear extrapolation secures the estimation, which means the error is exaggerated to some extend and the estimation on n is on the safe side.

Photon antibunching is perfect when there is only one photon emitter and it fades away while the number of photon emitters increases. Actually the antibunching phenomenon disappears faster than the increase of the number of photon emitters as shown in Fig. 4.19. When the fluorescence intensity drops from more than $2000\ counts/10ms$ at $t = 0\ s$ to around $750\ counts/10ms$ at $t = 9\ s$, or around 62.5%, at the same time the frequency of 2

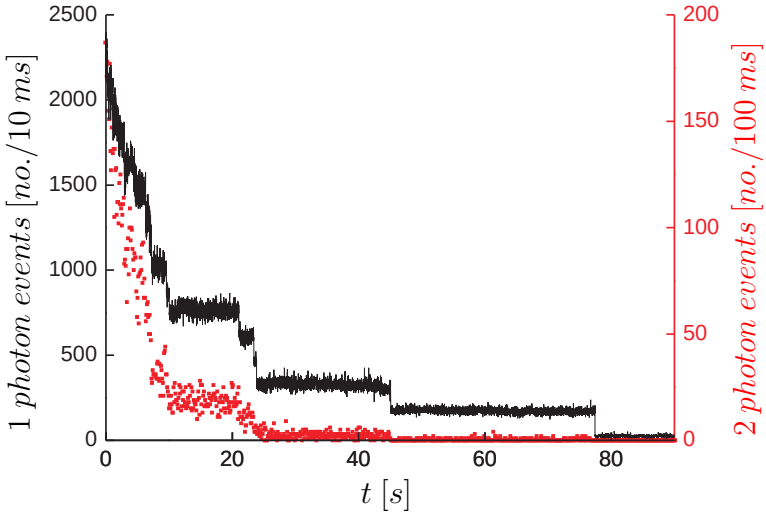

Figure 4.19: Two-photon-detection event trace: Two-photon-detection event time trace (red squares) is plotted with the fluorescence intensity time trace (black line). Experimental setting are the same as Fig. 4.18. The bin size of fluorescence intensity is $10\ ms$ and that of two-photon-detection trace is $100\ ms$.

photon detection events drops from $175\ counts/100ms$ at $t = 0\ s$ to $25\ counts/100ms$ at $t = 9\ s$, or about 86%. It partially explains that former attempts of using photon antibunching to count the number of fluorophores was limited to rather low number of fluorophores [79, 92].

4.3.4 Fluorescence lifetime

Fluorescence lifetime is an important parameter for application of fluorescence because it is very sensitive to the local environment of individual fluorophores, such as the existence of excited-state quenchers and resonance energy transfer, such as heterotransfer and homotransfer. Basically, the single molecule detection setup used in this work is a TCSPC system with pulsed laser excitation, so it is able to measure the decay of the excited state at the same time. The decay of excited-state population of a single dsDNA (red dots) is plotted with single exponential fitting (blue line) in Fig. 4.20. The χ^2 of the fitting is 1.20 and the residual is randomly distributed, which indicate that there is one species and the variation

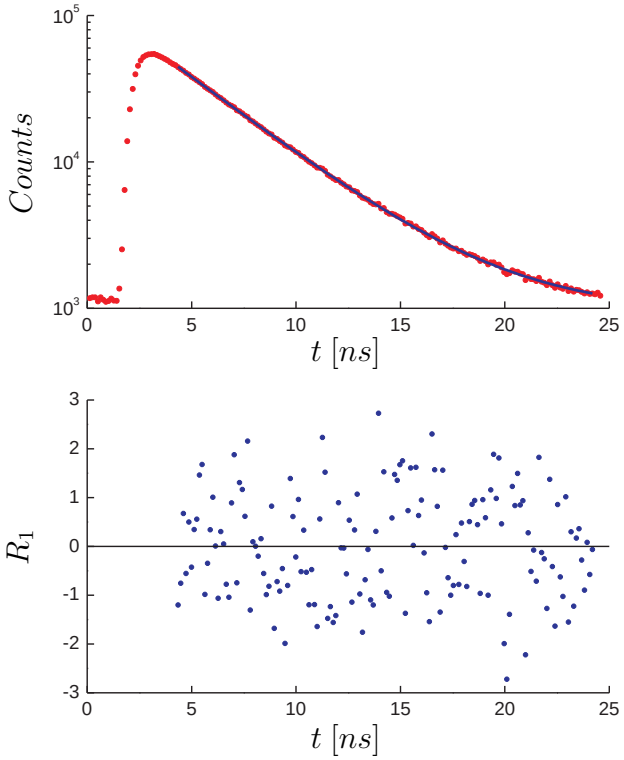

Figure 4.20: Excited-state decay of a single dsDNA: The decay (upper) of excited-state of single double strand DNA with 5 Atto-647N labels is plotted in a logarithmic scale in dependency of time t, with single exponential decay fitting (blue line). The residual of single exponential decay fitting (lower) is also plotted with respect of t. Fitting only corresponds to the data range from $4.3\ ns$ to $24\ ns$ since the instrument response function (IRF) is missing in this experiment. The lifetime of excited-state is $4.03 \pm 0.01\ ns$ with $\chi^2 = 1.199$.

of local environments surrounding each labels is not notable [45]. Due to the sensitivity of lifetime on local environments of fluorophores, there is no prominent cross talk, such as homo-transfer, among these Atto 647N molecules. Moreover, the lifetime of the dsDNA τ is $4.03 \pm 0.01\ ns$ according to the fitting, which is a little bit longer than that of free Atto 647N ($3.56 \pm 0.1\ ns$). However, it has been reported that some fluorophores show longer lifetime after coupled to dsDNA [43]. The reason may reside in that the adjacent dsDNA provide a shield against the solvent for the fluorophores. Therefore, quenching from the solvent decreases and consequently suppresses the non-radiative de-excitation. As a result, the lifetime of the fluorophores is prolonged.

Furthermore, the use of a photostabilizing buffer [86] dramatically increases the number of photons collected from single dsDNA. In an aqueous solution without photostabilizing buffer, one fluorophore can emit around 10^6 photons in average, and only 1% can be collected by a single molecule setup [56]. Thus, $5 \cdot 10^4$ photons can be observed from a dsDNA labeled with 5 Atto 647N and it is not enough to derive the lifetime. However, with help of the photostabilizing buffer, 100 times more photons can be collected, which results in more than 4 million photons from a single dsDNA with 5 labels. Consequently, a nice decay curve as shown in Fig. 4.20 can be obtained from a single dsDNA to estimate the lifetime of the fluorophores.

The single exponential decay of the fluorophores in single dsDNA suggests the existence of single species and verifies the assumption that there is no big difference in molecular brightness among the fluorophores. Therefore, the proposed method is applicable to this dsDNA.

4.3.5 Fluctuation of normalized molecular brightness

Fluctuations in normalized molecular brightness are inevitable for the following reasons. First, Atto 647N has several states with different fluorescence intensity [86]. Second, there

are differences in local laser power that the individual fluorophores experience. That is, the laser intensity at focus is not flat but rather a point spread function, and consequently fluorophores located at different positions will be illuminated with different laser intensity.

In order to investigate the fluorescence intensity fluctuations of fluorophores, photobleaching was explored to determine the molecular brightness of single fluorophores. Individual fluorescence intensity drops are mainly due to the photobleaching of single fluorophores. They indicate the molecular brightness of the fluorophore which has experienced photobleaching. Therefore, by determining the fluorescence intensity drops of all individual bleaching steps, the variation of normalized molecular brightness of all fluorophores in one molecule complex can be approached. The histogram (red line) of one fluorescence intensity trace (black line) is plotted in Fig. 4.21. Several bleaching steps can be identified clearly in the

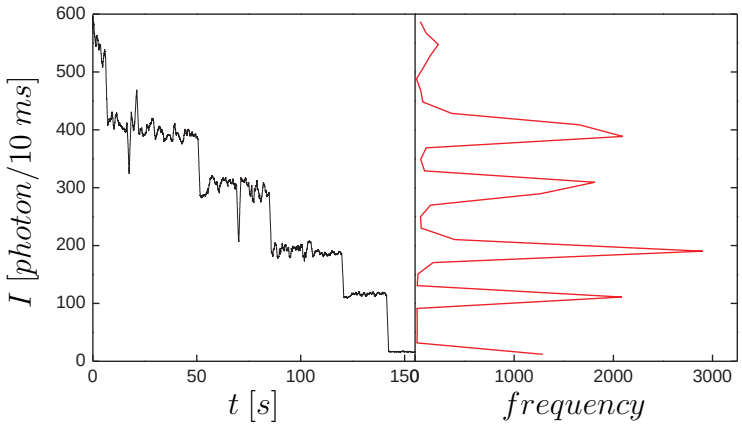

Figure 4.21: Fluorescence intensity histogram: The histogram (red line right) of fluorescence intensity of single dsDNA with 5 Atto 647N labels with the fluorescence intensity time trace (black line left). The peaks in the histogram corresponds to the fluorescence intensity plateaus in the fluorescence intensity time trace. The fluorescence intensity time trace is smoothed and the original bin size is $10\ ms$.

fluorescence intensity trace. Because the fluorescence intensity is rather stable and forms several plateaus between every two successive bleaching steps, the histogram is composed of several peaks. As a result, the difference of fluorescence intensity between two immediate

peaks gives the molecular brightness of one fluorophore.

A Statistics on 75 histograms shows the mean value of the standard deviation of normalized molecular brightness is 14.5%. The distribution of the relative standard deviation of normalized molecular brightness is not normally distributed (see the histogram of the standard deviation of molecular brithness in Fig. 4.22). It may be due to the different states, which

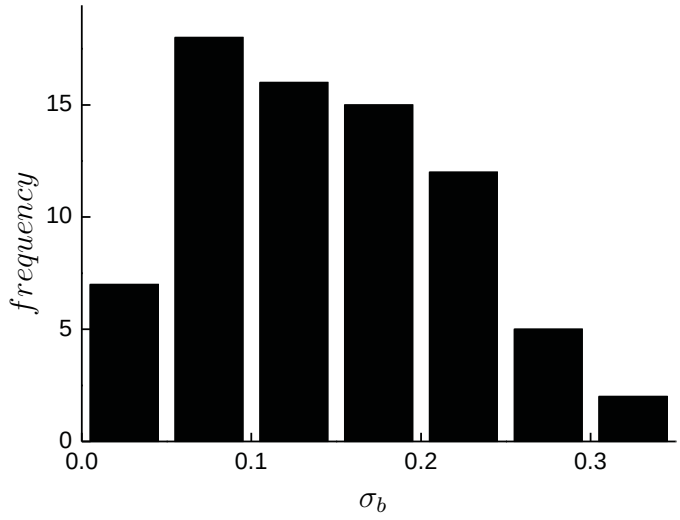

Figure 4.22: Distribution of the variation of molecular brightness: The histogram of the standard deviation σ_b of normalized molecular brightness of single dsDNA with 5 Atto0647N labels. The mean of the normalized molecular brightness standard deviation is 14.5%. Statistics are based on 75 samples.

Atto 647N resides [86]. Moreover, some of the traces show unexpected high fluorescence intensity drops. In addition, two overlapping photo bleaching steps are not excluded in the statistics and they contribute the abnormity of the distribution. Further studies are needed to explain the distributions.

Although fluctuations in normalized molecular brightness at room temperature and aqueous environment can not be avoided, and they violate the assumptions of the model, the model

still works very well on both simulated data and experimental data with even around 20% variation in molecular brightness.

Above all, a new method was built to extend the molecule counting ability of photon antibunching. A TCSPC setup was established with picosecond-pulsed laser excitation and four detectors, which is an extension of two-detector setup. A four-detector setup is able to detect more two simultaneous photon pairs than a two-detector setup and also detect multiple (triple/quadruple) simultaneous photons. A theoretical model was developed based on four (multiple) detection channels. Photobleaching is also included in the model to take advantage of all photons. Evaluation of the model by simulations predicts the feasibility of the method on 50 fluorescent molecules. The performance of the method on real experimental data proved that the method is able to resolve 15 fluorescent molecules.

5 Discussion and Outlook

The trend that biology is becoming a more quantitative science has been recently stimulated by advances in sensitivity of instruments, fast and automatic data acquisition and analysis facilitated with computing power. Quantitative approaches to biological problems will continue to extend our knowledge in understanding and predicting the behaviors of biological systems. However, limited by optical resolution of microscope, the structures of many macromolecules in their physiological conditions still remain unclear. Quantifying the stoichiometry of a biological system is one of the top demands of quantitative biology, especially when the size of the system is below the optical resolution of modern microscopes.

Photon antibunching has been used to determine the number of fluorescent copies in biological systems. However, former attempts were limited to about 3 molecules. A new method has been built based on photon antibunching to quantify more fluorescent molecules. Helped with four detectors and photostabilizing buffer, the method is able to collect more simultaneously detected photons from a certain number of fluorophores than former methods. The method uses a new theoretical model based on four (multiple) detection channels, which is able to describe photobleaching, and extends the ability of photon antibunching to count more than 10 molecules.

In this chapter, some discussions about the proposed model and the comparison between simulations and experiments are presented. Moreover, some potential applications of the proposed method in biological systems are prospected. In the end, some extensions and developments of photon antibunching are suggested.

5.1 Photon statistics enhancement

Former attempts to count molecules by photon antibunching with two detectors were limited by poor statistics [92, 79], especially the lack of enough correlated photon pairs (two-photon-detection events). To get better photon statistics, four independent detection channels are used. On one hand, they collect 1.5 times more two photon pairs, which is discussed in Section 4.1.2. On the other hand, they are also able to detect multiple(triple/quadruple)-photon-detection events, which is another advantage over two detection channels. Moreover, the maximum photon count rate of four independent detection channels is two times higher than two channels. Therefore, four channels have enabled us to collect the photons from a higher number of fluorophores without saturating detectors and data acquisition cards in a short time (seconds).

Beside four detection channels, a photostabilizing buffer is also used to achieve better photon statistics. Oxygen plays a very important role in fluorescence in two ways. On one hand, it is mainly responsible for photobleaching via photo-oxidation. On the other hand, it is an efficient triplet-state quencher. Triplet state is metastable and prevents the return of fluorophores to ground state for next excitation cycle. The photostabilizing buffer is composed of the agents to deplete the oxygen in the solution and delay photobleaching. It is also composed of both a reducing and an oxidizing agent, which is a compensation of oxygen as a triplet-state quencher. Therefore, it is able to both enhance fluorescent molecular brightness by diminishing blinking and prolong the lifetime of fluorophores by delaying photobleaching [86].

However, although the photon statistics can be increase by both four detection channels and photostabilizing buffer, photon antibunching method is still suffering from photobleaching because photonbleaching is inevitable, especial when the number of fluorophores is higher than 10. Therefore, in order to overcome this problem, I have established a new model which includes photobleaching (see Section 4.1.2) and, consequently, the method is able to use the

photons from all fluorophores theoretically. Experiments proved that the new method is able to resolve at least 15 fluorescent molecules.

Therefore, four detection channels, photostabilizing buffer and a new algorithm which considers photobleaching are combined to extend the molecule counting ability of photon antibunching.

5.1.1 A model with photobleaching

In practice, the model with photobleaching is able to provide more reliable performance than the model without photobleaching. If bleaching is not considered, only a part of the fluorescence trace, which is before the first bleaching happens, can be used to perform the estimation. Since photobleaching happens stochastically, the first bleaching is liable to take place early as the number of fluorophores is high. Therefore, the effective part of the fluorescence trace is heavily shortened. As an example shown in Fig. 5.1, four time intervals start all at $t = 0$ and end at different time point from $2.0s$ to $12.2s$. The estimation (Tab. 5.1) by the model without photobleaching gives reasonable values of the number of fluorophores when the time intervals (T_1 and T_2) do not include many photobleaching steps. If the time intervals (T_3 and T_4) include several bleaching steps, the estimation turns to provide fake numbers of fluorophores. However, as long as photobleaching is considered, the estimation becomes more stable even the time intervals span over a large range (Fig. 5.1 & Tab. 5.1).

Table 5.1: Estimation of the number of fluorophores with and without considering photobleaching.

		n_{est}	
Time intervals	Time	No bleaching	With bleaching
T_1	$0 - 2.0s$	5.85 ± 1.17	5.29 ± 1.05
T_2	$0 - 4.7s$	5.00 ± 1.00	4.71 ± 0.94
T_3	$0 - 9.3s$	10.60	5.16 ± 1.03
T_4	$0 - 12.2s$	54.73	5.38 ± 1.08

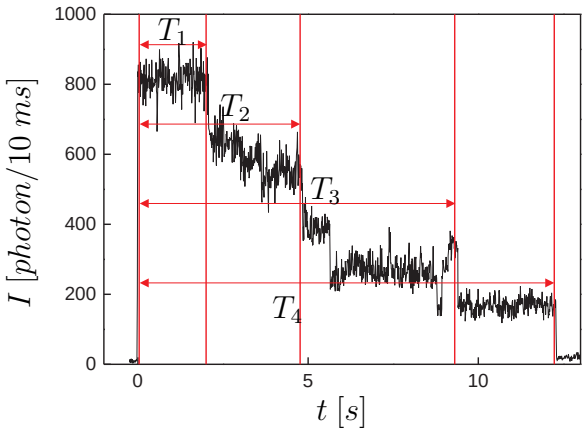

Figure 5.1: Influence of considering photobleaching: A dsDNA with 5 Atto 647N is illuminated by a 635nm laser with a repetition rate of $10MHz$ and laser power of $10\mu W$ or $8KW/cm^2$ at the focus. Four time intervals, T_1 $(0-2.0s)$, T_2 $(0-4.7s)$, T_3 $(0-9.3s)$ and T_4 $(0-12.2s)$ are chosen in the fluorescence intensity trace. The time intervals are subject to coincidence analysis without and with photobleaching. The estimation of the number of fluorophores is listed in Tab. 5.1. Background is taken into account in both cases and background photon probability is determined after all the fluorophores are bleached, which is $1.9 \cdot 10^{-4}$.

Although the model without photobleaching is able to provide reasonable estimation in most cases, the estimation is sensitive to the time intervals and more attention is therefore needed to choose proper time intervals. On the contrary, if photobleaching is included, there is more freedom to choose time intervals and the estimation is more reliable.

5.1.2 Instant number of fluorophores by fluorescence intensity

Photobleaching is unavoidable and results in losing fluorophores. In order to include photobleaching, the model is modified by considering the changes in the number of fluorophores (see Section 4.1.2). Because photobleaching is not predictable, the changes in the number of fluorophores can only be indicated by fluorescence intensity changes. Therefore, the instant number of fluorophores left in fluorescence-on state is approximately given by the instant fluorescence intensity according to the initial fluorescence intensity. However, the

fluorescence intensity is influenced not only by the changes in the number of fluorophores, but also by noise and the fluctuation of molecular brightness. Since fluorescence intensity in TCSPC (see Section 2.2) is given by the number of photons in a certain period, the noise is mainly from shot noise and the standard deviation of the photon number follows the square root of the intensity. Moreover, the fluctuation of molecular brightness is from the fluctuation of the local environment of the fluorophores and different states which the fluorophores reside. Therefore, even if the number of fluorophores remains constant, the fluorescence intensity fluctuates. However, the model makes use of the integration of multiple-photon-detection events. Thus, the fluctuation in fluorescence intensity by noise and the fluctuation in molecular brightness are canceled by integration.

Moreover, the measured fluorescence intensity is not the real fluorescence intensity. There are chances that multiple photons reach the same detector in one laser cycle. If more than one photon reaches one detector in a short time, only the first photon is detected and the rest are neglected due to the dead time of the detector and data acquisition card. Therefore, the measured fluorescence intensity has to be compensated by those neglected photons. However, if multiple-photon-detection events are rare, the measured fluorescence intensity can provide a good approximation to the real one.

By describing photobleaching with the instant fluorescence intensity, the method is able to use all photons and there is no limit to choose time intervals. Therefore, reliable estimation of the number of fluorophores is obtained by the method.

5.2 Influence of two-photon emission from one fluorophore

The adaption of photon antibunching in TCSPC results in that ”only” one photon can be emitted by one fluorophore in each laser cycle. The condition of the state is that the duration of a laser excitation pulse is much shorter than the excited-stated lifetime of the fluorophores. It is one of the most important assumptions of the model. However, the probability of observing two photons from one fluorophore in one laser cycle is not absolute zero. It has been explored in Section 4.1.1, but it is worth to examine it again by examining its influence on the algorithm.

To simplify the system, the incident laser pulse is roughly considered as a rectangular function with a width a, which is equal to the full-width at half-maximum (FWHM) of the laser pulse. The probability of one- and two-photon-detection events, $\widetilde{P}^{(1)}$ and $\widetilde{P}^{(2)}$, can be approximately given by Eq. 4.10 and Eq. 4.11 respectively. A direct conclusion of the two formulas is that the probability of two-photon-detection events is proportional to the square of the probability of one-photon-detection events, which is given by

$$\widetilde{P}^{(2)} = (\widetilde{P}^{(1)})^2(a/\tau_s)/6 \tag{5.1}$$

where τ_s is the excited-state lifetime of the fluorophore.

According to the definition of normalized molecular brightness p in Section 4.1.2, the probability of one-photon-detection events from one fluorophore is the normalized molecular brightness, which means $\widetilde{P}^{(1)} = p$. In reality $\widetilde{P}^{(1)} << 1$, so $\widetilde{P}^{(2)}$ is even smaller.

However, it is more interesting to examine the influence of two-photon-detection events from single fluorophores to those from different fluorophores. The ratio R of the probability of two-photon-detection events from single fluorophores $n\widetilde{P}^{(2)}$ (n is the number of

fluorophores.) to that from different fluorophores $P_4(n,p,i=2)$ (Eq. 4.18) is given by

$$R = \frac{n\widetilde{P}^{(2)}}{P_4(n,p,i=2)} = \frac{4}{9}\frac{a}{\tau_s}\frac{1}{(n-1)} \tag{5.2}$$

In this work, $a \approx 0.1ns$ and $\tau \approx 4ns$, therefore, $R \approx \frac{1}{90(n-1)}$. That is, as long as the number of fluorophore is higher than 1, the contribution of two-photon-detection events from single fluorophores is only about 1% or less of the overall two-photon-detection events.

If there is only one fluorophore, two-photon-detection events only come from the same fluorophore. The influence of two-photon-detection events can be explored by applying the estimation on the number of fluorophores. As $p << 1$, the estimated number can be given by Eq. 4.19, which is

$$n_{est} = \frac{3P_4(n,p,i=1)^2}{3P_4(n,p,i=1)^2 - 8\widetilde{P}^{(2)}} = \frac{1}{1-\frac{4}{9}\frac{a}{\tau_s}} \tag{5.3}$$

Here, $P_4(n,p,1)$ is approximated by Eq. 4.18. By substituting the value of a and τ_s with $0.1\ ns$ and $4\ ns$, n_{est} is equal to 1.01, which is only 1% more than the expected value 1.

Therefore, the influence of two-photon-detection events from single fluorophores is not significant. The assumption of no more than one photon per fluorophore per laser cycle is reasonable.

5.3 Bias and error of the estimation

The bias and error of the estimation by the method result from several factors.

- The model is a simplification of the real problem and the parameters of the model are also an approximation of the real ones;
- The noise in TCSPC is mainly shot noise;
- Background includes the Rayleigh scattering, Raman scattering, background photons and electronic noise from the devices, such as the dark count rate of the detectors;
- The multiple-photon-detection events are correlated, but they are still subject to the non-linear regression algorithm.

Although some of them have been explored in Chapter 4, the bias and the error of the method are discussed again from different respects in this part.

5.3.1 Underestimation induced by variation of molecular brightness

The model assumes that all the fluorophores have the same molecular brightness. In fact, the variation in molecular brightness is inevitable for the differences in laser intensity and local environments which the fluorophores experience. Nevertheless, simulations and experiments have demonstrated that the method is still applicable. Furthermore, simulations demonstrate that the method is inclined to underestimate the number of fluorophores when the variation of the molecular brightness increases (Fig. 4.12(b)). This underestimation can be explored theoretically in a simple case with two fluorophores.

Assume there are two fluorophores with normalized molecular brightness $p + \Delta p$ and $p - \Delta p$, $\Delta p < p$, under consideration. Thus, p and Δp are the average and variation of the normalized molecular brightness respectively. All other conditions are the same as that in Section 4.1.2. The probability $P(p,\Delta p,i)$ to observe i-photon-detection events in one laser

cycle, $i = 0, 1, ..., m$ where m is the number of detection channels, can be expressed similarly as Eq. 4.12 and given by

$$P(p,\Delta p,i) = \begin{pmatrix} m \\ i \end{pmatrix} ((i \cdot \frac{p+\Delta p}{m} + 1 - p - \Delta p)(i \cdot \frac{p-\Delta p}{m} + 1 - p + \Delta p) - \sum_{k=0,k>0}^{i-1} \frac{\begin{pmatrix} i \\ k \end{pmatrix}}{\begin{pmatrix} m \\ k \end{pmatrix}} P(p,k)) \tag{5.4}$$

Since four detection channels are mainly used in this work, here m is also given as 4. Therefore, Eq. 5.4 can be simplified as

$$\begin{aligned} P(p,\Delta p,0) &= 1 - 2p + p^2 - \Delta p^2 \\ P(p,\Delta p,1) &= 2p - \frac{7}{4}p^2 + \frac{7}{4}\Delta p^2 \\ P(p,\Delta p,2) &= \frac{3}{4}p^2 - \frac{3}{4}\Delta p^2 \\ P(p,\Delta p,3) &= P(p,\Delta p,4) = 0 \end{aligned} \tag{5.5}$$

If the proposed method is applied to these coincidence probabilities in Eq. 5.5, the number of fluorophores n can be calculated from Eq. 4.19 by taking into account that $\Delta p < p << 1$

$$n_{est} \approx \frac{4p^2}{2p^2 + 2\Delta p^2} \tag{5.6}$$

When the variation of the molecular brightness Δp is 0, the estimated number n_{est} is 2 as expected. However, when Δp increases, n_{est} decreases. It conveys the same information as simulations demonstrate that when the variation of the molecular brightness increases, the estimated number of fluorophores decreases.

At the same time, according to Eq. 5.5 when there is no variation of the molecular brightness,

$\Delta p = 0$, the probability for two-photon-detection events reaches its maximum value, if the fluorescence intensity, which is the sum of the molecular brightness of the two fluorophores $2p = p + \Delta p + p - \Delta p$, remains constant. Actually, this conclusion can be extended to more than two molecules, but more sophisticated deduction is needed.

5.3.2 Correlation of estimation

LM algorithm is used in the proposed method to obtain the best fit parameters based on the occurrence of multiple-photon-detection events. It requires the independence of the multiple-photon-detection events. However, multiple-photon-detection events are from a multinomial distribution. Therefore, they are correlated to each other and the correlations are expressed by Eq. 4.28. It partially explains the abnormality of the average value of the estimated normalized molecular brightness $\overline{p}_{est}$ (Fig. 5.2). $\overline{p}_{est}$ is fluctuating around the

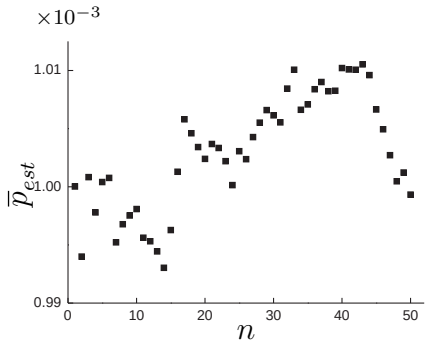

Figure 5.2: Estimation of normalized molecular brightness on simulated data: $\overline{p}_{est}$, the average of the estimated normalized molecular brightness p, is plotted against the number of fluorophores n with excitation laser pulses $N = 10^8$, $p = 10^{-3}$, and the statistics are based on 500 simulations.

expected value, but they are not randomly distributed. However, the deviation of $\overline{p}_{est}$ from their expected value is as low as 1% and has little effect on the performance of the method. Furthermore, a non-Gaussian behavior can also be identified with the estimated number of fluorophores. Moreover, the number of fluorophores in simulations is always an integer, but it can be any real number in Eq. 4.12 or 4.21. Thus, the LM algorithm base on these equations can not perfectly reflect the the simulated number of fluorophores.

Nevertheless, the influence of correlation among the multiple-photon-detection events and the integer requirement of fluorophore number are not considerable and do not destroy the calculations.

5.3.3 Error of the estimation

Multiple-photon-detection events are used to perform the estimation. They are identified by comparing the photon arrival times. If some photon arrival times fall into the same laser cycle, they are a multiple-photon-detection event. By scanning all the photons, the numbers of multiple-photons-detection events is obtained and ready to perform the estimation. An example of multiple-photon-detection events is shown in Fig. 5.3(b) (right, black square). They are from the part of a photon count trace in time interval T_1 recorded from

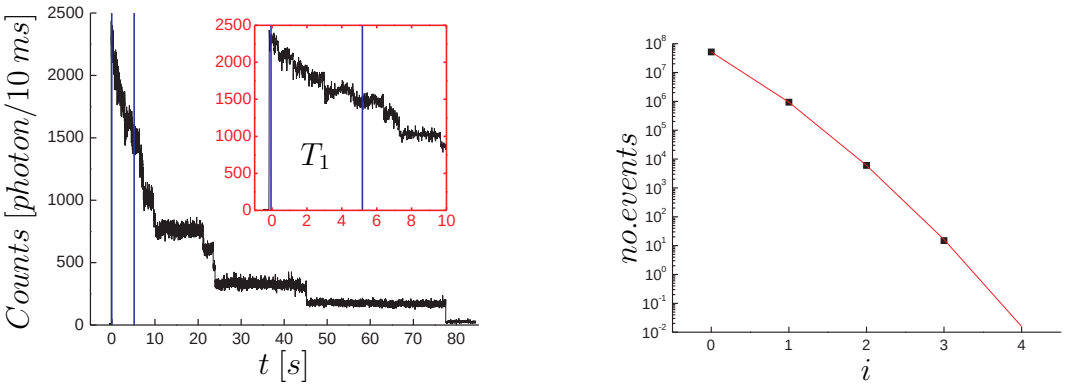

(a) (b)

Figure 5.3: An example of multiple detection events: A time interval $T1$ is chosen in a fluorescence intensity trace ((a) with a zoom inset) of a single ds-DNA complex with multiple Atto 647N dyes. The number of i-photon-detection events (black squares in (b)), $i = 0,1,...,4$, is obtained by analyzing the part of the photon trace in $T1$ and plotted with a fit (red line in (b)). The best fit parameters are $n = 15.452$ and $p = 1.3952$. The 95% confidential interval of the parameters are $15.378 \sim 15.526$ and $0.0013885 \sim 0.0014019$ respectively.

a dsDNA with multiple fluorophores (fluorescence intensity trace is shown in Fig. 5.3(b)

left). LM algorithm provides a fitting line (right, red line) with parameters $n = 15.452$ and $p = 1.3952$. The 95% confidential intervals of the parameters are very narrow with widths less than 1% of the corresponding parameters. However, simulations indicate that the error of estimated number of fluorophores is above 10% as discussed in Section 4.3.2. It appears that LM algorithm and statistics contradict to each other. Actually, on one hand, because the multiple-photon-detection events are anticorrelated to each other (Eq. 4.28), the error from LM algorithm is not able to reflect the real error of the estimation. On the other hand, the fluorophores have different molecular brightness even when they are in one dsDNA construct, which violates the assumptions of the model. Therefore, the model is only a simplification of the reality and provides parameters of the model instead of physical values. In fact, it is not possible to explore the molecular brightness of each fluorophore at the same time by this model because the degree of freedom exceeds the number of observable dependent values. As a result, even if the fitting provides a rather 'reliable' parameter estimation, the real error of the estimation is beyond the error given by LM algorithm.

The statistics of the estimation on systems with $1 - 5$ fluorophores (Fig. 4.16) indicates that there is an overestimation of the method in comparison with counting bleaching steps. However, counting bleaching steps is not a perfect reference because it may underestimate the number of fluorophore. For example, if two steps are so close to each other that they can not be discerned, the number of bleaching steps is underestimated. It means, on the contrary, an 'overestimation' is introduced to the proposed method. Furthermore, it is taken for granted that there is only one background photon in one laser cycle. However, according to the estimation on page 56 in Section 4.1.2, two background photons may occur more than once. These two background photons also lead to an overestimation of the number of fluorophores.

Therefore, simulations have provided a better evaluation of the error (standard deviation) of the estimation, which is 10-20 percent.

5.3.4 Occurrence of multiple-photon-detection events

In order to observe photon antibunching, it is necessary to examine the correlated photons. Therefore, a Hanbury Brown-Twiss setup with two detectors (one to start the measurement and the other to stop) is frequently used. A four-detector setup, as an extension of Hanbury Brown-Twiss setup, is able to detect not only two-photon events, but also triple- and quadruple-photon events. Although the probability to observe two-photon events is low, they are detectable and are able to provide good statistics under normal experimental conditions as long as there is more than one fluorophore under consideration. However, triple-photon-detection events are rare. Their occurrence is not significant unless the number of fluorophores is more than 10 according to my observation. When it comes to quadruple-photon-detection events, the chance is negligible. Simulations indicate that it is possible to observe quadruple-photon-detection events only if the number of fluorophores is close to 50 (see Section 4.2.1). No quadruple-photon-detection events have been identified under the experimental conditions in this work with less than 20 fluorophores.

If the triple-photon-detection events are populated and provide enough data, they will contribute to the parameter estimation. As discussed in Section 4.1.2, there are simple relations among the multiple-photon-detection events (Eq. 4.19 and 4.20). Although, only the two-photon-detection and single-photon-detection events are involved in these equations, it is also possible to include triple- and quadruple-photon-detection events. An example with the probability of triple-photon-detection events deduced from Eq. 4.18 is given by

$$n = \frac{2P_4(n,p,i=1)P_4(n,p,i=2)}{P_4(n,p,i=1)P_4(n,p,i=2) - 6P_4(n,p,i=3)} \tag{5.7}$$

$$p = \frac{1}{2}P_4(n,p,i=1) - \frac{3P_4(n,p,i=3)}{P_4(n,p,i=2)} \tag{5.8}$$

where all symbols have the same meanings as those in Eq. 4.18.

There are several combinations which provide estimation of n and p because the system

is overdetermined (two parameters n and p with 5 multiple-photon-detection events). It is also the reason that a regression was chosen to estimate the parameters. As long as the triple-photon-detection events start to populate, they will enhance the performance of the estimation.

5.4 Potential applications of coincidence analysis in biological systems

As the principle has been proved by both simulations and experiments, coincidence analysis has promising applications on many aspects of biological systems, such as determining the stoichiometry of DNA-dendrimer complexes, protein aggregations, receptor clusters on cell membrane and so on.

The dendrimers were firstly synthesized by several groups or companies such as Voegtle in 1978 [19], Denkewalter and coworkers at Allied Corporation in 1981 [26] and so on. Dendrimers have well defined structures resulting from stepwise synthetic processes and are distinct from less well-defined hyperbranched polymers. Because of the possibilities to be designed with both internal hydrophobicity and surface hydrophilicity, dendrimers has been attracting many interests for delivering genes [60] or hydrophobic drugs [33] into living cells. However, the mechanisms of the interaction of DNA and dendrimer are poorly understood [14]. By stoichiometrically labeling DNA and dendrimer, the interaction of them can be explored by coincidence analysis.

Macromolecular assembly and disassembly are essential for cellular structure and function. An example of assembly is protein aggregation. Abnormal protein aggregation characterizes many neurodegenerative disorders and severe diseases [42, 2]. Quantifying the stoichiometry of protein aggregation and disaggregation is important for controlling protein aggregation

and studying the mechanism of chaperone mediated protein disaggregation, such as Hsp104/ClpB and Hsp70 chaperone systems [90]. The dynamics and the size distribution of protein aggregations have been investigated by some methods [64]. Photon antibunching is a potential tool to provide the information of the stoichiometry of protein aggregation at single aggregation level by immobilizing them on a surface. Fluorescent labeled protein

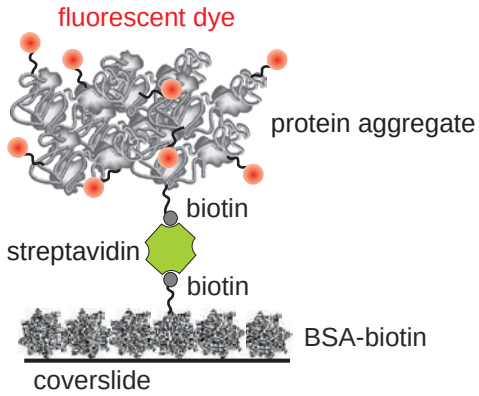

Figure 5.4: Protein aggregation stoichiometry exploration: Protein is labeled stoichiometrically with fluorescent dyes and induced to aggregate. Immobilization of aggregation can be realized by biotin-streptavidin system to BSA-biotin surface.

aggregation can be immobilized via biotin-streptavidin system to a BSA-biotin surface (Fig. 5.4). The stoichiometry of immobilized protein aggregations can be explored by the proposed method.

Furthermore, the number of receptors in a cluster on cell membrane is always interesting for biologists. As an example, the neuroreceptors on the post-synaptic membrane is one of the important components in the information flows from one neuron to another neuron across a synapse. Coincidence analysis provides the possibility to investigate the size or even the change in size of neuroreceptors, thus helps to understand and diagnose the abnormalities of neurons.

As a method, coincidence analysis is ready for applications in biological systems to enrich our understanding of the unknown world which can not be resolved by modern optical mi-

croscopy.

5.5 Further development of coincidence analysis and photon antibunching

The molecule counting by coincidence analysis is limited by the number of fluorophores which are labeled to single complexes. Therefore, some possible ways to achieve constructs with a higher number of fluorophores are explained in order to explore the limit of the method in counting molecules. Moreover, two kinds of stable fluorescent particles are suggested to circumvent the photobleaching problem of organic dyes. Furthermore, photon antibunching is also able to investigate protein-protein interaction by combining with other techniques, such as multiple-color labeling. In the end, as a phenomenon, photon antibunching is applicable not only to determine the stoichiometry of fluorescent molecules but also to other problems, such as imaging and determining the orientation of transition dipole moments.

5.5.1 dsDNA with a higher number of fluorophores

My observations indicate that 15 fluorophores can be resolved by coincidence analysis. However, its limit has probably not been reached. By labeling dsDNA with more fluorophores, the counting ability of coincidence analysis can be explored further. One way to obtain dsDNA with more labels is to extend the long ssDNA used in this work with more repeated short sequences. After hybridization with the short complementary sequences, the dsDNA can carry a higher number of fluorophores. Another way is an extensible fashion. First, a dsDNA with several labels in the middle and two biotins at each end can be constructed as shown in Fig. 5.5 (a). Second, dsDNA can be immobilized via streptavidin-biotin linkage as shown in Fig. 5.5 (b). After coupled to another streptavidin, the immobilized dsDNA can be linked to another dsDNA as shown in Fig. 5.5 (c) and (d). By repeating this procedure several times, higher number of fluorophores can be immobilized on a single spot for further evaluation. Further more, it is also possible to design DNA origamis

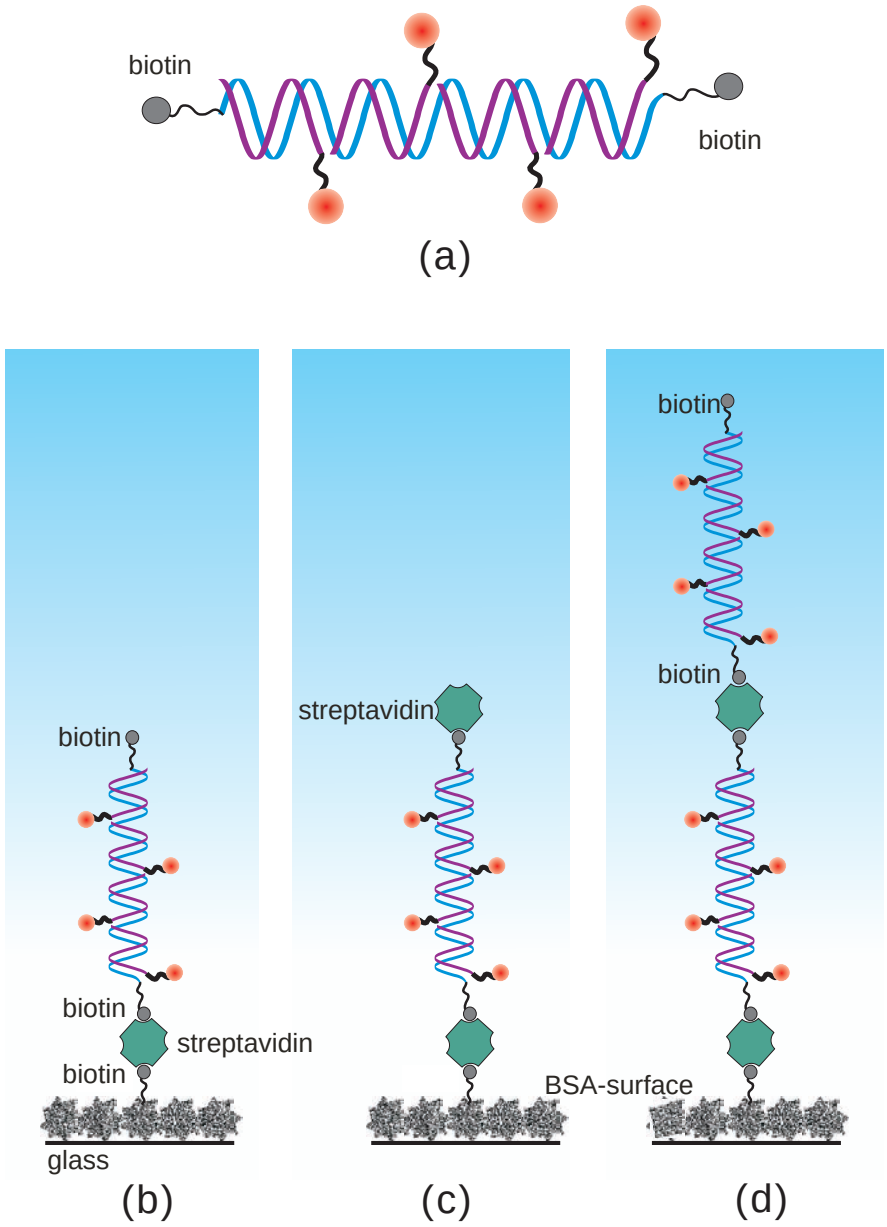

Figure 5.5: Immobilization of dsDNA with multiple labels: (a) A scheme of dsDNA with multiple labels in the strands and two biotins at each end, (b) a ds-DNA is immobilized on a surface, (c) additional streptavidin makes the immobilized dsDNA accessible to another biotin, (d) a second dsDNA can be linked to the immobilized dsDNA via streptavidin-biotin system. The surface is coated with a mixture of biotinylated BSA and BSA.

which have multiple labels. Although systems with a certain number of fluorophores can be programmed and realized, calibration of the method is not straightforward for the lack of ways to determine the exact number of fluorophores on single complexes.

5.5.2 Alternative fluorophores

An alternative to avoid photodestruction is to use more stable counterparts of organic dyes, such as quantum dots and fluorescent nanodiamonds, which are much more resistant to photobleaching and can be illuminated for hours or even longer [30, 85].

However, it will be more complicated to resolve the number of quantum dots when many quantum dots present at the same time due to their random blinking [57, 44] and possible multiple excitations [22]. Because the Auger ionization rate is much larger than the fluorescence decay [41], the multi-photon emission is suppressed. Therefore, Lounis *et al* observed perfect photon antibunching curves from a certain quantum dots over a wide range of excitation intensity [46]. Moreover, Wang *et al* were able to synthesize the first quantum dots without blinking [89]. Non-blinking quantum dots may be a good candidate for coincidence analysis.

There is also a limitation for fluorescent nanodiamonds because the occurrences of the fluorescent deficits in single nanodiamonds is not strictly 1:1 [83]. As a result, it is difficult to interpret the estimated number of fluorescent nanodiamods. However, if the number of nanodiamods is high, the statistics become better and the rough number of them still provides very interesting information.

5.5.3 Two-color coincidence analysis

A straightforward extension of coincidence analysis is to use two different fluorophores differing in emission spectra. The excitation beam path remains unchanged as one color coincidence analysis (Fig. 3.2). The detection beam path is separated into two by a dichroic mirror according to the wavelength of the fluorescence. Afterwards both are equally divided into m parts. The case with $m = 2$ is shown in Fig. 5.6. In an ideal case without background, the

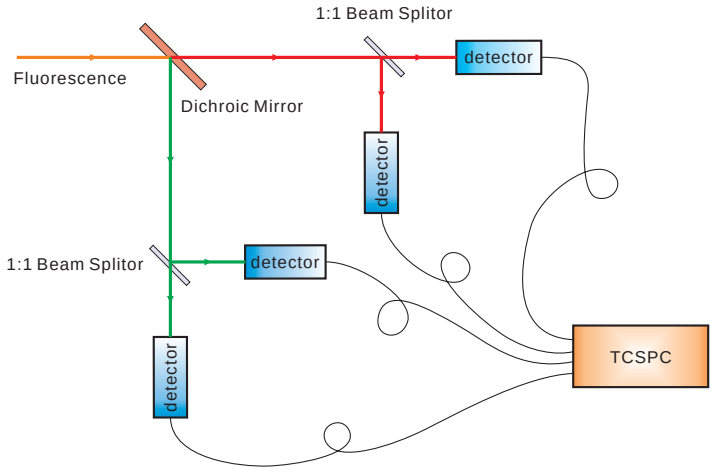

Figure 5.6: A scheme of the detection beam path of two-color coincidence analysis: Fluorescence radiation is separated with a dichroic mirror according to the wavelength (such as red and green) and each part is further divided into two parts by 1:1 beam splitters. The signals from detectors are fed to TCSPC cards.

probabilities of multiple photon detection can be given by

$$\begin{aligned} P_r(n_1,n_2,p_1,p_2,i) = \left(\begin{array}{c} mi \end{array} \right) ((1 - \frac{(m-1)p_1\rho_{1r}}{m})^{n_1}(1 - \frac{(m-1)p_2\rho_{2r}}{m})^{n_2} \\ - \sum_{k=0,k>0}^{i-1} \frac{\left(\begin{array}{c} ik \end{array} \right)}{\left(\begin{array}{c} mk \end{array} \right)} P(n_1,n_2,p_1,p_2,k)) \\ P_g(n_1,n_2,p_1,p_2,j) = \left(\begin{array}{c} mj \end{array} \right) ((1 - \frac{(m-1)p_1\rho_{1g}}{m})^{n_1}(1 - \frac{(m-1)p_2\rho_{2g}}{m})^{n_2} \\ - \sum_{k=0,k>0}^{j-1} \frac{\left(\begin{array}{c} jk \end{array} \right)}{\left(\begin{array}{c} mk \end{array} \right)} P(n_1,n_2,p_1,p_2,k)) \end{aligned} \tag{5.9}$$

where P_r and P_g are the coincidence probabilities of different colors; $i, j = 1, 2,..., m$; n_s and p_s ($s = 1, 2$) are the number and normalized molecular brightness of the s^{th} fluorophores respectively, ρ_{sc} ($s = 1, 2$ and $c = r, g$) are the percentages of the fluorescent contribution of the s^{th} fluorophore in c color channels. The ρ_{sc} can be determined by a calibration experiments beforehand by examining only the fluorophores or the single fluorophore labeled molecules. As proposed to obtain the number of fluorophores in this work, the nonlinear least square regression can be used to estimate n_s and p_s. The background can also be included in this model with a few efforts. In an ideal case there is no leakage between the two channels from the two fluorophores, or red channels only correspond to the red fluorophores and green channels to green. The estimation turns into two completely independent two-channel coincidence analyses. Two-color coincidence analysis can be applied to investigate protein-protein interactions, such as determining the stoichiometry of a complex formed by two different proteins.

5.5.4 Photon antibunching in imaging

It is also possible to apply coincidence analysis in imaging. Fluorescence intensity in an image is a relative indicator of the local richness of the fluorophores and influenced by many conditions surrounding the fluorophores, such as the existence of quenching molecules. Therefore, it is not always reliable to refer the concentration of the fluorophores to fluorescence intensity. Additional information derived from coincidence analysis can enrich the information of images by providing absolute numbers of fluorophores at each pixel. Moreover, the laser intensity always has a distribution, such as point spread function (PSF). Hence each fluorophore experience different laser intensity if they slightly differ in position. Therefore, when the laser focus moves across the fluorophores, the fluorescence intensity distribution will be broadened. For example, the superposition F_1 of the fluorescence intensity from two fluorophores provides a wider and higher peak at the middle of the two fluorophores (Fig. 5.7 (upper)). As a result, it is not possible to resolve the two fluorophores. However, the intensity

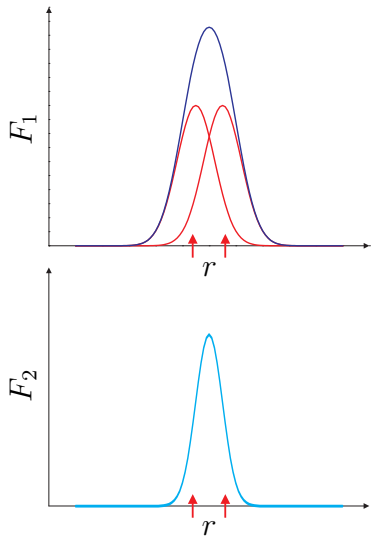

Figure 5.7: A scheme of photon antibunching in imaging: r is the position, F_1 is the fluorescence intensity in arbitrary unit. The blue curve (upper) is the superposition of the fluorescence intensity from two fluorophores. The arrows are where the two fluorophores are located. The fluorescence intensity of the two fluorophores is shown in red curve. The cyan curve F_2 (lower) is the intensity of correlated photon pairs in arbitrary unit.

of correlated photon pairs F_2 (blue curve in the lower picture of Fig. 5.7) indicates that there are more than one molecules and the width of F_2 is much narrower than F_1. Therefore, it is possible to determine the relative position of the fluorophores more precisely by the combination of intensity of fluorescence and correlated photon pairs than by fluorescence intensity alone.

5.5.5 Photon antibunching in orientation determination

The orientation of two transition dipole moments can be determined by examining the correlated photon pairs from them with linear polarized laser excitation. Assume that there are two transition dipole moments differing from each other by an angle θ as shown in Fig. 5.8. If a linear polarized laser is the excitation source, absorption of both the transition dipole moments can happen and may result in two-simultaneous-photon emission. However, when the polarization line of laser is perpendicular to one of the transition dipole moments, the photon antibunching is perfect and there are no correlated photon pairs at zero lag time. The

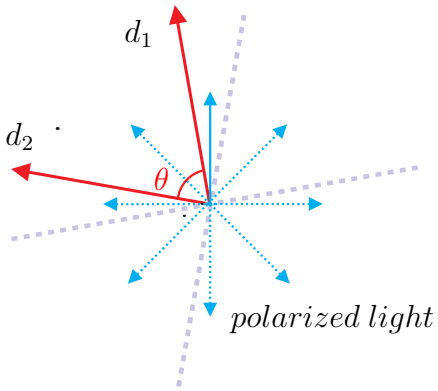

Figure 5.8: A scheme of coincidence analysis to determine the orientation of two transition dipole moments: θ is the angle between the dipoles of two transition dipole moments (d_1 and d_2). A rotation scan of linear polarized laser excitation (blue) can determine the orientation of the two transition dipole moments. When the orientation of the linear polarized laser is in certain planes (gray lines), only one of the transition dipole moments can be excited and photon antibunching will be perfect with no correlated photons at zero lag time.

reason is that no absorption will occur if the transition dipole moment and the polarization line of laser are perpendicular. For instance, a nanodiamond with two Nitrogen-Vacancy (NV) centers inside provides two defined transition dipole moments, which are close to each other. Therefore, photon antibunching can be used to determine the orientations of multiple stationary dipole moments.

As a conclusion, a new method is established to determine the stoichiometry of fluorescent molecules by photon antibunching. The method has several advantages. First, the method is not limited by optical resolution because photon antibunching is a quantum nature of fluorophores. For the same reason, it is also free of calibration. Second, it applies to single molecule complexes. An average over a large number of fluorescent complexes is not necessary. Third, coincidence analysis is implemented in a standard confocal and TCSPC system, which is a standard configuration of many labs. Therefore, it can be easily integrated. Moreover, all the advantages of TCSPC are inherited. The multiplexed signals from TCSPC can provide fluorescence intensity, lifetime, and images of single molecules as

well as the photon antibunching information at the same time. In addition, the background photons and the photobleaching are both included in the model, which makes coincidence analysis suitable for many circumstances. However, photon antibunching method requires the fluorophores to be very photostable. Even with the help of photostabilizing agents, photobleaching is still a big challenge, especially when many fluorophores is under consideration. Moreover, photostabilizing agents, such as ROXS [86] or Trolox system [3, 66] make the method not feasible in living cell for the compatibility problem of the agents with physiological conditions.

It is the first time that photon antibunching has been proved to be able to quantify the stoichiometry of up to 15 fluorescent molecules. Because it is not limited by optical diffraction, photon antibunching is able to explore the mostly unknown world, which is under the optical resolution of modern microscope and lack of proper methods to explore. Photon antibunching is a powerful tool to extend our knowledge in basic problems in biology and deepen our understanding of the mechanism of many biological functions.

Bibliography

[1] J. A. Abate, H. J. Kimble, and L. Mandel. Photon statistics of a dye laser. *Phys. Rev. A*, 14(2):788–795, Aug. 1976.

[2] A. Aguzzi and A. M. Calella. Prions: Protein aggregation and infectious diseases. *Physiol. Rev.*, 89(4):1105–1152, Oct. 2009.

[3] C. E. Aitken, A. R. Marshall, and J. Puglisi. An oxygen scavenging system for improvement of dye stability in single-molecule fluorescence experiments. *Biophys. J.*, pages 1826–1835, October 2007.

[4] A. P. Alivisatos. Semiconductor clusters, nanocrystals, and quantum dots. *Science*, 271(5251):933–937, 1996.

[5] W. P. Ambrose, P. M. Goodwin, J. C. Martin, and R. A. Keller. Single molecule detection and photochemistry on a surface using near-field optical excitation. *Phys. Rev. Lett.*, 72(1):160–163, Jan. 1994.

[6] E. S. Andersen, M. Dong, M. M. Nielsen, K. Jahn, R. Subramani, W. Mamdouh, M. M. Golas, B. Sander, H. Stark, C. L. P. Oliveira, J. S. Pedersen, V. Birkedal, F. Besenbacher, K. V. Gothelf, and J. Kjems. Self-assembly of a nanoscale dna box with a controllable lid. *Nature*, 459(7243):73–76, May 2009.

[7] B. Ballou, B. C. Lagerholm, L. A. Ernst, M. P. Bruchez, and A. S. Waggoner. Noninvasive imaging of quantum dots in mice. *Bioconjugate Chem.*, 15(1):79–86, Jan. 2004.

[8] T. Basche, W. E. Moerner, M. Orrit, and H. Talon. Photon antibunching in the fluorescence of a single dye molecule trapped in a solid. *Phys. Rev. Lett.*, 69(10):1516–1519, Sept. 1992.

[9] W. Becker. *The bh TCSPC Handbook*. 2006.

[10] R. E. Benesch and R. Benesch. Enzymatic removal of oxygen for polarography and related methods. *Science*, 118:447–448, 1953.

[11] A. Bergmann and R. Duncan. *Biological Application of FLIM by TCSPC*. 2006.

[12] E. Betzig and R. J. Chichester. Single molecules observed by near-field scanning optical microscopy. *Science*, 262(5138):1422–1425, Nov 1993.

[13] A. Beveratos, R. Brouri, T. Gacoin, J. P. Poizat, and P. Grangier. Nonclassical radiation from diamond nanocrystals. *Phys. Rev. A*, 64(6):061802–061805, 2001.

[14] A. U. Bielinska, J. F. Kukowska-Latallo, and J. R. Baker. The interaction of plasmid dna with polyamidoamine dendrimers: mechanism of complex formation and analysis of alterations induced in nuclease sensitivity and transcriptional activity of the complexed dna. *BBA-Gene Struct. Expr.*, 1353(2):180–190, Aug. 1997.

[15] E. M. Blalock, editor. *A Beginner's Guide to Microarrays*. Springer, 1 edition, July 2003.

[16] L. M. Bollinger and G. E. Thomas. Measurement of the time dependence of scintillation intensity by a delayed-coincidence method. *Rev. Sci. Instrum.*, 32(9):1044–1050, Sept. 1961.

[17] E. Brooks Shera, N. K. Seitzinger, L. M. Davis, R. A. Keller, and S. A. Soper. Detection of single fluorescent molecules. *Chem. Phys. Lett.*, 174(6):553–557, Nov. 1990.

[18] R. Brouri, A. Beveratos, J. P. Poizat, and P. Grangier. Photon antibunching in the fluorescence of individual color centers in diamond. *Opt. Lett.*, 25(17):1294–1296, 2000.

[19] E. Buhleier, W. Wehner, and F. Vagtle. "cascade"- and "nonskid-chain-like" syntheses of molecular cavity topologies. *Synthesis*, 1978(02):155–158, 1978.

[20] C. R. Calladine. *Understanding DNA: the molecule & how it works*. Elsevier, Amsterdam ; Heidelberg [u.a.], 3. ed. edition, 2004.

[21] M. Cavallini, M. Facchini, C. Albonetti, and F. Biscarini. Single molecule magnets: from thin films to nano-patterns. *Phys. Chem. Chem. Phys.*, 10(6):784–793, 2008.

[22] H.-S. Chang, W.-Y. Chen, T.-M. Hsu, T.-P. Hsieh, J.-I. Chyi, and W.-H. Chang. Origins of nonzero multiple photon emission probability from single quantum dots embedded in photonic crystal nanocavities. *Appl. Phys. Lett.*, 94(16):163111–3, Apr. 2009.

[23] Y. Chen, J. D. Muller, P. T. So, and E. Gratton. The photon counting histogram in fluorescence fluctuation spectroscopy. *Biophys. J.*, 77(1):553–567, July 1999.

[24] Y. Chen, M. Tekmen, L. Hillesheim, J. Skinner, B. Wu, and J. D. Mueller. Dual-color photon-counting histogram. 88(3):2177–2192, Mar. 2005.

[25] S. K. Das, M. Darshi, S. Cheley, M. I. Wallace, and H. Bayley. Membrane protein stoichiometry determined from the step-wise photobleaching of dye-labelled subunits. *ChemBioChem*, 8(9):994–999, 2007.

[26] K. J. L. W. J. Denkewalter, Robert G. Macromolecular highly branched homogeneous compound based on lysine units, September 1981.

[27] F. Diedrich and H. Walther. Nonclassical radiation of a single stored ion. *Phys. Rev. Lett.*, 58(3):203–206, Jan. 1987.

[28] M. A. Digman, R. Dalal, A. F. Horwitz, and E. Gratton. Mapping the number of molecules and brightness in the laser scanning microscope. *Biophys. J.*, 94(6):2320–2332, Mar. 2008.

[29] M. A. Digman, P. W. Wiseman, C. Choi, A. R. Horwitz, and E. Gratton. Stoichiometry of molecular complexes at adhesions in living cells. *PNAS*, 106(7):2170–2175, Feb. 2009.

[30] B. Dubertret, P. Skourides, D. J. Norris, V. Noireaux, A. H. Brivanlou, and A. Libchaber. In vivo imaging of quantum dots encapsulated in phospholipid micelles. *Science*, 298(5599):1759–1762, Nov. 2002.

[31] D.V.O'Connor and D. Phillips. *Time-Correlated Single Photon Counting*. Academic Press,London, 1984.

[32] E. Fuereder-Kitzmueller, J. Hesse, A. Ebner, H. J. Gruber, and G. J. Schuetz. Non-exponential bleaching of single bioconjugated cy5 molecules. *Chem. Phys. Lett.*, 404(1-3):13–18, Mar. 2005.

[33] E. R. Gillies and J. M. J. Frechet. Dendrimers and dendritic polymers in drug delivery. *Drug Discovery Today*, 10(1):35–43, Jan. 2005.

[34] K. G. Heinze, M. Jahnz, and P. Schwille. Triple-color coincidence analysis: One step further in following higher order molecular complex formation. *Biophys. J.*, 86(1):506–516, Jan. 2004.

[35] P. Kask, K. Palo, N. Fay, L. Brand, U. Mets, D. Ullmann, J. Jungmann, J. Pschorr, and K. Gall. Two-dimensional fluorescence intensity distribution analysis: Theory and applications. *Biophys. J.*, 78(4):1703–1713, 2000.

[36] P. Kask, K. Palo, D. Ullmann, and K. Gall. Fluorescence-intensity distribution analysis and its application in biomolecular detection technology. *PNAS*, 96(24):13756–13761, 1999.

[37] P. Kask, P. Piksarv, and . Mets. Fluorescence correlation spectroscopy in the nanosecond time range: Photon antibunching in dye fluorescence. *Eur. Biophys. J.*, 12(3):163–166, Aug. 1985.

[38] S.-K. Kim, C.-H. Cho, B.-H. Kim, S.-J. Park, and J. W. Lee. Electrical and optical characteristics of silicon nanocrystal solar cells. *Appl. Phys. Lett.*, 95(14):143120–3, Oct. 2009.

[39] H. J. Kimble, M. Dagenais, and L. Mandel. Photon antibunching in resonance fluorescence. *Phys. Rev. Lett.*, 39(11):691–695, Sept. 1977.

[40] H. J. Kimble and L. Mandel. Theory of resonance fluorescence. *Phys. Rev. A*, 13(6):2123–2144, June 1976.

[41] V. I. Klimov, A. A. Mikhailovsky, D. W. McBranch, C. A. Leatherdale, and M. G. Bawendi. Quantization of multiparticle auger rates in semiconductor quantum dots. *Science*, 287(5455):1011–1013, Feb. 2000.

[42] E. H. Koo, P. T. Lansbury, and J. W. Kelly. Amyloid diseases: Abnormal protein aggregation in neurodegeneration. *PNAS*, 96(18):9989–9990, Aug. 1999.

[43] M. U. Kumke, G. Li, L. B. McGown, G. T. Walker, and C. P. Linn. Hybridization of fluorescein-labeled dna oligomers detected by fluorescence anisotropy with protein binding enhancement. *Anal. Chem.*, 67(21):3945–3951, May 1995.

[44] M. Kuno, D. P. Fromm, H. F. Hamann, A. Gallagher, and D. J. Nesbitt. Nonexponential "blinking" kinetics of single cdse quantum dots: A universal power law behavior. *J. Chem. Phys.*, 112(7):3117–3120, Feb. 2000.

[45] J. R. Lakowicz. *Principles of fluorescence spectroscopy*. Springer, New York, 2006.

[46] B. Lounis, H. A. Bechtel, D. Gerion, P. Alivisatos, and W. E. Moerner. Photon antibunching in single cdse/zns quantum dot fluorescence. *Chem. Phys. Lett.*, 329(5-6):399–404, Oct. 2000.

[47] B. Lounis and W. E. Moerner. Single photons on demand from a single molecule at room temperature. *Nature*, 407(6803):491–493, Sept. 2000.

[48] M. Mandelkern, J. G. Elias, D. Eden, and D. M. Crothers. The dimensions of dna in solution. *J. Mol. Biol.*, 152(1):153–161, Oct. 1981.

[49] A. D. Mehta, M. Rief, J. A. Spudich, D. A. Smith, and R. M. Simmons. Single-molecule biomechanics with optical methods. *Science*, 283(5408):1689–1695, Mar. 1999.

[50] T. C. Messina, H. Kim, J. T. Giurleo, and D. S. Talaga. Hidden markov model analysis of multichromophore photobleaching. *J. Phys. Chem. B*, 110(33):16366–16376, Aug 2006.

[51] X. Michalet, F. F. Pinaud, L. A. Bentolila, J. M. Tsay, S. Doose, J. J. Li, G. Sundaresan, A. M. Wu, S. S. Gambhir, and S. Weiss. Quantum dots for live cells, in vivo imaging, and diagnostics. *Science*, 307(5709):538–544, Jan. 2005.

[52] P. Michler, A. Imamoglu, M. D. Mason, P. J. Carson, G. F. Strouse, and S. K. Buratto. Quantum correlation among photons from a single quantum dot at room temperature. *Nature*, 406(6799):968–970, Aug. 2000.

[53] W. E. Moerner. A dozen years of single-molecule spectroscopy in physics, chemistry, and biophysics. *J. Phys. Chem. B*, 106(5):910–927, Feb. 2002.

[54] W. E. Moerner and D. P. Fromm. Methods of single-molecule fluorescence spectroscopy and microscopy. *Rev. Sci. Instrum.*, 74(8):3597–3619, Aug. 2003.

[55] W. E. Moerner and L. Kador. Optical detection and spectroscopy of single molecules in a solid. *Phys. Rev. Lett.*, 62(21):2535–2538, May 1989.

[56] W. E. Moerner and M. Orrit. Illuminating single molecules in condensed matter. *Science*, 283(5408):1670–1676, Mar. 1999.

[57] M. Nirmal, B. O. Dabbousi, M. G. Bawendi, J. J. Macklin, J. K. Trautman, T. D. Harris, and L. E. Brus. Fluorescence intermittency in single cadmium selenide nanocrystals. *Nature*, 383(6603):802–804, Oct. 1996.

[58] M. Olek, J. Ostrander, S. Jurga, H. Mohwald, N. Kotov, K. Kempa, and M. Giersig. Layer-by-layer assembled composites from multiwall carbon nanotubes with different morphologies. *Nano Lett.*, 4(10):1889–1895, Oct. 2004.

[59] M. Orrit and J. Bernard. Single pentacene molecules detected by fluorescence excitation in a p-terphenyl crystal. *Phys. Rev. Lett.*, 65(21):2716–2719, Nov. 1990.

[60] C. M. Paleos, L.-A. Tziveleka, Z. Sideratou, and D. Tsiourvas. Gene delivery using functional dendritic polymers. *Expert Opinion on Drug Delivery*, 6(1):27–38, Jan. 2009.

[61] K. Palo, U. Metz, S. Jager, P. Kask, and K. Gall. Fluorescence intensity multiple distributions analysis: Concurrent determination of diffusion times and molecular brightness. *Biophys. J.*, 79(6):2858–2866, 2000.

[62] W. Patrick Ambrose, P. M. Goodwin, J. Enderlein, D. J. Semin, J. C. Martin, and R. A. Keller. Fluorescence photon antibunching from single molecules on a surface. *Chem. Phys. Lett.*, 269(3-4):365–370, May 1997.

[63] W. Press, S. Teukolsky, W. Vetterling, and B. Flannery. *Numerical recipes in C (2nd ed.): the art of scientific computing*. Cambridge University Press, New York, NY, USA, 1992.

[64] J. Puchalla, K. Krantz, R. Austin, and H. Rye. Burst analysis spectroscopy: A versatile single-particle approach for studying distributions of protein aggregates and fluorescent assemblies. *PNAS*, 105(38):14400–14405, Sept. 2008.

[65] R. Q. T. R. Hanbury Brown. Correlation between photons in two coherent beams of light. *Nature*, 177:27–29, 1956.

[66] I. Rasnik, S. A. McKinney, and T. Ha. Nonblinking and long-lasting single-molecule fluorescence imaging. *Nat Meth*, 3(11):891–893, Nov. 2006.

[67] R. R.Hanbury Brown. Correlation between photons in two coherent beams of light. *Nature*, 177:27–29, 1956.

[68] R. Rigler, . Mets, J. Widengren, and P. Kask. Fluorescence correlation spectroscopy with high count rate and low background: analysis of translational diffusion. *Eur. Biophys. J.*, 22(3):169–175, Aug. 1993.

[69] R. Rossetti, S. Nakahara, and L. E. Brus. Quantum size effects in the redox potentials, resonance raman spectra, and electronic spectra of cds crystallites in aqueous solution. *J. Chem. Phys.*, 79(2):1086–1088, July 1983.

[70] R. Roy, S. Hohng, and T. Ha. A practical guide to single-molecule fret. *Nat Meth*, 5(6):507–516, June 2008.

[71] C. R. Sabanayagam, J. S. Eid, and A. Meller. Long time scale blinking kinetics of cyanine fluorophores conjugated to dna and its effect on f[o-umlaut]rster resonance energy transfer. *J. Chem. Phys.*, 123(22):224708–7, Dec. 2005.

[72] J. SantaLucia. A unified view of polymer, dumbbell, and oligonucleotide dna nearest-neighbor thermodynamics. *PNAS*, 95(4):1460–1465, Feb. 1998.

[73] A. Schenzle and R. G. Brewer. Macroscopic quantum jumps in a single atom. *Phys. Rev. A*, 34(4):3127–3142, Oct. 1986.

[74] B. Schuler. Single-molecule fluorescence spectroscopy of protein folding. *ChemPhysChem*, 6(7):1206–1220, 2005.

[75] G. A. F. Seber and C. J. Wild. *Wiley series in probability and mathematical statistics : applied probability and statistics*. Wiley, New York, NY, 1989.

[76] M. T. Sheldon, P.-E. Trudeau, T. Mokari, L.-W. Wang, and A. P. Alivisatos. Enhanced semiconductor nanocrystal conductance via solution grown contacts. *Nano Lett.*, 9 (11):3676–3682, Aug. 2009.

[77] D. Shu, H. Zhang, J. Jin, and P. Guo. Counting of six prnas of phi29 dna-packaging motor with customized single-molecule dual-view system. *EMBO J*, 26(2):527–537, Jan. 2007.

[78] D. Stoler. Photon antibunching and possible ways to observe it. *Phys. Rev. Lett.*, 33(23):1397–1400, Dec. 1974.

[79] J. Sykora, K. Kaiser, I. Gregor, W. Bonigk, G. Schmalzing, and J. Enderlein. Exploring fluorescence antibunching in solution to determine the stoichiometry of molecular complexes. *Anal. Chem.*, 79(11):4040–4049, Jun 2007.

[80] H. Ta, J. Wolfrum, and D.-P. Herten. An extended scheme for counting fluorescent molecules by photon-antibunching. *Laser Phys.*, 19:online, 2009.

[81] P. Tinnefeld, C. Mueller, and M. Sauer. Time-varying photon probability distribution of individual molecules at room temperature. *Chem. Phys. Lett.*, 345(3-4):252–258, Sept. 2001.

[82] P. Tinnefeld, K. D. Weston, T. Vosch, M. Cotlet, T. Weil, J. Hofkens, K. Mullen, F. C. De Schryver, and M. Sauer. Antibunching in the emission of a single tetrachromophoric dendritic system. *J. Am. Chem. Soc.*, 124(48):14310–14311, Dec. 2002.

[83] J. Tisler, G. Balasubramanian, B. Naydenov, R. Kolesov, B. Grotz, R. Reuter, J.-P. Boudou, P. A. Curmi, M. Sennour, A. Thorel, M. Boersch, K. Aulenbacher, R. Erdmann, P. R. Hemmer, F. Jelezko, and J. Wrachtrup. Fluorescence and spin properties of defects in single digit nanodiamonds. *ACS Nano*, 3(7):1959–1965, July 2009.

[84] B. Valeur. *Molecular Fluorescence Principles and Applications*. Wiley-VCH, Weinheim [u.a.], 2002.

[85] I. I. Vlasov, A. S. Barnard, V. G. Ralchenko, O. I. Lebedev, M. V. Kanzyuba, A. V. Saveliev, V. I. Konov, and E. Goovaerts. Nanodiamond photoemitters based on strong narrow-band luminescence from silicon-vacancy defects. *Adv. Mater.*, 21(7):808–812, 2009.

[86] J. Vogelsang, R. Kasper, C. Steinhauer, B. Person, M. Heilemann, M. Sauer, and P. Tinnefeld. A reducing and oxidizing system minimizes photobleaching and blinking of fluorescent dyes. *Angew. Chem. Int. Ed.*, 47(29):5465–5469, 2008.

[87] M. Wahl. Technical note: Time tagged time-resolved fluorescence data collection. Technical report, PicoQuant GmbH, 2004.

[88] M. Wahl, H.-J. Rahn, T. Rohlicke, G. Kell, D. Nettels, F. Hillger, B. Schuler, and R. Erdmann. Scalable time-correlated photon counting system with multiple independent input channels. *Rev. Sci. Instrum.*, 79(12):123113–8, Dec. 2008.

[89] X. Wang, X. Ren, K. Kahen, M. A. Hahn, M. Rajeswaran, S. Maccagnano-Zacher, J. Silcox, G. E. Cragg, A. L. Efros, and T. D. Krauss. Non-blinking semiconductor nanocrystals. *Nature*, 459(7247):686–689, June 2009.

[90] J. Weibezahn, B. Bukau, and A. Mogk. Unscrambling an egg: protein disaggregation by aaa+ proteins. *Microb. Cell Fact.*, 3(1):1–12, Jan 2004.

[91] S. Weiss. Fluorescence spectroscopy of single biomolecules. *Science*, 283(5408):1676–1683, Mar. 1999.

[92] K. D. Weston, M. Dyck, P. Tinnefeld, C. Muller, D. P. Herten, and M. Sauer. Measuring the number of independent emitters in single-molecule fluorescence images and trajectories using coincident photons. *Anal. Chem.*, 74(20):5342–5349, Oct. 2002.

[93] J. Widengren and P. Schwille. Characterization of photoinduced isomerization and back-isomerization of the cyanine dye cy5 by fluorescence correlation spectroscopy. *J. Phys. Chem. A*, 104(27):6416–6428, July 2000.

[94] B. Wu, Y. Chen, and J. D. Müller. Fluorescence fluctuation spectroscopy of mcherry in living cells. 96(6):2391–2404, Mar. 2009.

[95] B. Wu and J. D. Müller. Time-integrated fluorescence cumulant analysis in fluorescence fluctuation spectroscopy. *Biophys. J.*, 89(4):2721–2735, Oct. 2005.

[96] X.-Q. Zhang, M. Chen, R. Lam, X. Xu, E. Osawa, and D. Ho. Polymer-functionalized nanodiamond platforms as vehicles for gene delivery. *ACS Nano*, 3(9):2609–2616, Sept. 2009.

List of Figures

List of Tables

Hiermit erkläre ich an Eides Statt, dass ich die vorliegende Arbeit selbstständig und ohne unerlaubte Hilfsmittel durchgeführt habe.

Heidelberg, den 19.12.2009 .....